Volume 9, Issue 16 – e2025916 January – December – 2025

ECORFAN

Journal - Taiwan

ISSN-On line: 2524-2121

ECORFAN®

ECORFAN Journal-Taiwan, Volume 9, Issue 16: e2025916 January - December 2025, is a Continuous publication – Journal edited by ECORFAN-Taiwan, Taipei. YongHe district, Zhong Xin, Street 69. Postcode: 23445. WEB: www.ecorfan.org/taiwan/journal@ecorfan.org. Editor in Chief: Vargas-Delgado, Oscar. PhD. ISSN: 2524-2121. Responsible for the latest update of this number ECORFAN Computer Unit. Escamilla-Bouchán, Imelda. PhD, Luna-Soto, Vladimir. PhD, last updated December 30, 2025.

ECORFAN Journal-Taiwan

Definition of Journal

Scientific Objectives

Support the international scientific community in its written production Science, Technology and Innovation in the Field of Physical Sciences Mathematics and Earth sciences, in Subdisciplines of optical astronomy, optical characterization, optical encoder, experimental research, planetary magnetic fields, ultraviolet radiation, lasers, algorithms and optical waves.

ECORFAN-Mexico, S. C. is a Scientific and Technological Company in contribution to the Human Resource training focused on the continuity in the critical analysis of International Research and is attached to CONACYT-RENIECYT number 1702902, its commitment is to disseminate research and contributions of the International Scientific Community, academic institutions, agencies and entities of the public and private sectors and contribute to the linking of researchers who carry out scientific activities, technological developments and training of specialized human resources with governments, companies and social organizations.

Encourage the interlocution of the International Scientific Community with other Study Centers in Mexico and abroad and promote a wide incorporation of academics, specialists and researchers to the publication in Science Structures of Autonomous Universities - State Public Universities - Federal IES - Polytechnic Universities - Technological Universities - Federal Technological Institutes - Normal Schools - Decentralized Technological Institutes - Intercultural Universities - S & T Councils - CONACYT Research Centers.

Scope, Coverage and Audience

ECORFAN Journal- Taiwan is a Journal edited by ECORFAN-Mexico S.C in its Holding with repository in Taiwan, is a scientific publication arbitrated and indexed with semester periods. It supports a wide range of contents that are evaluated by academic peers by the Double-Blind method, around subjects related to the theory and practice of optical astronomy, optical characterization, optical encoder, experimental research, planetary magnetic fields, ultraviolet radiation, lasers, algorithms and optical waves with diverse approaches and perspectives , That contribute to the diffusion of the development of Science Technology and Innovation that allow the arguments related to the decision making and influence in the formulation of international policies in the Field of Physical Sciences Mathematics and Earth sciences. The editorial horizon of ECORFAN-Mexico® extends beyond the academy and integrates other segments of research and analysis outside the scope, as long as they meet the requirements of rigorous argumentative and scientific, as well as addressing issues of general and current interest of the International Scientific Society.

Editorial Board

Arbitration Committee

Jimenez - Contreras, Edith Adriana. PhD
Instituto Politécnico Nacional • R-2935-2017 • 0000-0002-2792-7864 • 176565

Beltrán - Pérez, Georgina. PhD
Benémerita Universidad Autónoma de Puebla • JGW-3069-2023 • 0000-0001-6736-734X • 25762

Anzueto - Sánchez, Gilberto. PhD
Universidad Autónoma del Estado de Morelos • • 0000-0002-8905-8027 • 104099

Guzmán - Chávez, Ana Dinora. PhD
Universidad de Guanajuato • I-2111-2017 • 0000-0002-5545-6852 • 167827

Cano - Lara, Miroslava. PhD
Instituto Tecnológico Superior de Irapuato • ITU-0041-2023 • 0000-0002-3335-2710 • 1652459

Orozco - Guillén, Eber Enrique. PhD
Universidad Politécnica de Sinaloa • 0000-0001-9309-252X

Rojas - Laguna, Roberto. PhD
Universidad de Guanajuato • FP-7892-2022 • 0000-0001-9487-0354 • 19315

Jauregui - Vazquez, Daniel. PhD
Universidad de Guanajuato • 0000-0001-7621-8573 • 290595

García - Guerrero, Enrique Efrén. PhD
Universidad Autónoma de Baja California • 0000-0001-5052-6850 • 86932

Guerrero-Viramontes, J Ascención. PhD
Instituto Tecnológico de Aguascalientes • K-9042-2019 • 0000-0001-7408-5375 • 22162

Ibarra-Manzano, Oscar Gerardo. PhD
Universidad de Guanajuato • L-2432-2018 • 0000-0002-7487-2528 • 19462

Assignment of Rights

The sending of an Article to ECORFAN Journal-Taiwan emanates the commitment of the author not to submit it simultaneously to the consideration of other series publications for it must complement the Originality Format for its Article.

The authors sign the Authorization Format for their Article to be disseminated by means that ECORFAN-Mexico, S.C. In its Holding Taiwan considers pertinent for disclosure and diffusion of its Article its Rights of Work.

Declaration of Authorship

Indicate the Name of Author and Coauthors at most in the participation of the Article and indicate in extensive the Institutional Affiliation indicating the Department.

Identify the Name of Author and Coauthors at most with the CVU Scholarship Number-PNPC or SNI-CONACYT- Indicating the Researcher Level and their Google Scholar Profile to verify their Citation Level and H index.

Identify the Name of Author and Coauthors at most in the Science and Technology Profiles widely accepted by the International Scientific Community ORC ID - Researcher ID Thomson - arXiv Author ID - PubMed Author ID - Open ID respectively.

Indicate the contact for correspondence to the Author (Mail and Telephone) and indicate the Researcher who contributes as the first Author of the Article.

Plagiarism Detection

All Articles will be tested by plagiarism software PLAGSCAN if a plagiarism level is detected Positive will not be sent to arbitration and will be rescinded of the reception of the Article notifying the Authors responsible, claiming that academic plagiarism is criminalized in the Penal Code.

Arbitration Process

All Articles will be evaluated by academic peers by the Double Blind method, the Arbitration Approval is a requirement for the Editorial Board to make a final decision that will be final in all cases. MARVID® is a derivative brand of ECORFAN® specialized in providing the expert evaluators all of them with Doctorate degree and distinction of International Researchers in the respective Councils of Science and Technology the counterpart of CONACYT for the chapters of America-Europe-Asia- Africa and Oceania. The identification of the authorship should only appear on a first removable page, in order to ensure that the Arbitration process is anonymous and covers the following stages: Identification of the Journal with its author occupation rate - Identification of Authors and Coauthors - Detection of plagiarism PLAGSCAN - Review of Formats of Authorization and Originality-Allocation to the Editorial Board-Allocation of the pair of Expert Arbitrators-Notification of Arbitration -Declaration of observations to the Author-Verification of Article Modified for Editing-Publication.

Instructions for Scientific, Technological and Innovation Publication

Knowledge Area

The works must be unpublished and refer to topics of optical astronomy, optical characterization, optical encoder, experimental research, planetary magnetic fields, ultraviolet radiation, lasers, algorithms and optical waves and other topics related to Physical Sciences Mathematics and Earth sciences.

Presentation of the content

In the first article we present *Cryptographic Algorithms for Industry 4.0: Analysis of the learning with errors method, Feistel networks, and linear feedback shift registers* by Castillo-Pacheco, César Marcelino & Rodríguez-Olivares, Noé Amir, with adscription in the Centro de Ingeniería y Desarrollo Industrial, in the next article we present *Incorporation of Zinc Oxide Nanoparticles in Ceramic Materials* by Díaz-Silvestre, Sergio Enrique, Correa-Vazquez, Evanivaldo, Canales-Patiño, Eduardo Luis and Rico-Martinez, Alejandra Hikari, with adscription in the Universidad Tecnológica de Saltillo, in the next article we present *Ultrasound-assisted modification of MWCNTs with citric acid* by Díaz-Silvestre, Sergio Enrique, Ramírez-Mendoza, Leticia Arizbeth and Vazquez-Aguilar, Mario Leornardo, with adscription in the Universidad Tecnológica de Saltillo and Universidad Tecnológica de Coahuila, in the next article we present *Optical Sensing Technology for Capturing Vibrations in the Automotive Industry* by Hernández-González, Josué Iván, Torres-Cedillo, Sergio Guillermo, Hernández-Moreno, Hilario and Cortés-Pérez, Jacinto, with adscription in the Universidad Nacional Autónoma de México and Instituto Politécnico Nacional, in the next article we present *Effect of frying on pork rinds quality* by Reynoso-Ocampo, Carlos Abraham, Arroyo-Cruz, Celerino, Trejo-Trejo, Elia and Cervantes-Miranda, Jesús, with adscription in the Universidad Tecnológica del Valle del Mezquital, in the next article we present *PID control for tracking A 5 DOF robotic manipulator subjected to exogenous forces* by Pacheco, Jorge, Cortés-Vega, David, Sanchez-Lara, Rafael, Alazki, Hussain, with adscription in the Universidad Autónoma del Carmen, in the last article we present *Current sensorless robust voltage regulation discontinuous control for DC-DC buck converter* by Hernandez-Salazar, Jesus Emmanuel, Cortes-Vega, David, Alazki, Hussain and Vázquez-Ávila, José Luis, with adscription in the Universidad Autónoma del Carmen.

Content

ECORFAN-Journal Taiwan 9[16]1-13: e1916113
Article

Cryptographic Algorithms for Industry 4.0: Analysis of the learning with errors method, Feistel networks, and linear feedback shift registers

Algoritmos criptográficos para la Industria 4.0: Análisis del método de Aprendizaje con Errores, redes de Feistel y registros de desplazamiento con retroalimentación lineal

Castillo-Pacheco, César Marcelino*[a] & Rodríguez-Olivares, Noé Amir[b]

[a] Centro de Ingeniería y Desarrollo Industrial • T-9314-2025 • 0009-0007-8266-8838 • 1288544
[b] Centro de Ingeniería y Desarrollo Industrial • I-5012-2018 • 0000-0001-5892-0625 • 444191

SECIHTI classification:

Area: Engineering
Field: Technological Sciences
Discipline: Computer Technology
Subdiscipline: Code and coding systems

https://doi.org/10.35429/EJT.2025.9.16.1.1.13
History of the article:
Received: June 02, 2025
Accepted: December 15, 2025

* ✉ [cm.castillo@cidesi.edu.mx]

Abstract

In the context of Industry 4.0, the selection of suitable encryption schemes is essential to ensure cybersecurity without compromising computational efficiency. The wide variety of available algorithms, each with different levels of complexity and security, makes an objective selection challenging. This study presents a comparative analysis of three cryptographic techniques: lattice-based cryptography (Learning With Errors, LWE), the Feistel network, and the Linear Feedback Shift Register (LFSR). Each algorithm was implemented in MATLAB and evaluated using metrics such as execution time, memory consumption, entropy, avalanche effect, and correlation between the original and the encrypted signal. The results show that LWE provides the highest level of security, exhibiting a significantly stronger avalanche effect, whereas the Feistel network achieves a balanced trade-off between performance and security. LFSR proves to be highly efficient in terms of resource usage; however, it exhibits limited cryptographic robustness. The study also considers the PIG Geómetra system developed at CIDESI, highlighting the need for secure data encryption. LWE was found to be suitable for protecting continuous streams of industrial information.

Comparison of Cryptographic Schemes Based on LWE, Feistel Networks, and LFSRs

Goal	Methodology	Contribution
To evaluate performance. To encrypt signals. To analyze efficiency 	To *generate input signal*. To encrypt the signals with 3 schemes. To analyze metrics. 	Facilitate the understanding of advantages and limitations of three cryptographic schemes with different levels of security and efficiency. 

Cryptography, Encryption, Security

Resumen

En el contexto de la Industria 4.0, la selección de esquemas de encriptación adecuados es fundamental para garantizar la ciberseguridad sin comprometer la eficiencia computaciona, la variedad de algoritmos disponibles, con distintos niveles de complejidad y seguridad, dificulta una elección objetiva. Este estudio presenta un análisis comparativo de tres técnicas criptográficas: la criptografía basada en retículos (Learning With Errors, LWE), la red de Feistel y el registro de desplazamiento con retroalimentación lineal (LFSR). Cada algoritmo fue implementado en MATLAB y evaluado mediante métricas como tiempo de ejecución, consumo de memoria, entropía, efecto avalancha y correlación entre la señal original y la señal encriptada. Los resultados obtenidos muestran que LWE ofrece una mayor seguridad, con un efecto avalancha significativamente superior, mientras que la red de Feistel logra un balance entre rendimiento y seguridad. LFSR promete ser muy eficiente en el consumo de recursos, sin embargo, presenta propiedades criptográficas muy limitadas. El estudio también considera el sistema PIG Geómetra desarrollado en CIDESI, destacando la necesidad de un cifrado seguro de datos. LWE resultó adecuado para proteger flujos continuos de información industrial.

Comparación de esquemas criptográficos basados en LWE, redes de Feistel y registros de desplazamiento con retroalimentación lineal

Objetivo	Metodología	Contribución
Evaluar desempeño. Encriptar señales. Analizar eficiencia. 	Generar señal de entrada. Encriptar las señales con 3 esquemas. Analizar métricas. 	Facilitar la compresión de ventajas y limitaciones de tres esquemas criptográficos con distintos niveles de seguridad y eficiencia. 

Criptografía, Encriptado, Seguridad.

Área: Development of strategic leading-edge technologies and open innovation for social transformation

Citation: Castillo-Pacheco, César Marcelino & Rodríguez-Olivares, Noé Amir. [2025]. Cryptographic Algorithms for Industry 4.0: Analysis of the learning with errors method, Feistel networks, and linear feedback shift registers. ECORFAN-Journal Taiwan. 9[16]1-13: e1916113.

Introducción

In a world of constant digital evolution, information security has become a critical concern. Cryptography ensures the confidentiality, integrity, and authenticity of both stored and transmitted data. In industrial embedded systems, such as the PIG Geómetra developed at CIDESI, protecting the continuous flow of information through encryption is essential. Among modern encryption schemes, LWE (Learning With Errors) stands out for its high level of security, making it an ideal approach to strengthen the reliability of industrial dataloggers and other Industry 4.0 applications.

In a context where Industry 4.0 drives the interconnection of physical systems, sensor networks, and embedded devices, information protection becomes critically important. The evaluation of post-quantum encryption schemes within connected industrial environments is not only useful but also necessary. This is because traditional cryptographic algorithms, such as RSA (based on the factorization of large prime numbers) and ECC (Elliptic Curve Cryptography, which relies on the discrete logarithm problem in elliptic curves), are founded on mathematical problems that could be efficiently solved by quantum computers. Post-quantum schemes, such as LWE (Learning With Errors), rely on hard problems in lattice spaces and have been specifically designed to resist quantum attacks. In industrial applications, both cybersecurity and computational efficiency are critical factors, thus creating the need to identify which cryptographic schemes provide the best balance between robustness and performance.

At present, there are various encryption techniques, each designed to respond to different levels of attacks or threats, as well as to specific hardware capabilities. This diversity of schemes makes the selection of the most suitable algorithm for a given application more challenging, turning the search for an optimal balance between robustness and computational efficiency into a complex task. This situation becomes critical in modern environments such as Industry 4.0, where embedded resources are more constrained, and both technological risks and advancements evolve continuously. In this context, a reliable and rigorous comparative analysis is essential to understand the strengths and weaknesses of each cryptographic scheme.

This work compares three widely used cryptographic approaches:

a) Lattices (LWE – Learning With Errors).
b) Feistel Network.
c) Linear Feedback Shift Register (LFSR).

The decision to carry out this comparison arises from the interest in contrasting a traditional and well-established scheme (the Feistel network) with a modern one (LWE), where performance requirements are significantly more demanding. Through this comparison, it is possible to analyze the current trade-off between security and computational efficiency. Additionally, encryption based on Linear Feedback Shift Registers (LFSR) is included, offering extreme simplicity and high speed. By incorporating LFSR into the analysis, the evaluation spectrum is completed—comparing a highly secure scheme (LWE), a balanced one (Feistel), and an extremely efficient one (LFSR). This approach allows for the identification of specific advantages and limitations under controlled testing conditions. The central problem of this study lies in the comparative evaluation of the performance of three encryption methods with different theoretical foundations (Feistel, LWE, and LFSR), considering both their cryptographic strength and their feasibility for implementation in embedded systems in terms of:

– Security: theoretical resistance against attacks (brute-force, statistical analysis, and quantum attacks). [NIST, 2023; Katz & Lindell, 2020; Biryukov & Shamir, 2002].
– Efficiency: execution time, memory usage, and scalability across different platforms. [ARM, 2022; IEEE IoT, 2020]

To this end, implementations were developed in MATLAB, evaluating metrics such as:

– Entropy of the encrypted outputs (to measure randomness).
– Avalanche effect (sensitivity to small changes in the input or key).
– Correlation between the plaintext and the ciphertext (ideally close to zero).
– Computational performance for different data sizes.

ISSN: 2524-2121
RENIECYT-SECIHTI: 1702902

Castillo-Pacheco, César Marcelino & Rodríguez-Olivares, Noé Amir. [2025]. Cryptographic Algorithms for Industry 4.0: Analysis of the learning with errors method, Feistel networks, and linear feedback shift registers. ECORFAN-Journal Taiwan. 9[16]1-13: e1916113.
https://doi.org/10.35429/EJT.2025.9.16.1.1.13

These metrics were selected because they represent the fundamental pillars for evaluating a cryptographic algorithm applied to digital signals. Shannon entropy measures the randomness and dispersion of the signal, which once encrypted helps prevent predictable patterns (Shannon, 1949). The avalanche effect evaluates the impact of small changes in the input on the output (Upadhyay *et al*., 2022). The correlation between the original and encrypted signals reveals the degree of statistical independence achieved by the transformation (Krishnamurthy & Ramaswamy, 2010). Finally, computational performance helps quantify the practical feasibility of the algorithm for real-world implementation.

The results of this study make it possible to establish criteria for the selection of algorithms according to the required security level, the type of device, and the application context. Moreover, this analysis contributes to the global discussion on the adoption of post-quantum algorithms in connected industrial systems, a key aspect for ensuring cybersecurity in Industry 4.0.

Embedded systems dedicated to pipeline inspection (PIG Geómetra) have demonstrated the importance of protecting large volumes of data acquired by sensors during extended operations. In these mass storage systems, which use microSD or NAND Flash memories, variations in latency and vulnerabilities to data manipulation may occur. It is under these conditions that LWE emerges as an ideal solution to ensure both the integrity and authentication of the information. Its lattice-based nature makes it particularly suitable for critical embedded systems, where security must coexist with processing constraints and continuous data flow.

Theory

Feistel Network

The Feistel cipher is a symmetric structure widely used in cryptographic algorithms such as DES, Blowfish, and Twofish (Schneier, 1996; Schneier, 1993). Its popularity is due to its ability to provide acceptable security using simple operations such as XOR, rotations, and substitutions, which makes it easy to implement in both hardware and embedded software (Stallings, 2017; Schneier, 1996).

The network is a symmetric structure in which the data are divided into two halves that are repeatedly transformed through a series of operations known as rounds. Each round consists of a transformation function applied to one half of the block, combining it with the other through operations such as rotations and XOR. A block is a fixed-size unit of data on which an encryptor operates; it has a constant size, local independence, and reversibility properties.

It is a classic symmetric cryptography scheme, present in algorithms such as DES [NIST FIPS 46-3, 1999; Daemen & Rijmen, 2002] and Blowfish [Schneier, 1993; Schneier, 1996]. It stands out for its computational efficiency and ease of implementation in both hardware and software. Despite being a classical symmetric encryption scheme, the Feistel network continues to be widely used in modern algorithms due to its high efficiency and straightforward implementation in hardware and software alike. It features a flexible structure and very low computational cost, making it ideal for embedded systems and resource-constrained devices.

LWE-Based Cipher

Cryptographic method based on mathematical problems known as Learning With Errors (LWE), which consists of recovering a secret vector s from a system of noisy linear equations of the form $b = A * s + e$. This problem could be easily solved through algebraic methods; however, the introduction of noise (error) makes the system extremely difficult to solve. For this reason, LWE is considered one of the most robust pillars of post-quantum cryptography and has been proposed as a standard by NIST. Its high level of security lies in the difficulty of solving noisy linear equation systems in high-dimensional spaces, a fundamental feature for high-security applications, including interconnected industrial systems. (NIST, 2023).

To implement the LWE scheme in a secure and functional manner, it is necessary to carefully define a set of parameters that determine the computational difficulty of the problem. These parameters must be chosen so that the resulting instance is resistant to known cryptographic attacks, both classical and quantum. The main parameters that define an LWE instance are:

ISSN: 2524-2121
RENIECYT-SECIHTI: 1702902

Castillo-Pacheco, César Marcelino & Rodríguez-Olivares, Noé Amir. [2025]. Cryptographic Algorithms for Industry 4.0: Analysis of the learning with errors method, Feistel networks, and linear feedback shift registers. ECORFAN-Journal Taiwan. 9[16]1-13: e1916113.
https://doi.org/10.35429/EJT.2025.9.16.1.1.13

– n dimension of the secret vector.
– q modulus over which the vectors operate (a large prime integer).
– σ standard deviation of the error term.

LFSR-Based Cipher (Linear Feedback Shift Register)

It is a lightweight technique that generates pseudorandom sequences through simple logical operations; it offers high speed and low memory consumption, although its security level is lower if not used in combination with another suitable scheme.

The encryption mechanism is based on a bitwise XOR operation between each value of the original signal and the byte generated by the LFSR, which allows the implementation of a simple synchronous stream cipher with low computational cost. This technique is common in applications that require speed and efficiency, although its security level is limited if used without additional confusion or diffusion functions.

Methodology

In order to carry out a consistent and repeatable evaluation among the three selected cryptographic schemes, an experimental platform was designed in MATLAB that applies the same input, processing, and evaluation criteria for each algorithm. This ensures that the differences observed are not caused by external factors, but rather by the inherent properties of each cryptographic scheme.

Experimental Environment

All tests were performed five times on a system equipped with an AMD Ryzen 5 8645HS processor running at 4.30 GHz, 16 GB of RAM, and the Windows 11 Home operating system, using MATLAB® R2019b with a 200-sample discretized signal.

This environment was selected to ensure uniform and reproducible conditions during implementation. The implemented methodology focused on applying each cryptographic scheme to a digital signal normalized within the range $[-1, 1]$, which was then scaled and discretized to an 8-bit format in the interval [0, 255], simulating a typical analog-to-digital signal in embedded systems.

The behavior of each scheme was evaluated against a set of metrics designed to measure its security, robustness, and computational performance.

The input signal used as the base message to evaluate the three cryptographic methods consists of a single-cycle sinusoidal wave, generated with a sampling period of 1 ms (equivalent to a sampling frequency of 1000 Hz) and a fundamental frequency of 5 Hz. This choice is justified by its distinct visual form, which allows for a clear observation of distortion, dispersion, and information loss effects that may result from message manipulation.

$$N = \frac{f_s}{f_0} = \frac{1000\ \text{Hz}}{5\ \text{Hz}} = 200\ \text{samples} \qquad [1]$$

Where N is the total number of samples required to represent one complete cycle of the signal, $f0$ is the fundamental frequency of the sinusoidal wave (in Hz), and fs is the sampling frequency, that is, the number of samples per second taken to digitize the signal.

These 200 samples represent the sampling points of the sinusoidal signal during one complete cycle. In other words, they consist of the 200 discrete values obtained by digitizing a continuous 5 Hz wave using a sampling frequency of 1000 Hz. This set of samples is used as the quantized base message on which the different encryption methods analyzed in this study are applied.

Box 1

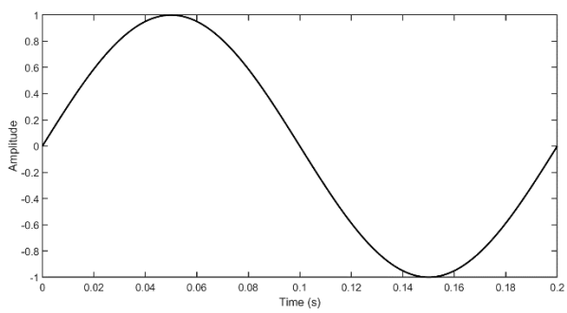

Figure 1
Single-cycle sinusoidal wave generated at 5 Hz and sampled at 1000 Hz
Source: Authors' own work

Figure 1 shows the sinusoidal waveform used as the input signal, composed of 200 samples representing one complete cycle.

ISSN: 2524-2121
RENIECYT-SECIHTI: 1702902

This visualization clearly illustrates the encoding and distortion effects produced by the different cryptographic schemes evaluated. Once quantized, the signal is processed by each of the encryption schemes. After completing the encryption process, a fully encoded and unreadable signal is obtained. Subsequently, this signal is subjected to an inverse process to carry out its recovery.

Box 2

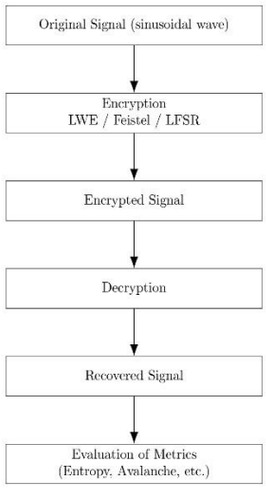

Figure 2
Methodological summary of the encryption system applied to signals.

Source: Authors' own work

Implementation of the Feistel Cipher

In this work, a 16-round network was employed, applied to an 8-bit quantized signal.

Box 3

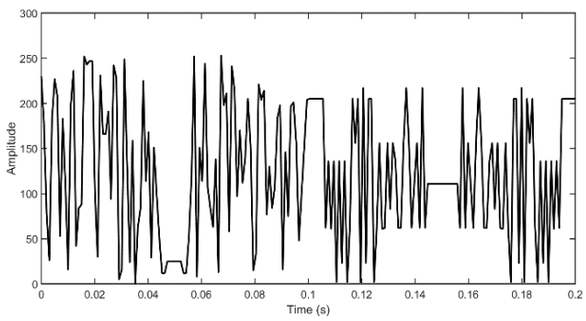

Figure 3
Signal encrypted by the Feistel network (discretized to the range [0,1])

Source: Authors' own work

Figure 3 shows how the 16-round process transforms the original sinusoidal wave, dispersing its values and eliminating any recognizable pattern.

Signal Division

The input signal is divided into two halves:

$$L_0 = S[1: N/2], \quad R_0 = S[N/2 + 1: N] \qquad [2]$$

Where:

S is the input vector composed of N simples *N* is the total number of samples. L_0 and R_0 represent the left and right blocks, respectively, which are obtained by dividing the signal into two halves.

The use of $N/2$ ensures that each half contains the same amount of initial information, which is necessary to maintain symmetry. By dividing the signal into two equal blocks, a recursive structure can be applied that exchanges information between both sides, progressively increasing the complexity and diffusion of the encrypted message.

Encryption Rounds

Each encryption round i applies a nonlinear permutation operation, including a process that reorders the bits within the byte, which breaks the linearity over the input domain:

$$L_{i+1} = R_i, \quad R_{i+1} = L_i \oplus F(R_i, K_i) \qquad [3]$$

The transformation function *F(R,K)* is defined as a bit rotation followed by an XOR operation:

$$F(R, K) = \text{bitxor}(\text{rot}(R, s_i), K) \qquad [4]$$

Where:
si represents the number of positions by which the byte R is rotated in round *i.*

The rotation function is implemented as:

$$\text{rot}(R, s) = (R \ll s) \oplus \big(R \gg (8 - s)\big) \qquad [5]$$

The rotation *rot(R,s)* is an operation designed to rearrange the bits within each byte cyclically, altering their positions through left and right shifts and combining them with XOR. This introduces internal complexity and diffusion, even before applying the key.

Where the shift s_i is calculated as:

$$s_i = \text{mod}(2i - 1,\ 8) + 1 \qquad [6]$$

ISSN: 2524-2121
RENIECYT-SECIHTI: 1702902

Castillo-Pacheco, César Marcelino & Rodríguez-Olivares, Noé Amir. [2025]. Cryptographic Algorithms for Industry 4.0: Analysis of the learning with errors method, Feistel networks, and linear feedback shift registers. ECORFAN-Journal Taiwan. 9[16]1-13: e1916113.
https://doi.org/10.35429/EJT.2025.9.16.1.1.13

The value of the shift s_i varies in each round according to a modular function that ensures different and cyclic rotations between 1 and 8 bits, thus avoiding repetitive patterns.

Subkey Generation

The master key *K* is an 8-byte vector that is reused cyclically:

$$K_i = K[\text{mod}(i - 1,\ 8) + 1] \quad [7]$$

This design allows for memory and processing efficiency, using only 8 bytes to cover the 16 rounds.

Decryption

The decryption process applies the same operations in reverse order:

$$R_i = L_{i+1}, \quad L_i = R_{i+1} \oplus F(L_{i+1}, K_i) \quad [8]$$

To validate that the encryption and decryption process was fully reversible, the original signal was compared with the decrypted signal, sample by sample. The mean absolute error (MAE) was then calculated, defined as:

$$\text{MAE} = \frac{1}{N}\sum_{i=1}^{N}\left|S_{\text{original}}(i) - S_{\text{descrypted}}(i)\right| \quad [9]$$

Where:
N is the total number of samples.
$S_{original}(i)$ is the i-th sample of the original signal (before being encrypted).
$S_{descrypted}(i)$ is the i-th sample recovered after decryption.

Implementation of the LWE-Based Cipher

It is considered one of the pillars of post-quantum cryptography and has been proposed as a standard by NIST due to its resistance to quantum algorithms, such as Shor's algorithm.

Parameter Generation

In this implementation, the following parameters were used:

$$n = 256, \quad q = 4096, \quad \sigma = 3 \quad [10]$$

These values provide a reasonable balance between security and efficiency for academic testing.

Key Generation

The key generation process includes three components:

a) Public matrix $A \in Z_q^{n \times n}$ containing random values.
b) Secret vector $s \in \{0,1\}^n$ composed of binary bits.
c) Error vector $e \sim \mathcal{N}(0, \sigma^2)$ that adds controlled noise to conceal the relationship between *A* y *s*.

The resulting public key:
$b = (A \cdot s + e)\ mod\ q$ [11]

And ***s*** is the private key.

Encryption Process

The quantized signal (message m) is converted into an LWE-compatible format and encrypted through a linear combination with noise. The previously induced noise, drawn from a distribution $\mathcal{N}(0, \sigma^2)$ ensuring that the encrypted message maintains security based on the computational hardness of the LWE problem.

a) Generation of random matrix R
$R \in \{0,1\}^{n \times m}$ [12]

b) Computation of the encrypted values *u* and *v*.

selected with binary values:

$u = (A^T \cdot R)\ mod\ q$ [13]
$v = (b^T \cdot R + m)\ mod\ q$ [14]

Here, m is the message scaled to the domain of Zq.

Box 4

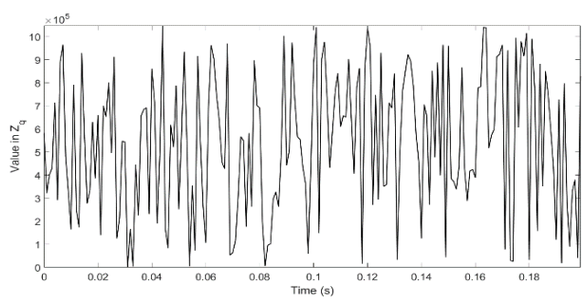

Figure 4
Signal encrypted using the LWE scheme. It is represented directly in the domain Zq with q = 1048583
Source: Authors' own work

Castillo-Pacheco, César Marcelino & Rodríguez-Olivares, Noé Amir. [2025]. Cryptographic Algorithms for Industry 4.0: Analysis of the learning with errors method, Feistel networks, and linear feedback shift registers. ECORFAN-Journal Taiwan. 9[16]1-13: e1916113.
https://doi.org/10.35429/EJT.2025.9.16.1.1.13

ISSN: 2524-2121
RENIECYT-SECIHTI: 1702902

Decryption Process

The receiver, knowing s, can reconstruct the message through:

$$\tilde{m} = (v - s^T \cdot u) \bmod q \quad [13]$$

Where $\tilde{m}$ represents the estimated version of the original message m btained after applying the inverse operation to the encryption process. Due to the presence of noise in the LWE scheme, the result is not an exact recovery, but rather an approximation that can later be refined using rescaling and rounding techniques to map it back to the original domain.

Implementation of the LFSR-Based Cipher (Linear Feedback Shift Register)

Linear Feedback Shift Registers (LFSRs) represent one of the oldest and most efficient methods for generating pseudorandom sequences. In this work, the use of an LFSR is explored as a keystream generator (pseudorandom key sequence) to encrypt a previously quantized input signal.

System Parameters

The implemented LFSR was defined with the following values:

a) Register length

$$n_{LFSR} = 8 \quad [14]$$

b) Initial seed (in hexadecimal):

semilla= 0xB3 [15]

c) Feedback polynomial

$$P(x) = x^8 + x^6 + x^5 + x^4 + 1 \quad [16]$$

This polynomial is primitive over the finite field $F2$ which guarantees that the LFSR will generate a pseudorandom sequence with the maximum possible period, that is, 2^8−1=255 cycles before repeating. This property ensures that the produced keystream traverses all possible combinations (except the zero state), thereby improving the dispersion of the encrypted data and reducing the likelihood of repetitive or predictable patterns in the output.

d) Active Taps

$$taps = \{8, 6, 5, 4\} \quad [17]$$

The active taps are the register positions used to calculate the feedback bit during each LFSR iteration. Each tap represents a bit of the register that participates in a joint XOR operation. In this case, the bits located at positions 8, 6, 5, and 4 (counting from the most significant end) are combined to generate a new bit, which is then inserted into the register after shifting its contents. This selection of taps corresponds to the previously defined feedback polynomial and is crucial for determining the properties of the keystream, including its period and degree of randomness.

State Initialization

The seed is converted into an 8-bit binary vector representing the initial state of the register:

$$state_0 = de2bi(0xB3) \quad [18]$$

The de2bi function is a MATLAB utility that converts a decimal integer into its binary representation, returning it as a logical vector (composed of zeros and ones).

Example:

$$\boldsymbol{state_0} = [1\ 0\ 1\ 1\ 0\ 0\ 1\ 1] \quad [19]$$

This value is updated in each iteration based on the defined taps. It represents the LFSR seed, expressed as the initial state of the shift register.

Keystream Generation

The pseudorandom sequence is generated as follows:

For each iteration i:

– Compute the feedback bit:

$$f_i = \oplus_{j \in taps}\, state_j \quad [20]$$

Shift the state to the right and insert f_i:

$$state_{i+1} = [f_i,\ state_i(1:n-1)] \quad [21]$$

– Convert the current state to decimal to obtain the cipher byte:

ISSN: 2524-2121
RENIECYT-SECIHTI: 1702902

Castillo-Pacheco, César Marcelino & Rodríguez-Olivares, Noé Amir. [2025]. Cryptographic Algorithms for Industry 4.0: Analysis of the learning with errors method, Feistel networks, and linear feedback shift registers. ECORFAN-Journal Taiwan. 9[16]1-13: e1916113.
https://doi.org/10.35429/EJT.2025.9.16.1.1.13

$\text{keystream}_i = bi2de(\text{state}_i)$ [22]

This process is repeated until completing a sequence with a length equal to the input signal *N*.

Box 5

Table 1
Evolution of the Internal State of the LFSR

Iteration	Binary State	Decimal Value
1	10110011	179
2	11011001	217
3	11101100	236
4	11110110	246

Source: Authors' own work

Encryption Process

The quantized input signal $S \in Z^{N}_{256}$ is encrypted using XOR:

$$C = S \oplus K \quad [23]$$

Where:
K: pseudorandom sequence generated by the LFSR.
C: encrypted signal.

This scheme operates as a synchronous stream cipher, generating a sequence that depends solely on the seed and the polynomial.

Box 6

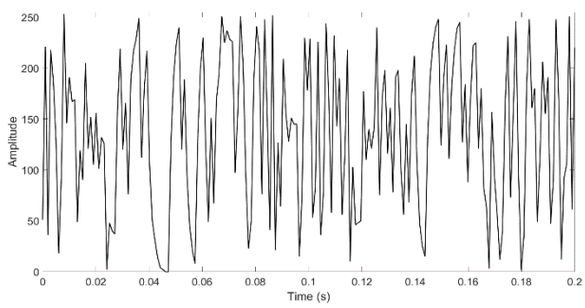

Figure 6
Signal encrypted using the LFSR scheme
Source: Authors' own work

Decryption Process

The decryption process is identical to the encryption process due to the XOR operator property:

$$S = C \oplus K \quad [24]$$

This mechanism allows for a highly efficient implementation, making it ideal for resource-constrained environments.

Decryption Validation

It was verified that:

$$\forall i, \quad S_i = (S_i \oplus K_i) \oplus K_i \quad [25]$$

which guarantees the exact recovery of the original signal, provided that the keystream is correctly replicated.

Evaluation Metrics

To perform a quantitative and objective comparison of the three encryption algorithms evaluated (Feistel, LWE, and LFSR), a set of evaluation metrics was defined to analyze their performance in terms of computational efficiency and statistical security.

Each metric was selected for its relevance in the context of encrypted digital signal processing and was measured under controlled conditions, using the same input signal, compatible parameters, and a common execution environment.

The following section describes each of the metrics used, their formal definitions, and the measurement methods applied in this study.

Execution Time

It is defined as the total time required to execute the encryption and decryption process of the signal. It was measured in milliseconds (ms) using the tic–toc function in MATLAB®. This metric is useful for determining temporal efficiency, which is especially important in real-time systems.

$$T_{proc} = T_{end} - T_{start} \quad [\text{ms}] \quad [26]$$

To reduce variability, each test was executed five times, and the average value was taken.

Where:
T_{proc}: total execution time in milliseconds.
T_{start}: starting time of the process.
T_{end}: ending time of the process.

ISSN: 2524-2121
RENIECYT-SECIHTI: 1702902

Castillo-Pacheco, César Marcelino & Rodríguez-Olivares, Noé Amir. [2025]. Cryptographic Algorithms for Industry 4.0: Analysis of the learning with errors method, Feistel networks, and linear feedback shift registers. ECORFAN-Journal Taiwan. 9[16]1-13: e1916113.
https://doi.org/10.35429/EJT.2025.9.16.1.1.13

Memory Usage

Memory usage represents the amount of space required to perform the encryption and decryption operations, considering both input and output data, as well as all auxiliary structures needed such as matrices, keys, temporary vectors, and state registers, among others.

To calculate it, the byte size of each structure used by the algorithm was summed:

$$M_{\text{total}} = \sum_{i=1}^{n} \text{bytes}(E_i) \quad [27]$$

Where:
M_{total}: total memory used.
E_i: individual structures employed (e.g., matrices, vectors).

Finally, the value was converted to kilobytes for presentation:

$$M\ [\text{KB}] = \frac{M_{\text{total}}}{1024} \quad [28]$$

The estimation was performed using MATLAB®'s whos function, which allows querying the size of each variable in memory. Only the structures strictly necessary for encryption were included, in order to avoid overestimating memory consumption.

Entropy of the Encrypted Signal

Entropy is a central metric in information theory. In the context of cryptography, higher entropy in the encrypted signal implies a greater level of randomness, which is desirable since it reduces the likelihood of patterns and enhances the confusion property of the system.

The Shannon formula was used to calculate the entropy of the encoded signals:

$$H = -\sum_{i=1}^{N} p_i \log_2(p_i) \quad [29]$$

Where:
H: entropy, in bits per sample.
P_i: probability of occurrence of value i, calculated as:

$$p_i = \frac{f_i}{\sum_{j=1}^{256} f_j} \quad [30]$$

where f_i is the absolute frequency of the value in the encrypted signal (uint8). A histogram with 256 bins (one for each possible value from 0 to 255) was used and normalized to obtain the probabilities.

An ideal entropy approaches:

$$H_{\max} = \log_2(256) = 8 \text{ bits/sample} \quad [31]$$

Shannon entropy measures the amount of uncertainty or randomness present in a signal. The higher the entropy, the more difficult it is to predict the next value, and therefore, the greater the statistical security of the encrypted signal.

Avalanche Effect

The avalanche effect measures how sensitive an encryption algorithm is to minimal changes in the input. A robust algorithm should produce a completely different signal if a single bit of the original signal is altered. This principle is key in cryptography, especially in block algorithms, as it ensures adequate diffusion. To quantify it, one bit in the first byte of the input signal was modified. Then, the original and modified encrypted bytes were compared, measuring how many bits changed using the Hamming distance.

The formula used were:

$$\text{Avalanche} = \frac{\sum_{i=1}^{n} \text{Hamming}(C_i, C_i')}{n \cdot 8} \times 100\% \quad [32]$$

n_l: total number of bytes analyzed.
Hamming (C_iC_i''): number of bits that differ between the two bytes.

This result is expressed as the percentage of bits altered.

Correlation Between Original and Encrypted Signals

This metric evaluates how independent the encrypted signal is from the original signal. In an ideal encryption scheme, there should be no apparent linear relationship between the two signals.

The Pearson correlation coefficient was calculated as:

$$\rho_{x,y} = \frac{\sum(x_i - \bar{x})(y_i - \bar{y})}{\sqrt{\sum(x_i - \bar{x})^2 \cdot \sum(y_i - \bar{y})^2}} \quad [35]$$

ISSN: 2524-2121
RENIECYT-SECIHTI: 1702902

Castillo-Pacheco, César Marcelino & Rodríguez-Olivares, Noé Amir. [2025]. Cryptographic Algorithms for Industry 4.0: Analysis of the learning with errors method, Feistel networks, and linear feedback shift registers. ECORFAN-Journal Taiwan. 9[16]1-13: e1916113.
https://doi.org/10.35429/EJT.2025.9.16.1.1.13

Where:
$X_{i:}$ original sample.
$Y_{i:}$ encrypted sample.
$\bar{x}, \bar{y}$: mean values of the signals.

Values of ρ close to zero or negative indicate greater independence, which is desirable in a secure cryptographic scheme. The calculation was performed in MATLAB® using the corrcoef(x, y) function and extracting the ρ value from the resulting matrix.

Box 7

Table 2
Scheme for the Presentation of Results

Metric	Unit	Measurement Tool
Encryption time	ms	*tic–toc* in MATLAB
Decryption time	ms	*tic–toc* in MATLAB
Memory usage	kB	*whos*, sum of structures
Entropy	bits/muestra	Shannon formula (histogram)
Avalanche effect	% de bits	Hamming distance, bit-by-bit comparison
Correlation	Pearson Coef..	*corrcoef*() between signals

Source: Authors' own work

In this section, the results obtained after applying the three encryption algorithms evaluated — Feistel, LWE, and LFSR — are presented and analyzed. Each algorithm was implemented in MATLAB® under the previously described experimental conditions, using the same 8-bit quantized sinusoidal input signal. The metrics considered were: processing time, memory usage, entropy of the encrypted signal, avalanche effect, and correlation between the original and the encrypted signals.

Execution Time

The encryption and decryption time was measured in milliseconds for each algorithm, averaging five consecutive runs.

Box 8

Table 3
Processing Time of Each Cipher

Algorithm	Encryption (ms)	Decryption (ms)
Feistel	0.35	0.41
LWE	1.87	2.32
LFSR	0.04	0.04

Source: Authors' own work

The LFSR algorithm demonstrated significantly superior performance in terms of speed, being 46 times faster than LWE and approximately 9 times faster than Feistel during the encryption stage. This behavior is expected, since LFSR operates with bit-level rotations and XOR operations, without the need for large data structures or matrix operations. LWE was the slowest algorithm, due to the requirement for matrix multiplications over Z_q and noise handling. This makes it less suitable for real-time applications, although its cryptographic robustness is higher.

Memory Usage

The total memory usage, measured in kilobytes, includes all the structures required by each algorithm during the encryption process.

Box 9

Table 4
Memory Used by Each Method

Algorithm	Memory (kB)
Feistel	0.20
LWE	1.53
LFSR	0.18

Source: Authors' own work

Once again, LWE showed a significantly higher memory consumption, resulting from the storage of the matrix $A \in Z_q^{nxn}$, the error vector, and the intermediate vectors. In contrast, Feistel and LFSR are limited to simple manipulations of the original signal, requiring less than 1 kB in total.

Entropy of the Encrypted Signal

The entropy was evaluated using Shannon's formula for the three encoded signals. A histogram with 256 bins (corresponding to all possible uint8 values) was used to estimate the probability of each value.

ISSN: 2524-2121
RENIECYT-SECIHTI: 1702902

Box 10

Table 5
Average Entropy of the Encrypted Signal

Algorithm	Entropy (bits/sample)
Feistel	7.85
LWE	9.21
LFSR	6.73

Source: Authors' own work

LWE achieved the highest entropy, even exceeding the theoretical maximum value of 8 bits/sample for uint8 signals, due to the dispersion introduced by operations in Z_q and the effect of Gaussian noise. Feistel produced a highly random signal, although slightly lower, while LFSR obtained the lowest value, suggesting a less dispersed and more predictable sequence.

Avalanche Effect

A single bit in the first input sample was altered, and the percentage of modified bits in the encrypted signal was measured using the Hamming distance.

Box 11

Table 6
Avalanche Effect by Algorithm

Algorithm	Avalanche Effect (% bits)
Feistel	0.31
LWE	45.7
LFSR	0.08

Source: Authors' own work

LWE exhibited a high avalanche effect, close to ideal behavior. This result is a consequence of the diffusive nature of the lattice-based scheme. Feistel showed minimal dispersion, which could potentially be improved by increasing the number of rounds. As expected, LFSR responded almost linearly to the change, demonstrating its weakness in diffusion.

Correlation Between Original and Encrypted Signals

The Pearson correlation coefficient between each original signal and its corresponding encrypted version was calculated to measure statistical independence.

Box 12

Table 7
Correlation Coefficient

Algorithm	Correlation (ρ)
Feistel	- 0.0012
LWE	–0.0341
LFSR	0.4412

Source: Authors' own work

LWE showed the lowest correlation (close to zero), indicating that the encrypted signal does not preserve linear information from the original. Feistel also achieved good independence, while LFSR exhibited a relatively high correlation, reflecting its limited ability to break relationships between the original and encoded data.

Conclusions

In this work, a detailed technical comparison was carried out among three encryption algorithms with different structures and theoretical foundations: Feistel, LWE (Learning With Errors), and LFSR (Linear Feedback Shift Register). The objective was to evaluate their performance on the same discretized input signal by applying a homogeneous set of metrics that cover both computational performance and cryptographic robustness.

The results obtained allowed for the identification of substantial differences among the analyzed algorithms, in terms of speed, memory consumption, and statistical properties of the encrypted signal.

From a computational efficiency perspective, the LFSR algorithm proved to be notably faster and lighter, with execution times below 0.05 ms and memory usage under 0.2 KB. This characteristic makes it an attractive candidate for implementation in embedded systems, remote sensors, and IoT devices, where resources are limited and cryptographic requirements may be basic. However, its entropy, avalanche, and correlation metrics revealed a significant structural weakness in terms of security, which restricts its applicability to low-criticality contexts.

ISSN: 2524-2121
RENIECYT-SECIHTI: 1702902

Castillo-Pacheco, César Marcelino & Rodríguez-Olivares, Noé Amir. [2025]. Cryptographic Algorithms for Industry 4.0: Analysis of the learning with errors method, Feistel networks, and linear feedback shift registers. ECORFAN-Journal Taiwan. 9[16]1-13: e1916113.
https://doi.org/10.35429/EJT.2025.9.16.1.1.13

he Feistel cipher, based on a 16-round symmetric network, provided a good balance between speed, memory, and security. Although it did not reach the entropy or avalanche effect levels of LWE, it maintained an almost null correlation with the original signal and showed greater robustness than LFSR. Its low computational cost and ease of implementation make it a viable option for real-world systems that require moderate security and efficiency, such as secure industrial control communications or mobile devices.

On the other hand, the LWE-based encryption exhibited lower computational performance due to its algorithmic complexity involving matrix operations over large domains, noise generation, and modular arithmetic management which resulted in higher execution times and greater memory consumption. Nevertheless, it outperformed the other algorithms in entropy, avalanche effect, and low correlation, demonstrating a superior level of cryptographic security. These properties make it particularly suitable for applications where quantum-attack resistance and statistical robustness are priority requirements, such as post-quantum digital signatures, sensitive data encryption, or secure cloud communications.

This study highlights the importance of considering both performance and statistical security metrics when selecting an encryption algorithm, especially in digital signal and discrete data transmission applications.

Finally, based on the results obtained, it can be stated that the statistical superiority of the LWE scheme makes it ideal for industrial continuous-storage environments, such as the PIG Geómetra system developed by CIDESI.

The implementation of LWE encryption in this architecture would provide the system with attack-resistant cryptographic protection, ensuring that the collected information remains intact and confidential. The LWE scheme is therefore the ideal complement for next-generation industrial dataloggers.

Conflict of Interest Statement

The authors declare that there is no financial, professional, or personal conflict of interest that could have influenced the results or the interpretation of the present work.

Authors' Contribution

C. M. Castillo Pacheco: conceptualization, implementation, technical writing, results analysis, and manuscript editing.

N. A. Rodríguez Olivares: conceptualization of the methodological approach, critical content review, academic supervision, and results validation.

Data and Code Availability

The source code of the implemented algorithms, as well as the test data used, are available in the following repository: https://github.com/CesarCastillo5/M-todos-de-encriptaci-n
This ensures the reproducibility of the results presented.

Funding

This work was partially funded by the Secretaría de Ciencia, Humanidades, Tecnología e Innovación, through the project MADTEC-2025-M-125, titled "Instrumented equipment for geometric inspection of hydrocarbon transport pipelines (Geómetra)".

No private external funding was received.

Abreviaciones

LWE	Learning With Errors
LFSR	Linear Feedback Shift Register
DES	Data Encryption Standard
XOR	Exclusive OR (operador lógico)
IoT	Internet of Things
RAM	Random Access Memory
Z_q	Set of integers modulo q
ρ	Pearson correlation coefficient
ms	Milliseconds
KB	Kilobytes

References

Basics

NIST. (2023). Post-Quantum Cryptography Standardization. National Institute of Standards and Technology.

Schneier, B. (1993). Description of a new variable-length key, 64-bit block cipher (Blowfish). In Fast Software Encryption (pp. 191–204). Springer.

ISSN: 2524-2121
RENIECYT-SECIHTI: 1702902

Castillo-Pacheco, César Marcelino & Rodríguez-Olivares, Noé Amir. [2025]. Cryptographic Algorithms for Industry 4.0: Analysis of the learning with errors method, Feistel networks, and linear feedback shift registers. ECORFAN-Journal Taiwan. 9[16]1-13: e1916113.
https://doi.org/10.35429/EJT.2025.9.16.1.1.13

Schneier, B. (1996). Applied Cryptography: Protocols, Algorithms, and Source Code in C (2nd ed.). John Wiley & Sons. ISBN: 0471128457

Stallings, W. (2017). Cryptography and Network Security: Principles and Practice (7th ed.). Pearson Education.

Shannon, C. E. (1949). Communication Theory of Secrecy Systems. Bell System Technical Journal, 28(4), 656–715.

Menezes, A. J., van Oorschot, P. C., & Vanstone, S. A. (1996). Handbook of Applied Cryptography. CRC Press.

European Telecommunications Standards Institute (ETSI). (2021). Security Algorithms Group of Experts (SAGE) Report on LFSR-based Stream Ciphers. ETSI TR 103 456.

Upadhyay, D., Gaikwad, N., Zaman, M., & Sampalli, S. (2022). Investigating the avalanche effect of various cryptographically secure hash functions and hash-based applications. IEEE Access, 10, 112472–112486.

Krishnamurthy, G. N., & Ramaswamy, V. (2010). Encryption quality analysis and security evaluation of CAST-128 algorithm and its modified version using digital images. International Journal of Network Security & Its Applications, 2(4), 50–60.

Supports

Su, Y., Yang, C., Tian, L., & Zhao, J. (2020). FPGA-based hardware accelerator for leveled Ring-LWE fully homomorphic encryption. IEEE Access, 8, 32640–32651.

Agrawal, R., Bu, L., Ehret, A., & Kinsy, M. A. (2020). Fast Arithmetic Hardware Library for RLWE-Based Homomorphic Encryption. In Proceedings of the 28th IEEE International Symposium on Field-Programmable Custom Computing Machines (FCCM 2020) (p. 206). IEEE.

Regev, O. (2009). On Lattices, Learning with Errors, Random Linear Codes, and Cryptography. Journal of the ACM, *56*(6), 1–40.

NIST. (1999). Data Encryption Standard (DES). Federal Information Processing Standards Publication 46-3.

Schneier, B. (1993). Description of a New Variable-Length Key, 64-Bit Block Cipher (Blowfish). In Fast Software Encryption (pp. 191–204). Springer.

Schneier, B. (1996). Applied Cryptography: Protocols, Algorithms, and Source Code in C (2nd ed.). Wiley.

Daemen, J., & Rijmen, V. (2002). The Design of Rijndael: AES – The Advanced Encryption Standard. Springer.

Roman, R., et al. (2019). *Feistel-Based Lightweight Cryptography for IoT*. IEEE

ARM Limited. (2022). *Optimizing Feistel Ciphers for ARM Cortex-M*.

Differences

Biryukov, A., & Shamir, A. (2002). Cryptanalytic Time/Memory/Data Tradeoffs for Stream Ciphers. In ASIACRYPT 2002 (pp. 1–13). Springer.

Katz, J., & Lindell, Y. (2020). Introduction to Modern Cryptography (3rd ed.). CRC Press. ISBN: 978-0815354369.

Pineda Rodríguez, M. L. (2025). Arquitectura basada en tecnología Blockchain para sistemas de información de registro turístico [Tesis doctoral, Universidad del Norte]. Repositorio Universidad del Norte.

Saldaña Trejo, L. M., Gallegos García, G., & Aldeco Pérez, R. (2025). Protocolos criptográficos de consenso en Blockchain para el Internet de las cosas. Computación y Sistemas, 29(3).

Peixoto, B. M. S. (2025). *Blockchain e novas engines para a indústria 4.0* [Monografía de grado, Universidade Federal de Ouro Preto]. Repositorio UFOP.

ISSN: 2524-2121
RENIECYT-SECIHTI: 1702902

Castillo-Pacheco, César Marcelino & Rodríguez-Olivares, Noé Amir. [2025]. Cryptographic Algorithms for Industry 4.0: Analysis of the learning with errors method, Feistel networks, and linear feedback shift registers. ECORFAN-Journal Taiwan. 9[16]1-13: e1916113.
https://doi.org/10.35429/EJT.2025.9.16.1.1.13

ECORFAN-Journal Taiwan 9[16]1-5: e2916105
Article

Incorporation of Zinc Oxide Nanoparticles in Ceramic Materials

Incorporación de Nanopartículas de Óxido de Zinc en Materiales Cerámicos

Díaz-Silvestre, Sergio Enrique[a], Correa-Vazquez, Evanivaldo*[b], Canales-Patiño, Eduardo Luis[c] and Rico-Martinez, Alejandra Hikari[d]

[a] Universidad Tecnológica de Saltillo • LBH-9981-2024 • 0000-0002-6765-3415 • 334151
[b] Universidad Tecnológica de Saltillo • NRY-8691-2025 • 0009-0002-9377-2474 • 484939
[c] Universidad Tecnológica de Saltillo • MSW-0505-2025 • 0000-0002-4327-2714 • 636576
[d] Universidad Tecnológica de Saltillo • ODM-3060-2025 • 0009-0007-1218-0079 • 704920

SECIHTI classification:

Area: Engineering
Field: Technological Sciences
Discipline: Material Technology
Subdiscipline: Ceramic materials

https://doi.org/10.35429/EJT.2025.9.16.2.1.5
History of the article:
Received: June 25, 2025
Accepted: December 19, 2025

* ✉ [sdiaz@utsaltillo.edu.mx]

Abstract

Recently, the incorporation of nanomaterials into industry has increased. The diverse applications of these different nanocomposites have allowed for a wide variety of studies, and with them, their applications have grown. In general, zinc oxide nanocomposites are used for medical applications due to their antimicrobial properties; however, little is known about this material in ceramic applications. This work studies the incorporation of nanostructured materials, such as zinc oxide nanoparticles, into ceramic materials. An XRD and optical microscopy study was performed to ensure the presence of nanoparticles and their effect on the final product.

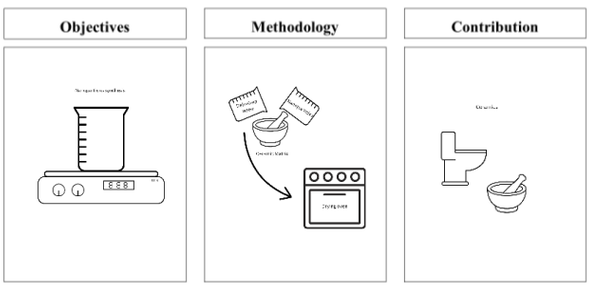

ZnO, Nanoparticles, ceramics

Resumen

Recientemente la incorporación de nanomateriales en la industria ha ido en aumento, diversas aplicaciones de los diferentes nanocompuestos han permitido una gran variedad estudios y con ello las aplicaciones han crecido. En general los nanocompuestos de óxido de zinc se utilizan para aplicaciones médicas por su capacidad antimicrobiana, sin embargo, poco se habla de este material en aplicaciones cerámicas. En este trabajo se estudia la incorporación de materiales nanoestructurados como lo es las nanopartículas de óxido de zinc en materiales cerámicos. Se realizó un estudio de DRX y microscopia óptica para asegurar la presencia de las nanopartículas y su efecto en el producto final.

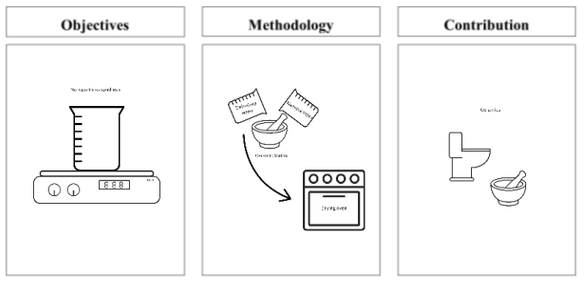

ZnO, Nanopartículas, cerámicos

Area: Promotion of frontier research and basic science in all fields of knowledge

Citation: Díaz-Silvestre, Sergio Enrique, Correa-Vazquez, Evanivaldo, Canales-Patiño, Eduardo Luis and Rico-Martinez, Alejandra Hikari. [2025]. Incorporation of Zinc Oxide Nanoparticles in Ceramic Materials. ECORFAN-Journal Taiwan. 9 [16]1-5: e2916105.

Introduction

Zinc oxide nanoparticles (ZnO) have found diverse applications in the ceramics industry due to their unique properties, including enhanced mechanical performance, antibacterial activity, improved thermal conductivity, and use in ceramic coatings, among others. These characteristics make ZnO nanoparticles highly attractive across various scientific fields (Esquivel, 2017; Carreón, 2020). Furthermore, it was reported to use different nanoparticles for the prevention of bacterial biofilms in titanium-based implants (Cajiao, 2025).

In particular, the incorporation of ZnO nanoparticles into ceramic matrices has demonstrated improvements in mechanical strength, thermal stability, and added functionalities such as ultraviolet (UV) radiation protection and antimicrobial capabilities (Surichaqui, 2013). The addition of ZnO can modify the microstructure of ceramics, enabling the development of novel applications in electronic devices, sensors, biomedical materials, and anticorrosive coatings (Bakhsheshi-Rad, 2017; Zhang, 2013; De La Rosa, 2022). In 2025, Quintanilla *et al* worked with epoxy compounds reinforced with silica nanoparticles (Quintanilla Cherrez, 2025). In addition, it was reported the use of silica nanoparticles at different filler contents, as a result of concentration, they improved stability and compressive strength (Conde Alania, 2025).

Moreover, the integration of ZnO nanoparticles into ceramics has shown significant effects in enhancing sintering behavior and reducing processing temperatures, thereby enabling more efficient and cost-effective production of high-performance ceramic materials. Research on the interaction mechanisms between ZnO nanoparticles and the ceramic matrix remains an active area of investigation, as precise control over these interactions is crucial for optimizing the final properties of the resulting materials (De la Garza, 2024).

In recent years, the incorporation of nanostructured materials into ceramics has increased significantly. In particular, zinc oxide nanoparticles have drawn considerable attention due to their antimicrobial properties. However, in other cases, different types of nanoparticles have been introduced into ceramic materials to enhance specific properties.

It should be noted that, despite the growing interest in nanoparticle-modified ceramics, ZnO nanoparticles have not been widely recognized for their potential to improve mechanical strength. Therefore, this study aims to explore the use of ZnO nanoparticles in ceramic materials for a purpose different from those previously reported. While previous studies have demonstrated that the incorporation of nanomaterials can enhance the mechanical resistance of ceramics, the mechanical reinforcement potential of ZnO nanoparticles remains underexplored. This work seeks to address this gap by investigating their role in improving the mechanical properties of ceramic composites.

Methodology

The zinc oxide (ZnO) nanoparticles used in this study were synthesized via the sol-gel method (Martinello, 2012). After synthesis, the ZnO nanoparticles were incorporated into a ceramic matrix by adding all materials simultaneously. Initially, all raw materials in powder form were placed into a ball mill crucible in the quantities specified in Table 1. The following materials were weighed:

Box 1

Table 1
Materials used in the ceramic formulatión

Feldespar
Calcium carbonate
Barium carbonate
Calcium silicate
Silica
Sodium tripolyphosphate
Zirconium silicate
Aluminum silicate
FT-1
ZnO nanoparticles

Created by the authors

The quantities were adjusted to prepare a total of 100 g of sample. The powders were then manually mixed using a spatula to achieve preliminary homogenization. Subsequently, 50 mL of deionized water was added to the mixture, along with one drop of a dispersant (flocculant) to control the suspension of solid particles, aiming to obtain a homogeneous and stable mixture. The slurry was then transferred to a ball mill and milled for 25 minutes to complete the homogenization process.

ISSN: 2524-2121
RENIECYT-SECIHTI: 1702902

Díaz-Silvestre, Sergio Enrique, Correa-Vazquez, Evanivaldo, Canales-Patiño, Eduardo Luis and Rico-Martinez, Alejandra Hikari. [2025]. Incorporation of Zinc Oxide Nanoparticles in Ceramic Materials. ECORFAN-Journal Taiwan. 9 [16]1-5: e2916105.
https://doi.org/10.35429/EJT.2025.9.16.2.1.5

The resulting liquid mixture was poured into an aluminum dish and placed in a drying oven to remove excess moisture. Once completely dried, the material was ground into a fine powder using a mortar and pestle. The powdered sample was then loaded into a pellet die and compacted into cylindrical pellets using a hydraulic press.

Finally, the green pellets were sintered in a muffle furnace at a predetermined temperature for 16 hours to obtain the final ceramic product. Figure 1 shows photographic images of the ceramic fabrication process.

Box 2

Figure 1
Images of the ceramic fabrication process

The quantities of the materials added were not specified because this is a collaborative project currently under development.

Results

X-ray diffraction (XRD) analysis also confirms the presence of zinc oxide nanoparticles. As shown in Figure 2, the diffraction peak at 37° appearing in the modified sample verifies the successful incorporation of the nanoparticles, consistent with the findings reported by Martinello (Martinello, 2012) and Colonia (Colonia, 2013). According to Martinello and Esquivel, the crystalline structure exhibited by the nanoparticles corresponds to the wurtzite phase.

Box 3

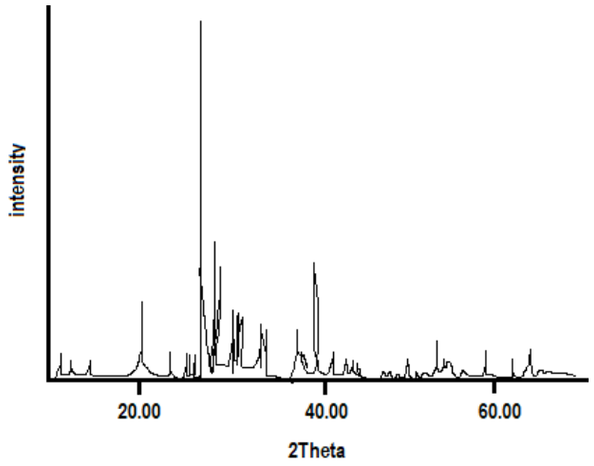

Figure 2
XRD patterns obtained for the unmodified sample and the sample incorporating ZnO nanoparticles
Source: [Origin 2018]

Ceramic product fabrication

The results after the sintering process show good densification of the material and adequate mechanical strength for ceramic coatings. The properties of zinc oxide nanoparticles are expected to enable the dispersion and reflection of ultraviolet (UV) radiation.

The incorporation of nanomaterials into the ceramic matrix was successful. As observed in the micrographs, the modified ceramic exhibits a surface with finer cracks, indicating a reduced grain size. This refinement suggests an improvement in mechanical strength. Figure 3 presents the fabricated ceramic samples, comparing the unmodified material (without nanoparticle addition) with the modified ceramic containing ZnO nanoparticles.

Box 4

Figure 3
Ceramic materials fabricated without modification (left side) and modified (right side) with the incorporation of ZnO nanoparticles using optical microscope
Created by the authors

ISSN: 2524-2121
RENIECYT-SECIHTI: 1702902

Díaz-Silvestre, Sergio Enrique, Correa-Vazquez, Evanivaldo, Canales-Patiño, Eduardo Luis and Rico-Martinez, Alejandra Hikari. [2025]. Incorporation of Zinc Oxide Nanoparticles in Ceramic Materials. ECORFAN-Journal Taiwan. 9 [16]1-5: e2916105.
https://doi.org/10.35429/EJT.2025.9.16.2.1.5

(De la Garza, 2024) reports in their study that porosity has a direct impact on the properties of ceramic tiles, concluding that the addition of ceramic oxide nanoparticles significantly reduces porosity in ceramic tiles. In another study, the incorporation of nanomaterials was shown to enhance the physical, mechanical, thermal and thermo-mechanical properties of refractory materials, depending on the concentration range and type of nanomaterial used (Carreón, 2020).

The study with other nanoparticles such as silica oxide as reinforcement demonstrated that they improve mechanical properties, therefore it is considered that the use of zinc oxide nanoparticles can improve mechanical properties in addition to contributing as a bacteria inhibitor on surfaces. (Quintanilla Cherrez, 2025), (Conde Alania, 2025).

The fabricated ceramic material was analyzed via micrographs. As shown in Figure 4, three optical microscope images reveal surface differences between the samples. In the unmodified material, small edge features are visible, which may indicate microcracks. In contrast, these features are not observed in the modified sample.

Although the modified sample appears to exhibit scratches that could be mistaken for fractures, these are artifacts resulting from surface scraping performed to reduce light reflection, as the modified material exhibited higher whiteness.

Box 5

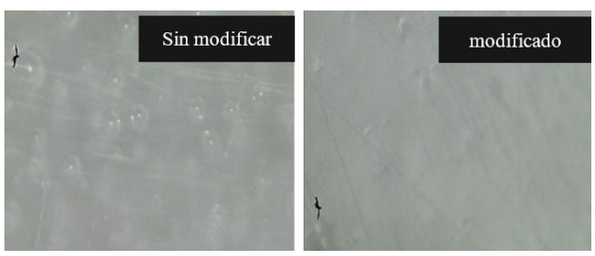

Figure 4
Micrographs of the unmodified ceramic material and the ceramic modified with ZnO nanoparticles. Image taken from the Quasar Qm 33 Science microscope

Conclusions

The incorporation of ZnO nanoparticles was successfully achieved and carried out without complications during the mixing process.

The addition of ZnO nanoparticles has the potential to increase the hardness and abrasion resistance of the ceramic coating, enhancing its durability and resistance to wear — findings that are consistent with previous literature regarding the influence of nanoparticle morphology. As observed in this study, the surface appearance of the modified ceramic is promising for application in the ceramic industry. However, further mechanical strength tests are required to confirm the improved performance of the modified material, as microstructural analysis revealed a reduction in crack formation, suggesting enhanced mechanical integrity.

Declarations

Conflict of interest

The authors declare no interest conflict. They have no known competing financial interests or personal relationships that could have appeared to influence the article reported in this article.

Author contribution

Evanivaldo Correa Vazquez: Contributed to investigation, material synthesis, and writing – original draft.

Sergio Enrique Díaz Silvestre: Contributed to conceptualization, project administration, writing – review & editing.

Eduardo Canales Patiño: Contributed to methodology, data analysis, and interpretation of results.

Alejandra Hikari Rico Marinez: Contributed to conceptualization and validation of results.

Availability of data and materials

Further information regarding the data is available upon request. Please contact the corresponding author for inquiries.

Funding

This work was supported by the Universidad Tecnológica de Saltillo.

ISSN: 2524-2121
RENIECYT-SECIHTI: 1702902

Díaz-Silvestre, Sergio Enrique, Correa-Vazquez, Evanivaldo, Canales-Patiño, Eduardo Luis and Rico-Martinez, Alejandra Hikari. [2025]. Incorporation of Zinc Oxide Nanoparticles in Ceramic Materials. ECORFAN-Journal Taiwan. 9 [16]1-5: e2916105.
https://doi.org/10.35429/EJT.2025.9.16.2.1.5

Acknowledgements

The authors thank Ing. Fernando Molina for his support in the preparation of the ceramic materials.

Abbreviations

Zno	Zinc oxide
XRD	X-ray Diffraction

References

Antecedents

H. R. Bakhsheshi-Rad E. Hamzah A.F. Ismail M. Aziz M. Kasiri-Asgarani E. Akbari S. Jabbarzare A. Najafinezhad Z. Hadisi. (2017). Synthesis of a novel nanostructured zinc oxide/baghdadite coating on Mg alloy for biomedical application: In-vitro degradation behavior and antibacterial activities. Ceramics International 43(17), 14842–14850.

Roberto Colonia, Vanessa C. Martínez, José L. Solís, Mónica M. Gómez. (2013). Síntesis de nanopartículas de ZnO2 empleando ultrasonido: caracterización estructural y morfológica para aplicaciones bactericidas. Revista de la Sociedad Química del Perú, 79(2), 126-135.

Y. Zhang T.R. Nayak H. Hong W. Cai. (2013). Biomedical Applications of Zinc oxide Nanomaterials. Current Molecular Medicine, 13(10), 1633-16–45.

Cajiao Checchin, Valentina Chiara. (2025). Desarrollo de nanoestructuras de óxido de titanio y nanopartículas/nanopelículas para la prevención de la formación de biofilms bacterianos sobre materiales implantables de base titanio. Tesis de doctorado. Universidad Nacional de La Plata

Basics

Bruna Martinello Savi, Larissa Rodrigues, Adriano Michael Bernardin. (2012). Síntesis de Nanopartículas de ZnO por el Proceso SOL-GEL. En QUALICER (Ed.), Qualicer 12.

Luis Alejandro Esquivel Rodríguez, María Blanca Nieves Cancino González. (2017). Estudio de las propiedades antimicrobianas de nanopartículas de ZnO y ZnO/Ag sintetizadas por el método de reacción en microemulsión" [Tesis de maestría, Centro de Investigación en Materiales Avanzados S. C.].

Supports

De La Garza, D. A. A. (2024). Efecto de la Adición de Nanopartículas Cerámicas en la Microestructura y Propiedades de Baldosas Cerámicas [Tesis de Doctorado, Universidad Autónoma de Nuevo León].

Surichaqui, R. C. C. (2013). Síntesis y Caracterización de nanopartículas de ZnO2 y su actividad antimicrobiana [Tesis de licenciatura, Universidad Nacional de Ingeniería].

Differences

De La Rosa-Reta Héctor Zermeño-González Magdalena Galindo-Guzmán, A. P. G.-G. M. F.-H. C. V. (2022). Síntesis química de nanopartículas de óxido de zinc y su evaluación en plántulas de Lactuca sativa. Revista Mexicana de Ciencias Agrícolas, 13(28), 299-308.

Discussions

Marco Vinicio Carrión V. & Fernanda Pilaquinga F. (2 de junio 2020). Nanotecnología Aplicada en Materiales Refractarios: Una Revisión. InfoANALÍTICA, 8(2), 21–44.

Quintanilla Cherrez, A. D. (2025). Caracterización mecánica de materiales compuestos de matriz epóxica reforzados con partículas a base de dióxido de silicio: componente A: caracterización mecánica de materiales compuestos de matriz epóxica reforzados con nanopartículas de sílice. 85 páginas. Quito :EPN.

Conde Alania, E. S., & Ñañez Saldaña, D. I. (2025). Efecto de la aplicación de nanopartículas de óxido de silicio como filler en las propiedades físicas y mecánicas de mezclas asfálticas frías Huancayo 2024. [Tesis de licenciatura, Universidad Continental]. Repositorio Institucional Continental.

ISSN: 2524-2121
RENIECYT-SECIHTI: 1702902

Díaz-Silvestre, Sergio Enrique, Correa-Vazquez, Evanivaldo, Canales-Patiño, Eduardo Luis and Rico-Martinez, Alejandra Hikari. [2025]. Incorporation of Zinc Oxide Nanoparticles in Ceramic Materials. ECORFAN-Journal Taiwan. 9 [16]1-5: e2916105.
https://doi.org/10.35429/EJT.2025.9.16.2.1.5

ECORFAN-Journal Taiwan 9[16]1-6: e3916106
Article

Ultrasound-assisted modification of MWCNTs with citric acid

Modificación asistida por ultrasonido de MWCNT con ácido cítrico

Díaz-Silvestre, Sergio Enrique*[a], Ramírez-Mendoza, Leticia Arizbeth[b] and Vazquez-Aguilar, Mario Leornardo[c]

[a] Universidad Tecnológica de Saltillo • LBH-9981-2024 • 0000-0002-6765-3415 • 334151
[b] Universidad Tecnológica de Coahuila • LBH 6830-2024 • 0009-0009-7093-0813 • 511901
[c] Universidad Tecnológica de Saltillo • MXJ-6634-2025 • 0009-0009-2421-9019 • 2104434

SECIHTI classification:

Area: Engineering
Field: Technological Sciences
Discipline: Material Technology
Subdiscipline: Properties of materials

https://doi.org/10.35429/EJT.2025.9.16.3.1.6
History of the article:
Received: June 23, 2025
Accepted: December 06, 2025

* ✉ [sdiaz@utsaltillo.edu.mx]

Abstract

Multi-walls carbon nanotubes (MWCNTs) were modified by ultrasound-assisted with citric acid (MWCNTs-citric acid). This modification was assisted by ultrasonic irradiation by 4 hours and 60°C. MWCNTs-citric acid were characterization by spectroscopy FT-IR (ATR) show the characteristics bands of carboxylic acids, and RAMAN spectroscopy shows the D and G bands to relation to sp^2 bonds, showing order and disorder structural. MWCNTs-citric acid contact angle value indicates the hydrophilic nature of nanostructure. MWCNTs-citric acid turbidity assay using different solvents is increase to MWCNTs. The measure of percentage of acid groups is 16.5%. The different characterizations are a probe of excellent superficial modification of MWCNT using ultrasonic energy.

Resumen

Los nanotubos de carbon de pared multiple (NTCPM) fueron modificados emplendo energía ultrasonica y ácido cítrico (NTCPM-ácido cítrico). Estas modificaciones se llevaron acabo por 4 horas a 60°C. Los NTCPM-ácido cítrico fueron caracterizados por FT-IR(ATR) mostrando bandas características del ácido carboxilíco, espectroscopia RAMAN mostrando las bandas D y G relacionadas con los enlaces sp^2, mostrando el orden y el desorden estructural. El valor de ángulo de contacto indicó la naturaleza hirdrofobíca de las nanoestrusturas. Los ensayos de turbidez indicaron que esta propiedad incrementa en los NTCPM-ácido cítrico. Las mediciones del % de grupos ácido fue del 16.5%. Las diferentes caracterizaciones son una prueba de la excelente modificación superficial de los NTCPM usando energía de ultrasonido.

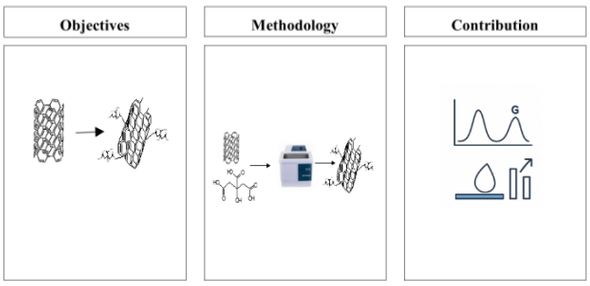

NTCPM, Ultrasound, Acid citric

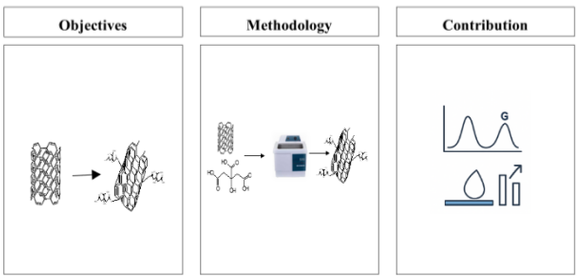

NTCPM, Ultrasonido, Ácido Cítrico

Area: Promotion of frontier research and basic science in all fields of knowledge

Citation: Díaz-Silvestre, Sergio Enrique, Ramírez-Mendoza, Leticia Arizbeth and Vazquez-Aguilar, Mario Leornardo. [2025]. Ultrasound-assisted modification of MWCNTs with citric acid. ECORFAN-Journal Taiwan. 9 [16]1-6: e3916106.

Introduction

Carbon nanotubes (CNTs) are allotropes of carbon such as diamond, graphite and fullerenes; which are presents in 1991 by Sumio Iijima, when he was worked in electronic microscopic showed tubular molecules (Iijima, 1991). CNTs have a structure with carbon atoms in hexagons and pentagons and sp^2 hybridization. Nanotubes are classified as simple-walls (SWCNTs) or multi-walls carbon nanotubes (MWCNTs), formed by single or multiple layers of graphene rolled up into a seamless tube. Since discovery of these nanostructures, multiple researches are focused in different research areas because exceptionally high material properties such as electrical and thermal conductivity, strength, stiffness, and toughness (Maubert *et al*., 2009).

MWCNTs showed several applications and technological solutions in different areas like automotive industry, optoelectronic, medicine, and water treatment. However, the major problem in several applications is the poor dispersion and solubility of nanomaterials of carbon. MWCNTs superficial modification might to help and change the poor dispersion. Several ways to performed superficial modification by covalent and not covalent bond of functional groups and molecules are reported (Sujata *et al*., 2013)

These modifications are accompanied by "green" modification methods. In the global effort to reduce hazardous waste generated by industry, the green chemistry philosophy is integrating and re-designed processes. Green chemistry bases in 12 fundamental principles. These principles are a guide in minimizing the use of unsafe reagents and maximizing the efficiency of chemical processes. One of the most important principles is the sixth, Design for Energy Efficiency, which states that the energy requirements of chemical processes should be acknowledged for their environmental and economic impacts and should be minimized. The ultrasound is an alternative energy source that reduces reaction time, decrease reagents and solvents, and contributes to an efficient process (Li *et al*., 2009).

In the search of novel strategies of reaction process, the ultrasound is an excellent method to MWCNTs dispersion and energy activation in the superficial modifications of MWCNTs.

The literature reports several approaches to MWCNTs modification using H_2SO_4/HNO_3 and ultrasound and high temperature. Additionally, other oxidizing agents, such as stearic acid, H_2SO_4, and $KMnO_4$, have also been employed in ultrasound-assisted modifications of CNTs (Chen *et al*., 2005).

Actually, it´s proposed the use of novel methods less aggressive to add functional groups on MWCNTs. For example, the Sonochemistry in MWCNTs modifications with citric acid; an organic acid of natural source, which found it in several fruits such as lemon, orange, plum, etc. Citric acid is a carboxylic acid used in pharmaceutical, food and cosmetics products (Wang *et al*., 2006).

Sonochemistry is used to development chemistry bonds in nanometric particles. Literature reports showed the use of ultrasound to MWCNT dispersion and activation of chemistry bonds to promote the superficial modification (Xu *et al*., 2012). In this article, present the results about the superficial modification of MWCNT's with citric acid using ultrasound like alternative activation.

Methodology

Develop give the meaning of the variables in linear writing and important is the comparison of the used criteria.

Materials

MWCNTs industrial grade with 90% of purity, 20-50 nm of diameter, 5-15 μm of length and superficial area of 200 m^2/g were used. Citric acid of analytical grade (Faga Lab) is used.

Superficial modification of MWCNT's

A saturate solution of citric acid (20 g in 25 mL of distillate water) was prepared. Then adding MWCNTs (0.04 mg). Placed this mixture into an ultrasonic bath (Branson 5510, 20-50 kHz and 10-60 Kw/m^2 of intensity) at 60 °C by 4 hours. Finish time of sonication, the mixture was filtered and washed with distilled water several times. Finally, dried the MWCNTs were dried into a stove at 40 ºC for 24 hours.

ISSN: 2524-2121.
RENIECYT-SECIHT: 1702902

Díaz-Silvestre, Sergio Enrique, Ramírez-Mendoza, Leticia Arizbeth and Vazquez-Aguilar, Mario Leornardo. [2025]. Ultrasound-assisted modification of MWCNTs with citric acid. ECORFAN-Journal Taiwan. 9 [16]1-6: e3916106
https://doi.org/10.35429/EJT.2025.9.16.3.1.6

Spectroscopic characterization

Infrared using a spectrophotometer Perkin-Elmer GX00 with ATR (Attenuated Total Reflectance) dispositive and diamond tip performed spectroscopic characterization. The samples were analyzed in powder form without prior treatment, using 32 scans at room temperature within the 4000–600 cm^{-1} range (Skoog, 2008).

Raman studies were development in a spectrophotometer Micro Raman (RENISHAW), Neon laser of 633 nm of length with 40 seconds of integrations and 6% of potency. Deposited the Samples on holder and stick with double-face tape and not previous preparation (Ferrari & Robertson, 2000).

Contact angle determination

Samples were compacted to form tablets. Then added a drop of 100 to surface of sample and the angle contact between the sample tablets and measured the water drop. For these experiments, a Rame-Hart contact angle gonio meter (model 100-00) was used.

Turbidity determination

The turbidity was determined in the solvents water, ethyl acetate, methanol, and ethanol (polar) and hexane and petroleum ether (nonpolar). For this determination, 0.02 mg of the sample in 8 mL of solvent was used as well as a Hach model 2100P turbidimeter for determinations.

Determination of percentage of acid groups by titration

Acid groups determination was carried out to weight 0.00125 mg of sample and then was put into a Schlenk flask, added a mixture of 0.01 N of NaOH (5 mL) and NaCl (0.01 N). The flask was hermetic closed and stirred by 4 hours in nitrogen atmosphere. Then the sample is filtered and added 2 drops of phenolphthalein like indicator and titillated with solution of NaOH (0.01 N). Executed the experiments by triplicate (Boehm, 1994).

Results

FTIR (ATR)

The performed MWCNTs modification in mild conditions using citric acid under ultrasonic irradiation. First, to demonstrate the modification, FTIR (ATR) of sample of MWCNTs performed the characterization and MWCNTs modified with citric acid (MWCNTs-citric acid). Fig.1 shows FTIR (ATR) spectrum of MWCNTs unmodified. The expected spectrum of the nanostructure not exhibits important bands, which is due to only C-H bond present in the structure. In contrast, Fig. 2 shows the FTIR (ATR) of MWCNT-citric acid.

The spectrum of the MWCNTs-citric acid exhibits important IR bands. For example, the O-H stretching (2900 cm^{-1}), the C=O stretching (1700 cm^{-1}) and the O-C-H bending (1390 cm^{-1}). These IR bands are an important suggestion of the superficial modification of MWCNTs and the presence of carboxylic acid group of the citric acid. In conforming to literature reports, (Chen *et al*., 2005) reported a study about MWCNTs modification with citric acid promoted by ultrasound.

Box 1

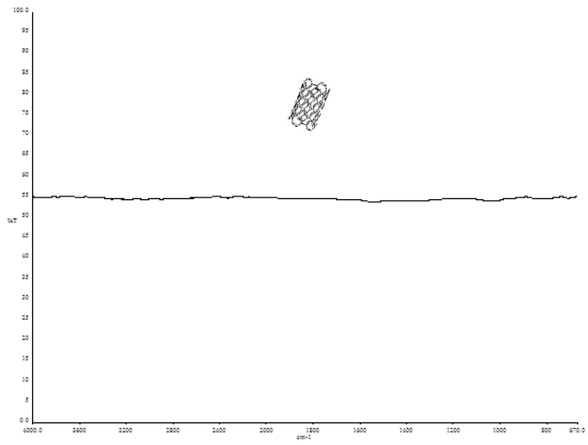

Figure 1
FT-IR (ATR) spectrum of MWCNTs
Source [in italic]

ISSN: 2524-2121.
RENIECYT-SECIHT: 1702902

Díaz-Silvestre, Sergio Enrique, Ramírez-Mendoza, Leticia Arizbeth and Vazquez-Aguilar, Mario Leornardo. [2025]. Ultrasound-assisted modification of MWCNTs with citric acid. ECORFAN-Journal Taiwan. 9 [16]1-6: e3916106
https://doi.org/10.35429/EJT.2025.9.16.3.1.6

Box 2

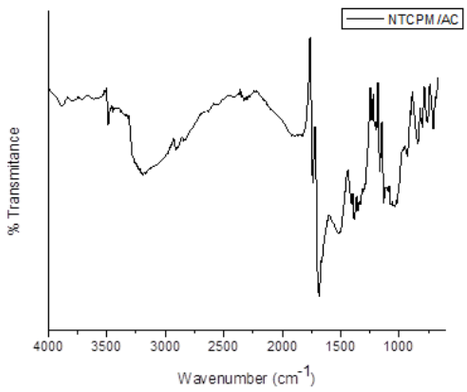

Figure 2

FT-IR (ATR) spectrum of MWCNTs-citric acid.

Source [in italic]

Raman characterization

In the Fig. 3 is present the Raman spectrum in which are observed the characteristic peaks in 1350 cm^{-1} (D band) and 1580 cm^{-1} (G band), to assigned to ordered and disordered structured of C-C layers respectively. Maiti and col. (2013) reported a study in which MWCNTs showed in 1331 cm^{-1} and 1604 cm^{-1} the D and G bands and assignation to C-C sp^2 hybridization (Maiti *et al.*, 2013).

Box 3

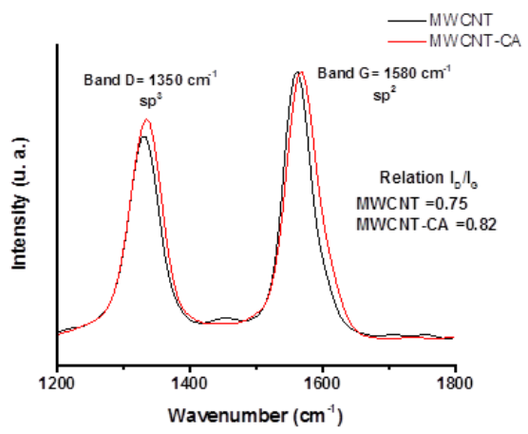

Figure 3

RAMAN spectra of MWCNTs and MWCNTs-citric acid

Source [in italic]

MWCNTs and MWCNTs-citric acid contact angle determination

Contact angle characterization determinate the hydrophilic or hydrophobic nature sample. In this case, the contact angle of MWCNTs and MWCNTs-citric acid determination was performed using a tablet of MWCNTs and MWCNTs-citric acid. The results show that MWCNTs formed a 90°C contact angle between the sample table and the drop of water. This is indicative that not exist interaction between MWCNTs and the water because the character hydrophobic of the nanostructure. In the other hand, the contact angle of MWCNTs-citric acid was 0 °C, because the sample tablet and the drop of water have an excellent interaction, Fig. 4. This behavior indicates that the modification of MWCNTs with citric acid was performed because the character on superficial nanostructure changes of hydrophobic to hydrophilic. The hydrophilic MWCNTs-citric acid is due to different interactions such as hydrogen bonds, Van der Waals and others.

Box 4

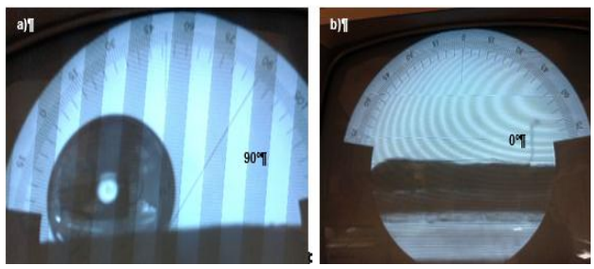

Figure 4

Contact angle of a) MWCNTs and b) MWCNTs-citric acid. The photographs show an angle of 90°C and 0°C respectively.

Source [in italic]

(Ellis & Ingham, 2012) reported that MWCNTs are hydrophobic nature, but with the superficial modification with acetic acid is changed to hydrophilic. This previous report shows that the modification of MWCNTs is possible using a green organic acid. For instance, the results in the contact angle determination are according with the literature.

Turbidity determination

Several technological applications of carbon nanostructures have not been developed due to their poor dispersion in various solvents and matrices.

ISSN: 2524-2121.
RENIECYT-SECIHT: 1702902

Díaz-Silvestre, Sergio Enrique, Ramírez-Mendoza, Leticia Arizbeth and Vazquez-Aguilar, Mario Leornardo. [2025]. Ultrasound-assisted modification of MWCNTs with citric acid. ECORFAN-Journal Taiwan. 9 [16]1-6: e3916106
https://doi.org/10.35429/EJT.2025.9.16.3.1.6

The surface modification of CNTs improved their dispersion, potentially addressing the issue of poor solubility. Turbidity determination is a physical analysis that shows if a nanomaterial is modified or unmodified to change this property. In the Fig. 5 are show the results in the turbidity assay, performed in different solvents; the MWCNTs-citric acid sample has a good dispersion because the light in the determination was not cross the MWCNTs-citric acid dispersion. The measure of turbidity in the solvents ethanol, pentanol and petroleum ether was not determinate because an excellent dispersion of the nanoparticles. In addition, MWCNTs-citric acid in ethyl acetate is different with the MWCNTs.

Box 5

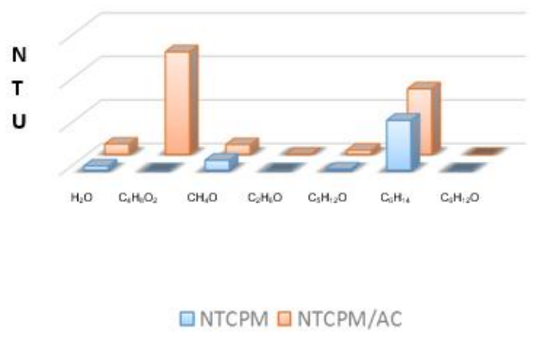

Figure 5
Turbidity determination in different solvents.
Source [in italic]

Acid groups quantification by titration

The determination of acid groups in MWCNTs-citric acid treated by titration in an assay by triplicate. The amount of acid groups in percentage of MWCNTs-citric acid was 16.5%. In according to literature, Cabello and col. reported a percentage of acid groups to MWCNTs-citric acid of 18.57%, using a treatment of 8 hours in the ultrasound irradiation (Cabello *et al*., 2014). In contrast, in the present work, MWCNT–citric acid composites were obtained through ultrasound-assisted treatment, requiring only 4 hours of irradiation.

MWCNTs covalent modification is possible due to the superficial defects in the nanostructure. It is important to mention that the percentage of acid groups should not be to high value because a total modification of the nanostructure may be to affect the MWCNTs properties.

Conclusions

In conclusion, citric acid superficial modification of MWCNTs performed by ultrasound assisted. FT-IR (ATR), Raman, contact angle determination, turbidity and measure of percentage of acid groups, characterized this modification. FT-IR (ATR) results show characteristic bands in MWCNTs-citric acid. Raman spectroscopy results show order and disorder in nanostructures. Turbidity results show that the dispersion of MWCNTs is poor in contrast with MWCNTs modified in different solvents such as ethanol, methanol, and petroleum ether. For polar solvents the electronegative atoms may be interact with the polar groups in MWCNTs-citric acid by hydrogen bond principally and the increase the dispersion. In the case of nonpolar solvents interacts with MWCNTs-citric acid by Van der Waals interactions. Contac angle in MWCNTs-citric acid is decrease in comparison with the MWCNTs. Finally, the percentage of acid groups is a measure of superficial modification of MWCNTs by covalent bond.

Declarations

Conflict of interest

The authors declare no interest conflict. They have no known competing financial interests or personal relationships that could have appeared to influence the article reported in this article.

Author contribution

Díaz-Silvestre, Sergio E: Contributed to investigation, writing –original draft and editing.

Ramirez-Mendoza, Leticia: Contributed to the project idea, research method and technique.

Vazquez-Aguilar Mario: Contributed to review amp; amp; editing.

Availability of data and materials

Further information regarding the data is available upon request. Please contact the corresponding author for inquiries.

Funding

This work was supported by the Universidad.

ISSN: 2524-2121.
RENIECYT-SECIHT: 1702902

Díaz-Silvestre, Sergio Enrique, Ramírez-Mendoza, Leticia Arizbeth and Vazquez-Aguilar, Mario Leornardo. [2025]. Ultrasound-assisted modification of MWCNTs with citric acid. ECORFAN-Journal Taiwan. 9 [16]1-6: e3916106
https://doi.org/10.35429/EJT.2025.9.16.3.1.6

Abbreviations

CNTs	Carbon nanotubes
FT-IR	Fourier-transform infrared spectroscopy
MWCNTs	Multi-walls carbon nanotubes

References

Antecedents

Iijima, S. (1991). Helical microtubules of graphitic carbon. Nature, 354(6348), 56–58.

Maubert, Ana; Soto, Laura; León, Ana; Flores, Jorge. (2009). Nanoturbos de carbono: La era de la nanotecnología. Razón y palabra, ISSN 1605-4806, Nº. 68, 2009.

Sujata Pramanik, Nilakshi Barua, & Alak K. Buragohain. (2013). Biofunctionalized Multiwalled Carbon Nanotube: A Reactive Component for the in Situ Polymerization of Hyperbranched PoIy(ester amide) and its Biophysico Interfacial Properties. The journal of physical chemistry, C. Nanomaterials and interfaces. 117.47

Basics

Skoog D.; Holler F.; Grouch S. "PRINCIPIOS DE ANÁLISIS INSTRUMENTAL". 6ª Ed., Cengage Learni, 2008,1063 ,90-103.

Ferrari, A. C., & Robertson, J. (2000). Interpretation of Raman spectra of disordered and amorphous carbon. Physical Review B, 61(20), 14095–14107.

Boehm, H. P. (1994). Some aspects of the surface chemistry of carbon blacks and other carbons. Carbon, 32(5), 759–769.

Supports

Qiuying Li, Yulu Ma, Chuang Mao, Chifei Wu. (2009). Grafting modification and structural degradation of multi-walled carbon nanotubes under the effect of ultrasonics sonochemistry. Ultrasonics Sonochemistry. 16. 752-757

C.S. Chen, X.H. Chen, L.S. Xu, Z. Yang, W.H. Li. 2005. Modification of multi-walled carbon nanotubes with fatty acid and their tribological properties as lubricant additive. Carbon. 43.8.1660-1666

Wang, Y.; Iqbal, Z.; Mitra, S. 2006. Rapidly Functionalized, Water-Dispersed Carbon Nanotubes at High Concentration. Journal of the American Chemical Society. 128 (1), 95-99

Yihui Xu, Qifang Li, Da Sun, Wenjing Zhang, and Guang-Xin Chen. (2012). A Strategy To Functionalize the Carbon Nanotubes and the Nanocomposites Based on Poly(l-lactide). Industrial & Engineering Chemistry Research. *51* (42), 13648-13654

Differences

Cabello J.; Sáenz A.; Pérez C.; López Ll.; Ávila C.; Valdés J.; Moran D. 2014. Modificación superficial de MWCNTs asistida por ultrasonido con ácido acético y ácido cítrico. Afinidad: Revista de química teórica y aplicada. 71.566.139-145

Discussions

Maiti, S., Shrivastava, N. K., Suin, S., & Khatua, B. B. (2013). Polystyrene/MWCNT/graphite nanoplate nanocomposites: efficient electromagnetic interference shielding material through graphite nanoplate-MWCNT-graphite nanoplate networking. *ACS applied materials & interfaces*, *5*(11), 4712–4724.

Ellis, B., & Ingham, M. (2006). Magnetic properties of multiwalled carbon nanotubes as a function of acid treatment. Journal of Magnetism and Magnetic Materials, 302(2), 378–381.

ISSN: 2524-2121.
RENIECYT-SECIHT: 1702902

Díaz-Silvestre, Sergio Enrique, Ramírez-Mendoza, Leticia Arizbeth and Vazquez-Aguilar, Mario Leornardo. [2025]. Ultrasound-assisted modification of MWCNTs with citric acid. ECORFAN-Journal Taiwan. 9 [16]1-6: e3916106
https://doi.org/10.35429/EJT.2025.9.16.3.1.6

ECORFAN-Journal Taiwan 9[16]1-11: e4916111
Article

Optical Sensing Technology for Capturing Vibrations in the Automotive Industry

Tecnología Sensorial Óptica para Capturar Vibraciones en la Industria Automotriz

Hernández-González, Josué Iván[a], Torres-Cedillo, Sergio Guillermo*[b], Hernández-Moreno, Hilario[c] and Cortés-Pérez, Jacinto[d]

[a] Centro Tecnológico Aragón, Universidad Nacional Autónoma de México • 0009-0003-5489-1611 • 1270905
[b] Centro Tecnológico Aragón, Universidad Nacional Autónoma de México • 0000-0002-3297-6409 • 229481
[c] SEPI-ESIME Ticomán, Instituto Politécnico Nacional • 0000-0002-4055-0037 • 40443
[d] Centro Tecnológico Aragón, Universidad Nacional Autónoma de México • 209116

SECIHTI classification:

Area: Engineering
Field: Engineering
Discipline: Mechanical Engineering
Subdiscipline: Automotive Industries

https://doi.org/10.35429/EJT.2025.9.16.4.1.11
History of the article:
Received: June 11, 2025
Accepted: December 10, 2025

* ✉ [sgtorres.c@gmail.com]

Abstract

Vibrational analysis in automotive rotodynamic systems faces technical limitations that hinder accurate fault diagnosis. This study proposes the use of fiber optic Bragg grating (FBG) sensors as an advanced alternative to conventional piezoelectric accelerometers, highlighting their electromagnetic immunity and distributed sensing capabilities. An experimental test bench was designed and instrumented with an FBG sensor array, and its functionality was validated through free vibration tests. Results reveal adequate sensitivity of the optical sensors in capturing structural deformations, with damping factor estimates consistent with those from accelerometers. This work constitutes a preliminary step toward comprehensive modal characterization, paving the way for industrial applications in predictive maintenance and structural monitoring.

Objectives	Methodology	Contribution
Evaluate FBG sensors as an alternative to accelerometers for vibrational analysis in automotive rotodynamic systems. 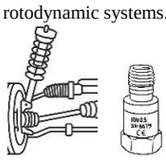	Test bench instrumented with FBG sensors and accelerometers. Validation through free vibration tests . 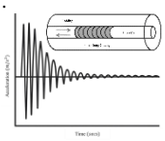	– New technologies applied to the automotive industry – Advances in monitoring and maintenance – Innovation in vehicle stability and safety. 

FBG, Capturing Vibrations, Automotive Industry

Resumen

El análisis vibracional en sistemas rotodinámicos automotrices enfrenta limitaciones técnicas que obstaculizan el diagnóstico preciso de fallas. Este estudio propone la implementación de sensores ópticos de fibra con rejillas de Bragg (FBG) como alternativa avanzada frente a los acelerómetros piezoeléctricos convencionales, destacando su inmunidad electromagnética y capacidad de monitoreo distribuido. Se diseñó e instrumentó un banco de pruebas experimental con un arreglo de sensores FBG, validando su funcionalidad mediante ensayos de vibración libre. Los resultados revelan una adecuada sensibilidad de los sensores ópticos para capturar deformaciones estructurales, con estimaciones del factor de amortiguamiento coherentes respecto a los acelerómetros. Este trabajo representa un primer avance hacia la caracterización modal integral del sistema, abriendo camino a aplicaciones industriales en mantenimiento predictivo y monitoreo estructural.

Objetivos	Metodología	Contribución
Evaluar sensores FBG como alternativa a acelerómetros para el análisis vibracional en sistemas rotodinámicos automotrices. 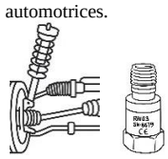	Banco de pruebas instrumentado con sensores FBG y acelerómetros. Validación mediante ensayos de vibración libre. 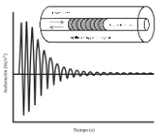	– Nuevas tecnologías aplicadas a la industria automotriz – Avances en monitoreo y mantenimiento – Innovación en estabilidad vehicular y seguridad. 

Fibra óptica con rejillas de Bragg, Captura de vibraciones, Industria Automotriz

Area: Promotion of frontier research and basic science in all fields of knowledge

Citation: Hernández-González, Josué Iván, Torres-Cedillo, Sergio Guillermo, Hernández-Moreno, Hilario and Cortés-Pérez, Jacinto. [2025]. Optical Sensing Technology for Capturing Vibrations in the Automotive Industry. ECORFAN-Journal Taiwan. 9 [16]1-11: e4916111.

1. Introduction

Since ancient times, vibrational analysis has been a highly relevant field of study in engineering, serving as a fundamental pillar to ensure the safety and stability of systems [*Au et al.*, 2008]. Such analysis requires the development of advanced measurement instruments that allow for precise evaluation of component performance, enabling timely fault detection and design optimization [T. Li *et al.*, 2017; Xu *et al.*, 2020].

In the automotive field, innovative proposals for the design of mechanical elements increasingly incorporate economic criteria in the optimization of rotodynamic systems. Currently, rotating shafts used in transmission systems and tire assemblies feature lighter and more compact configurations with reduced damping levels, adapting to increasingly restricted structural spaces [Emmanuel Augustine Etukudoh *et al.*, 2024]. During operation, the vehicle chassis serves as the primary medium for transmitting vibrations to the bodywork, originating from both the engine and the tire-surface interaction [Lim & Singh, 1991]. These vibrations pose a technological challenge for the automotive industry, which seeks to minimize their propagation to enhance user comfort and reduce maintenance costs simultaneously.

In this context, controlling vibration levels in rotating systems becomes essential, as phenomena such as imbalance and misalignment not only compromise the useful life of components but also vehicle safety as a whole [Hossain *et al.*, 2024]. Poor control of these conditions can lead to instability during driving and, in extreme cases, to fatal accidents.

Therefore, the study of the dynamic behavior of rotodynamic systems represents a growing interest both in academia and in the generation of practical solutions for the automotive industry, particularly in the design of new predictive maintenance schemes [Jazar, 2008].

Figure 1 illustrates the configuration of a suspension system, where key elements—such as the constant velocity joint and the steering knuckle—are affected by vibratory phenomena that induce misalignment and premature wear.

Among the most common indicators of wheel imbalance are perceptible vibrations in the steering wheel (which intensify with speed), global vibrations in the vehicle body, rear-end skidding sensations during cornering maneuvers, and abnormal tread wear patterns [Ledesma & Shih, 1999]. The causes of such imbalance include various manufacturing defects, improper tire mounting on the rim, irregularities in brake drums or discs, and uneven tire wear [Charles, 1943].

Box 1

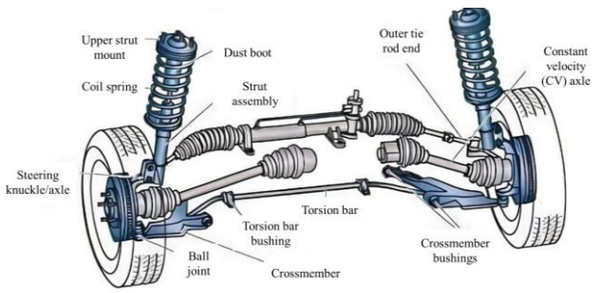

Figure 1
Automotive suspension system.
Source: [Jazar, 2008]

Imbalance in rotodynamic systems has driven the development of a wide range of diagnostic techniques, among which modal balancing and influence coefficient methods stand out [Jazar, 2008]. However, both approaches require the installation of trial masses and sensors directly on the rotor, which limits their applicability under real operating conditions due to space constraints and exposure to elevated temperatures [Randall, 2011]. In light of these limitations, the need has arisen to implement non-invasive inverse procedures for imbalance identification. These methods rely on prior knowledge of the chassis's modal parameters and the analysis of vibrational signals captured at the vehicle body to infer the dynamic state of the rotating system [Hossain *et al.*, 2024].

Within this context, an up-and-coming alternative lies in the development of experimental test benches designed to validate methodologies based on nonlinear inverse problems applied to automotive rotordynamics. These test benches serve as practical tools for the precise identification of mechanical faults in rotating systems through indirect diagnostic techniques [Vance *et al.*, 2010; Yang *et al.*, 2017].

ISSN: 2524-2121
RENIECYT-SECIHTI: 1702902

Hernández-González, Josué Iván, Torres-Cedillo, Sergio Guillermo, Hernández-Moreno, Hilario and Cortés-Pérez, Jacinto. [2025]. Optical Sensing Technology for Capturing Vibrations in the Automotive Industry. ECORFAN-Journal Taiwan. 9 [16]1-11: e4916111.
https://doi.org/10.35429/EJT.2025.9.16.4.1.11

Derived from this need, a representative test bench of a rotodynamic system was designed, capable of operating at speeds of up to 60 Hz. This bench is currently located at the Aragón Technology Center of the National Autonomous University of Mexico, as shown in Figure 2.

Box 2

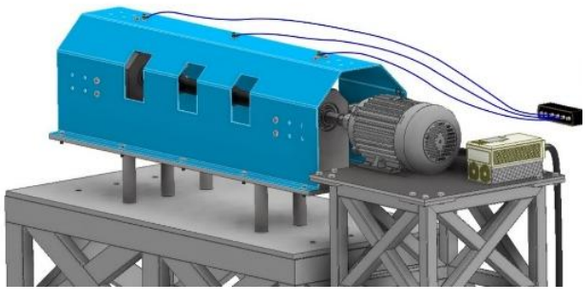

Figure 2
Experimental test bench.
Source: Own Elaboration

As background, the test bench was initially instrumented with piezoelectric accelerometer-type sensors, widely used in experimental rotordynamic analysis studies [T. Li *et al*., 2020]. However, such devices present inherent limitations in their operating principle: since they function with low-voltage signals, they are susceptible to environmental disturbances due to electromagnetic fields. This drawback is compounded by the requirement for complex cabling and electrical connections [T. Li *et al*., 2020; Xiong *et al*., 2021].

In light of these limitations, an alternative was identified in the implementation of fiber optic sensors based on Fiber Bragg Gratings (FBG), which have garnered increasing interest due to their high sensitivity, compact dimensions, and immunity to electromagnetic interference by virtue of utilizing light energy for operation [Hernández-Moreno *et al*., 2009b; Kim *et al*., 2022; K. Li *et al*., 2014]. Their operating principle, based on wavelength modulation, enables their installation at multiple sensing points along a single fiber, allowing for analysis through wavelength-division multiplexing interrogation techniques. This approach not only expands monitoring capabilities but also optimizes the efficiency of the measurement system by requiring only a single light source and a unique detection unit, thereby significantly reducing costs associated with the use of such instruments, known as optical interrogators [García *et al*., 2010; Hernández-Moreno *et al*., 2009a].

2. Theoretical Framework

Through a contemporary literature review based on primary sources, two particularly relevant approaches for the implementation of FBG sensors in dynamic applications have been identified. The first corresponds to the development of optical accelerometer-type sensors, as illustrated in Figure 3, whose operating principle is based on wavelength displacement. The second focuses on the construction of experimental setups specifically designed for the monitoring of engineering systems, as shown in Figure 4 [Hernández-González *et al*., 2023].

Box 3

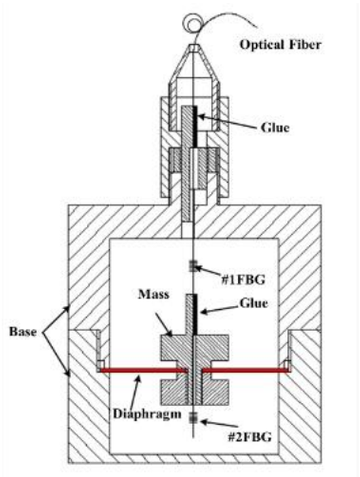

Figure 3
Optical accelerometer-type sensor.
Source [T. Li et al., 2017]

Box 4

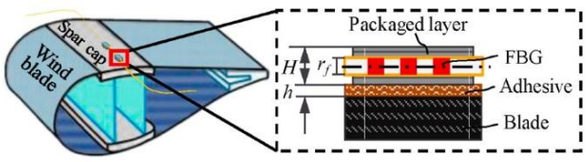

Figure 4
Experimental setup of FBG sensors.
Source [Javdani et al., 2016]

The essential distinction between the two application approaches lies in the number and distribution of analysis points. While an optical accelerometer-type sensor serves as a substitute for a conventional accelerometer, limiting its measurement to a specific point, experimental setups permit the installation of multiple sensors along a single fiber, thereby enabling the distributed characterization of the system under study.

ISSN: 2524-2121
RENIECYT-SECIHTI: 1702902

Hernández-González, Josué Iván, Torres-Cedillo, Sergio Guillermo, Hernández-Moreno, Hilario and Cortés-Pérez, Jacinto. [2025]. Optical Sensing Technology for Capturing Vibrations in the Automotive Industry. ECORFAN-Journal Taiwan. 9 [16]1-11: e4916111.
https://doi.org/10.35429/EJT.2025.9.16.4.1.11

Thus, due to the sensitive characteristics of Bragg gratings, any variation on the monitored surface—whether in terms of strain, temperature, or hydrostatic pressure—is directly reflected in the grating through a change in wavelength [García *et al*., 2010; Kim *et al.*, 2022].

The development of optical accelerometers remains an active field of innovation, aimed at improving sensitivity and design through adjustments in materials and geometries [K. Li *et al*., 2014]. In parallel, FBG experimental arrays are consolidating as a promising alternative for structural monitoring, as they allow distributed detection with minimal impact on the mechanical integrity of the structure since they can be adhered or integrated into the material [T. Li *et al.*, 2020]. Both approaches present advantages and limitations: optical accelerometers stand out for their versatility, while arrays offer a more comprehensive view, though requiring high precision in their installation.

In recent years, interest in FBG arrays has grown significantly, driven by advances in interrogation systems for monitoring, which has expanded their applicability in dynamic studies [Tozzetti *et al*., 2021]. Consequently, the choice between the two strategies must be based on the nature of the system and on technical, economic, and experimental feasibility criteria.

3. Experimental Design

Once the theoretical foundation was established, experimental design required determining the most suitable strategy for the implementation of FBG sensors. In this study, an experimental array of three sensors adhered to the surface of the test bench casing was chosen, based on the premise that phenomena occurring in the rotational shaft are transmitted through the bearings to the casing. This decision responds to the need for multiple analysis points in the bearing support zones—front, middle, and rear—recognized in the literature as critical positions for rotodynamic evaluation [Hou & Cao, 2019; Torres Cedillo & Bonello, 2016].

Although FBG-based optical accelerometers represent an up-and-coming alternative in vibrational contexts, their development entails significant investment of time and resources, in addition to being limited to instrumentation at a single point per sensor.

In contrast, arrays take advantage of the multiplexing capability of FBGs, facilitating simultaneous coverage of several points with a single optical interrogator. In this case, the choice was supported by the operational characteristics of the test bench, which reaches a speed of 60 Hz, and the availability of a si425 optical interrogator with a 250 Hz bandwidth, sufficient under the Nyquist-Shannon theorem for obtaining efficient data under dynamic conditions [Hernández-González *et al*., 2023; Preizler *et al*., 2017]. Thus, the array proposal responds not only to technical and economic efficiency but also to the experimental relevance of adapting FBG technology to the real context of the study.

Subsequently, the formal design of the FBG sensor array was carried out, which required defining both the materials and dimensions for experimental applications. The result was a design consisting of single-mode optical fiber coated with acrylate and polyamide, FC-APC connector, and three Bragg gratings with a physical length of 10 mm, staggered in 5 nm intervals (1535 nm, 1540 nm, and 1545 nm).

This configuration addresses the need to instrument critical areas of the test bench—both support bearings and the intermediate region between them. Due to the technological complexity involved in the manufacture of FBG arrays, particularly the precise inscription of gratings in the fiber, production was delegated to a specialized company capable of ensuring optical parameters such as reflectivity above 80%, a bandwidth of 0.20 nm, and a signal-to-noise ratio greater than 15 dB.

The installation process was carried out with maximum precision criteria, ensuring at all times the structural and functional integrity of the sensors during their installation. Figure 5 shows a top view of the experimental test bench, where the optical fiber sensor array was carefully integrated into the surface using epoxy adhesive.

To reinforce its protection, fiber sections not covered by gratings were coated with a transparent PVC layer, which also allowed the use of adhesive clips to limit axial displacement of the fiber without the need to perforate the test bench casing.

ISSN: 2524-2121
RENIECYT-SECIHTI: 1702902

Hernández-González, Josué Iván, Torres-Cedillo, Sergio Guillermo, Hernández-Moreno, Hilario and Cortés-Pérez, Jacinto. [2025]. Optical Sensing Technology for Capturing Vibrations in the Automotive Industry. ECORFAN-Journal Taiwan. 9 [16]1-11: e4916111.
https://doi.org/10.35429/EJT.2025.9.16.4.1.11

Box 5

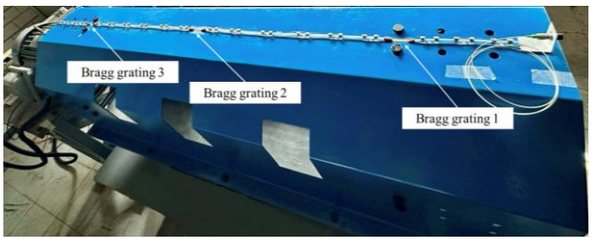

Figure 5
Optical fiber with Bragg gratings installed on an experimental test bench.
Source: Own Elaboration

4. Experimental Study

4.1 Considerations for Rotordynamic Study

In the field of applied rotordynamics, mechanical transmission systems and rolling assemblies in vehicles incorporate components whose vibrational response can be analyzed and understood through simplified configurations. Based on this premise, the developed experimental test bench is conceived as a scaled representation of the actual system, in which the shaft serves as the principal transmission element, the bearings act as supports conditioning the dynamic response, and the motor operates as the source of mechanical excitation [Lim & Singh, 1991].

This reduction to a fundamental shaft–bearing–motor scheme not only facilitates analysis but, from a rotordynamic standpoint, the casing enclosing the test bench preserves the most relevant phenomena associated with the dynamic coupling between the rotating elements and their supports [Lim & Singh, 1992; Vance *et al*., 2010].

Additionally, the experimental bench is capable of analogously emulating half of a rotating shaft in a real transmission system. This approach is justified by the symmetry of vibrational phenomena in longer shafts, whereby studying a representative section is sufficient to extrapolate the overall behavior. Consequently, this experimental simplification does not entail a loss of analytical rigor; rather, it serves as a methodological strategy that enhances the study of rotational dynamics while providing an suitable framework for the validation of analytical and numerical models under controlled conditions [Bugaru & Vasile, 2022; Zingoni, 2014].

4.2 Considerations for Vibrational Study

In this context, free vibration analysis constitutes the essential first stage in the dynamic characterization of a system, as it enables precise identification of natural frequencies and inherent vibration modes before subjecting the structure to external excitation. This procedure provides a reliable reference framework for understanding the intrinsic behavior of the system. It is indispensable for subsequent analysis of forced vibration, in which the motor directly imposes excitation frequency onto the rotating shaft [Feng *et al*., 1998].

It is worth noting that the present work addresses exclusively the introduction to free vibration analysis, to establish the foundation for future, more in-depth investigations that include the study of forced vibration.

Free vibration manifests when a system, after being initially disturbed, oscillates without the action of additional external forces [Beards, 1995]. Its behavior may be classified as stable or unstable: in the former, the presence of positive damping gradually attenuates the oscillation; in the latter, negative damping leads to a self-excitation phenomenon in which amplitude grows progressively until the system's stability is compromised [Lim & Singh, 1991]. In both scenarios, the amplificated vibratory response occurs at one of the natural frequencies of the rotating system, underscoring its close relationship with the fundamental modes of structural dynamics [Matsushita *et al*., 2017].

The parameters that define this behavior—principally the natural frequency and damping ratio—not only allow for the characterization of the vibratory system but also enable the anticipation of resonance scenarios under forced excitation conditions. In particular, the critical speed associated with imbalance-induced vibration is directly related to the shaft's natural frequency, highlighting the importance of precise analysis under free conditions [Matsushita *et al*., 2017].

The transient response generated by a sudden disturbance, such as an impact, constitutes another essential aspect of free vibration analysis.

ISSN: 2524-2121
RENIECYT-SECIHTI: 1702902

Hernández-González, Josué Iván, Torres-Cedillo, Sergio Guillermo, Hernández-Moreno, Hilario and Cortés-Pérez, Jacinto. [2025]. Optical Sensing Technology for Capturing Vibrations in the Automotive Industry. ECORFAN-Journal Taiwan. 9 [16]1-11: e4916111.
https://doi.org/10.35429/EJT.2025.9.16.4.1.11

This stimulus introduces energy into the system, triggering vibratory motion whose evolution depends solely on the system's intrinsic properties—mass, stiffness, and damping—and not on the magnitude of the impact [Beards, 1996; Szeidl & Kiss, 2020]. for its experimental characterization, techniques such as impact hammer testing are employed, providing a controlled environment for system excitation and enabling the identification of multiple vibration modes.

Through the analysis of the resulting response, it becomes possible to estimate the damping ratio and determine the natural frequencies associated with each mode, delivering essential information for the validation of dynamic models and the prediction of critical operational behaviours [Doebling *et al*., 1996].

4.3 Free Vibration Testing

As a first step, this study aims to establish a correlation between the data provided by FBG sensors and accelerometers, given that the measurements obtained from each technology are inherently not directly equivalent. Due to their sensitivity characteristics, the Bragg gratings installed on the experimental test bench are primarily responsive to strain variations, neglecting effects from temperature and hydrostatic pressure, whereas accelerometers quantify acceleration.

Consequently, a comparative framework is necessary to verify the consistency and reliability of the results obtained from both sensing techniques.

In this regard, the present study seeks to establish an initial quantitative framework concerning the energy dissipation behavior of the system through the damping ratio. However, this preliminary approach does not exhaust the dynamic characterization of the test bench, as the precise identification of the natural frequencies and the corresponding vibration modes remains pending. Such a modal analysis—excluded from this work due to temporal constraints—emerges as an essential step to complement the damping information obtained and to support the validation of FBG sensors in rotordynamic.

Box 6

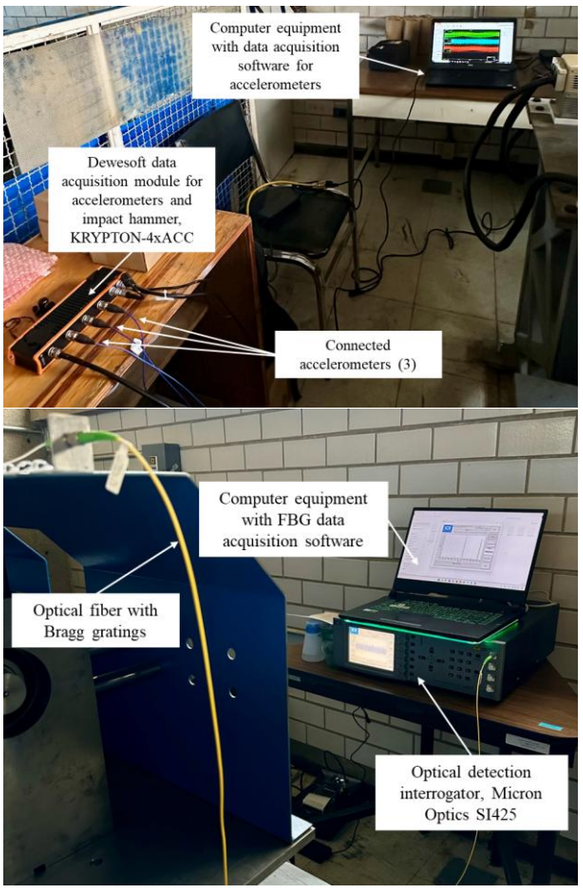

Figure 6
Data acquisition system for experimental testing.
Source: Own Elaboration

To conduct the free vibration study, the monitoring instrumentation depicted in Figure 6 was employed. This setup integrates acquisition devices based on accelerometers and FBG sensors, installed on the outer casing of the test bench. The system includes an optical interrogator model si425, a KRYPTON-4xACC acquisition module responsible for recording both the force exerted by the impact hammer and the accelerometer signals, and dedicated computing systems for data collection.

Although this study does not evaluate reproducibility or impact accuracy, its exploratory approach is valuable in early research stages, allowing the collection of preliminary results to formulate hypotheses, identify limitations, and establish methodological guidelines for future investigations. Practically, each test involved three impacts on the test bench casing near predefined monitoring points (Figure 7), strategically chosen to maximize vibratory response capture in key areas.

ISSN: 2524-2121
RENIECYT-SECIHTI: 1702902

Hernández-González, Josué Iván, Torres-Cedillo, Sergio Guillermo, Hernández-Moreno, Hilario and Cortés-Pérez, Jacinto. [2025]. Optical Sensing Technology for Capturing Vibrations in the Automotive Industry. ECORFAN-Journal Taiwan. 9 [16]1-11: e4916111.
https://doi.org/10.35429/EJT.2025.9.16.4.1.11

Box 7

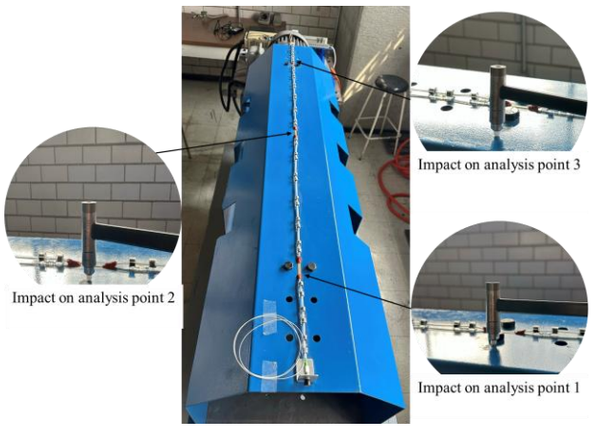

Figure 7
Impact points for free vibration tests.
Source: Own Elaboration

5. Results

As a representative example of the results obtained, Figures 8 and 9 present the experimental records. These include both the force exerted by the impact hammer [N] and the responses of the optical FBG sensors and the accelerometers, expressed in their original acquisition units—wavelength and acceleration, respectively. This test enables a morphological comparison between the responses of both types of sensors to the same dynamic stimulus, offering a reference framework for the comprehensive characterization of free vibration behavior in the system.

Box 8

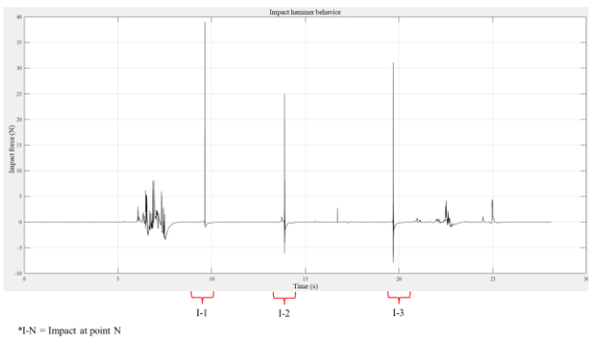

Figure 8
Behavior of the impact hammer.
Source: Own Elaboration

Box 9

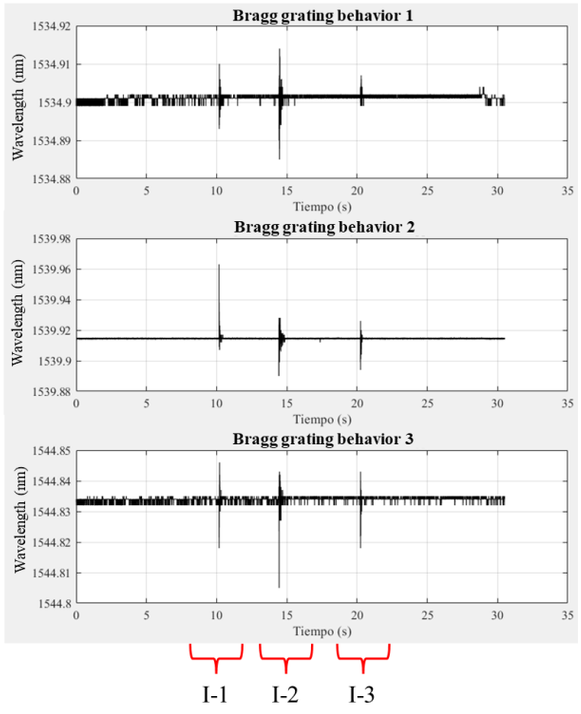

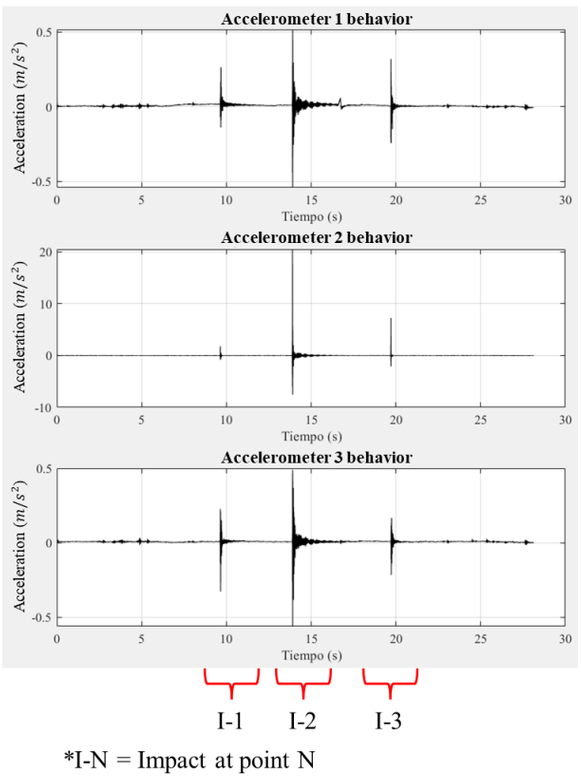

Figure 9
Behavior of the sensors during the free vibration test.
Source: Own Elaboration

ISSN: 2524-2121
RENIECYT-SECIHTI: 1702902

Hernández-González, Josué Iván, Torres-Cedillo, Sergio Guillermo, Hernández-Moreno, Hilario and Cortés-Pérez, Jacinto. [2025]. Optical Sensing Technology for Capturing Vibrations in the Automotive Industry. ECORFAN-Journal Taiwan. 9 [16]1-11: e4916111.
https://doi.org/10.35429/EJT.2025.9.16.4.1.11

To enhance the analytical approach to the study of FBG, the strain captured by each grating is first determined using Equation 1, which is expressed as a function of the relative wavelength shift $\Delta\lambda_B/\lambda_B$ —where λ_B is the central wavelength of the Bragg grating and $\Delta\lambda_B$ is the wavelength variation induced by mechanical strain—and the photoelastic coefficient of the optical fiber core material, $p_e = 0.219355$ (an estimated value for silica fibers) [Hernández-Moreno *et al*., 2009b].

Thus, for practical purposes in data processing, the responses of the FBG optical sensors and accelerometers will be considered in terms of strain and acceleration, respectively.

$$\varepsilon = \frac{1}{(1-p_e)}\frac{\Delta\lambda_B}{\lambda_B} \quad [1]$$

The data processing applied to the free vibration study was based on the use of the logarithmic decrement and the damping ratio, calculated through Equations 2 and 3 [Matsushita *et al*., 2017]. The former allows the logarithmic decrement δ to be determined from the amplitude ratio a_n over a defined number of complete cycles N_c, while the latter yields the corresponding damping ratio ζ.

$$\delta = \frac{1}{N_c} ln\left(\frac{a_n}{a_{n+N}}\right) \quad [2]$$

$$\zeta = \frac{\delta}{\sqrt{(2\pi)^2+\delta^2}} \quad [3]$$

Based on the impact responses recorded by both the FBG sensors and the accelerometers on the experimental bench, the maximum amplitudes of each signal in the time domain were identified, and the cycles used in the calculation were determined. This made it possible to accurately estimate the logarithmic decrement and, consequently, the damping ratio.

Figure 10 illustrates, as an example, the response of the FBG sensors and accelerometers to an impact applied at point 2 (center) of the test bench, highlighting the initial amplitude (P_{Max}) and final amplitude (P_{Fn}) used in the calculation over a total of 10 cycles.

Box 10

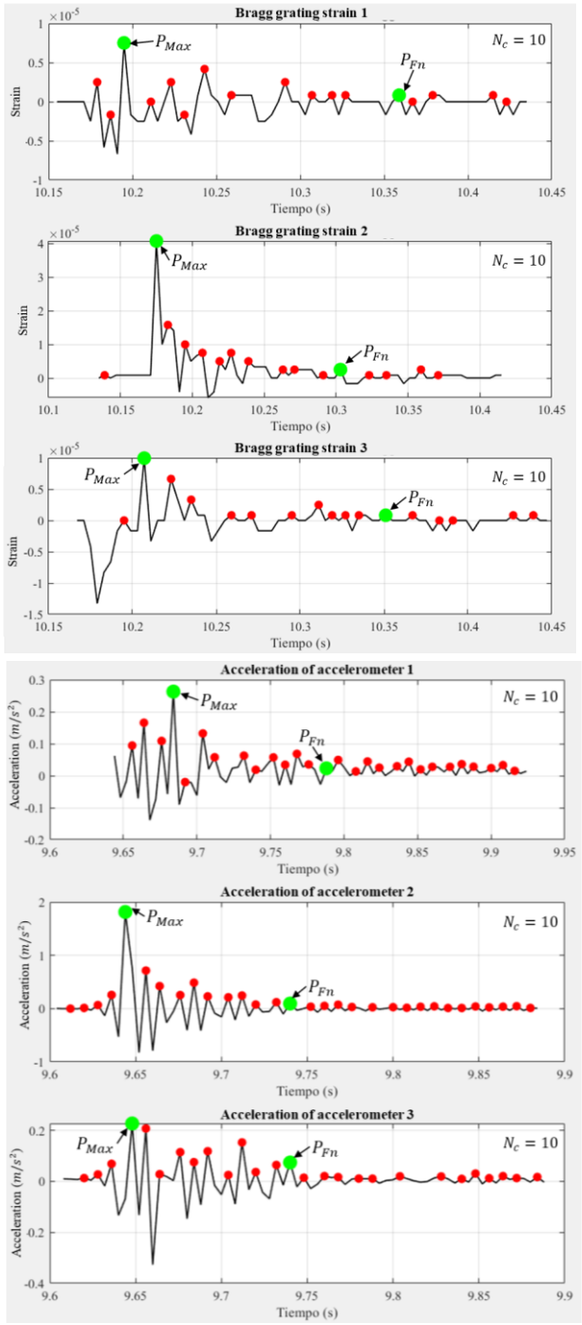

Figure 10
Sensor response at each analysis point.
Source: Own Elaboration

Based on the results obtained from a total of 27 experimental trials—individualized by sensor type and impact location—the equivalent damping ratio for an average force at each analyzed point, along with the corresponding value of the logarithmic decrement, is summarized in Table 1.

ISSN: 2524-2121
RENIECYT-SECIHTI: 1702902

Hernández-González, Josué Iván, Torres-Cedillo, Sergio Guillermo, Hernández-Moreno, Hilario and Cortés-Pérez, Jacinto. [2025]. Optical Sensing Technology for Capturing Vibrations in the Automotive Industry. ECORFAN-Journal Taiwan. 9 [16]1-11: e4916111.
https://doi.org/10.35429/EJT.2025.9.16.4.1.11

Box 11

Table 1
Equivalent damping factors

Test	Sensor	Average impact force	δ	ζ
Impact on analysis point 1	Bragg grating 1	37.8006	0.2042	0.0325
	Accelerometer 1		0.2981	0.0474
Impact on analysis point 2	Bragg grating 2	34.2359	0.2095	0.0334
	Accelerometer 2		0.4279	0.0679
Impact on analysis point 3	Bragg grating 3	40.1864	0.2119	0.0337
	Accelerometer 3		0.2809	0.0446

Source: Own Elaboration

5.1 Discussion of results

The Bragg grating sensors recorded consistent vibration patterns among themselves, with slight variations in amplitude and frequency attributable to their relative position with respect to the impact point. In contrast, the accelerometers exhibited a more uniform and stable response, likely associated with their higher sensitivity and greater precision in measuring accelerations compared to strain detection. These differences are reflected in the estimation of the damping ratio, as summarized in Table 1.

A more pronounced attenuation was observed in the signals from the Bragg gratings, an effect attributable both to a combination of structural damping factors and to potential interferences resulting from their direct installation on the surface of the test bench. In the comparison between the two sensing systems, the accelerometers systematically reported higher damping ratios at each analysis point.

Globally, the estimated damping ratios confirm that the rotodynamic system under study exhibits low energy dissipation, characteristic of configurations with high stiffness and minimal damping. This behavior is consistent with structures designed to ensure vibratory stability and minimize energy losses per cycle [Beards, 1996].

6. Conclusion

The results confirm that Bragg grating sensors represent a viable alternative for detecting vibrational responses in rotodynamic systems, showing overall agreement with accelerometers, albeit with variations inherent to the nature of each sensing technique.

Nonetheless, the estimation of the damping ratio constitutes only a preliminary step; a precise determination of the natural frequencies associated with the vibration modes of the experimental bench remains pending. This future modal analysis will enable a more comprehensive characterization of structural dynamics. It will consolidate the implementation of FBG sensors as a robust tool in rotodynamic instrumentation, with strong potential for specialized scientific and industrial applications.

Industrial implications include structural health monitoring, performance optimization, and enhanced operational safety. At the same time, in the academic domain, the integration of optical technologies promotes the development of lighter, more compact, and more reliable systems. Furthermore, this technology paves the way toward intelligent diagnostics in predictive maintenance, reinforcing its relevance in sectors such as the automotive industry.

Declarations

Conflict of interest

The authors declare no conflict. They have no known competing financial interests or personal relationships that could have appeared to influence the article reported in this article.

Author contribution

Hernández-Gonzalez, Josué Iván: Contributed to the overall conception of the project, as well as to the methodology, research techniques, experimental development and data analysis.

Torres-Cedillo, Sergio Guillermo: Contributed to the overall conception of the project, experimental development and data analysis.

Hernández-Moreno Hilario: Contributed to the overall conception of the project, the planning of the experimental design, and the analysis of results.

Cortés-Pérez, Jacinto: Contributed to the execution of experimental tests and the experimental setup.

Funding

The research did not receive any funding.

ISSN: 2524-2121
RENIECYT-SECIHTI: 1702902

Hernández-González, Josué Iván, Torres-Cedillo, Sergio Guillermo, Hernández-Moreno, Hilario and Cortés-Pérez, Jacinto. [2025]. Optical Sensing Technology for Capturing Vibrations in the Automotive Industry. ECORFAN-Journal Taiwan. 9 [16]1-11: e4916111.
https://doi.org/10.35429/EJT.2025.9.16.4.1.11

Acknowledgements

This research was conducted with the support of the "Investigadoras e Investigadores COMECyT 2025" Program. Acknowledgment is also given to DGAPA-PAPIIT through project number IN110923.

Abbreviations

FBG	Fiber Bragg Grating
N	Newtons
nn	Nanometers
nm	Millimeters
dB	Decibels
Hz	Hertz

References

Antecedents

Hernández-González, J. I., Torres-Cedillo, S. G., Hernández-Moreno, H., & Cortés-Pérez, J. [2023]. Identification of an instrumental proposal based on fiber optic sensors of the Bragg grating type for implementation in an experimental platform for dynamic analysis. ECORFAN Journal Taiwan, 7–15.

Hernández-Moreno, H., Collombet, F., Douchin, B., Choqueuse, D., Davies, P., & González Velázquez, J. L. [2009a]. Entire Life Time Monitoring of Filament Wound Composite Cylinders Using Bragg Grating Sensors: I. Adapted Tooling and Instrumented Specimen. Applied Composite Materials, 16(3), 173–182.

Hernández-Moreno, H., Collombet, F., Douchin, B., Choqueuse, D., Davies, P., & González Velázquez, J. L. [2009b]. Entire Life Time Monitoring of Filament Wound Composite Cylinders Using Bragg Grating Sensors: II. Process Monitoring. Applied Composite Materials, 16(4), 197–209.

Torres Cedillo, S. G., & Bonello, P. [2016]. An equivalent unbalance identification method for the balancing of nonlinear squeeze-film damped rotordynamic systems. Journal of Sound and Vibration, 360, 53–73.

Basics

Au, H. Y., Khijwania, S. K., & Tam, H. Y. [2008]. Fiber Bragg grating based accelerometer. D. D. Sampson, Ed.; p. 70042S.

Beards, C. F. [1995]. Engineering Vibration Analysis with Application to Control Systems. Elsevier.

Beards, C. F. [1996]. Structural Vibration. Elsevier.

Bugaru, M., & Vasile, A. [2022]. A Physically Consistent Model for Forced Torsional Vibrations of Automotive Driveshafts. Computation, 10(1), 10.

Charles, H. N. [1943]. The Performance Characteristics of Steering Gears and Notes on Some Factors in Vehicle Design Which affect the Operation of the Steering Gear. Proceedings of the Institution of Automobile Engineers, 37(2), 387–413.

Doebling, S. W., Farrar, C. R., Prime, M. B., & Shevitz, D. W. [1996]. Damage identification and health monitoring of structural and mechanical systems from changes in their vibration characteristics: A literature review.

Emmanuel Augustine Etukudoh, Favour Oluwadamilare Usman, Valentine Ikenna Ilojianya, Cosmas Dominic Daudu, Aniekan Akpan Umoh, & Kenneth Ifeanyi Ibekwe. [2024]. Mechanical engineering in automotive innovation: A review of electric vehicles and future trends. International Journal of Science and Research Archive, 11(1), 579–589.

Feng, M. Q., Kim, J.-M., & Xue, H. [1998]. Identification of a Dynamic System Using Ambient Vibration Measurements. Journal of Applied Mechanics, 65(4), 1010–1021.

García, Y. R., Corres, J. M., & Goicoechea, J. [2010]. Vibration detection using optical fiber sensors. In Journal of Sensors (Vol. 2010).

Hossain, M. N., Rahman, M. M., & Ramasamy, D. [2024]. Artificial Intelligence-Driven Vehicle Fault Diagnosis to Revolutionize Automotive Maintenance: A Review. Computer Modeling in Engineering & Sciences, 141(2), 951–996.

Hou, L., & Cao, S. [2019]. Evaluation Method for Vibration Measurement on Casing in Aeroengine: Theoretical Analysis and Experimental Study. Shock and Vibration, 2019, 1–15.

ISSN: 2524-2121
RENIECYT-SECIHTI: 1702902

Hernández-González, Josué Iván, Torres-Cedillo, Sergio Guillermo, Hernández-Moreno, Hilario and Cortés-Pérez, Jacinto. [2025]. Optical Sensing Technology for Capturing Vibrations in the Automotive Industry. ECORFAN-Journal Taiwan. 9 [16]1-11: e4916111.
https://doi.org/10.35429/EJT.2025.9.16.4.1.11

Javdani, S., Fabian, M., Carlton, J. S., Sun, T., & Grattan, K. T. V. [2016]. Underwater Free-Vibration Analysis of Full-Scale Marine Propeller Using a Fiber Bragg Grating-Based Sensor System. IEEE Sensors Journal, 16(4), 946–953.

Jazar, R. N. [2008]. Vehicle Dynamics: Theory and Application. Springer US.

Kim, D. G., Lee, A., Park, S. W., Yeo, C., Bae, C., & Park, H. J. [2022]. Experimental Study on Leak-induced Vibration in Water Pipelines Using Fiber Bragg Grating Sensors. Current Optics and Photonics, 6(2), 137–142.

Ledesma, R., & Shih, S. [1999]. Heavy and Medium Duty Vehicle Suspension-Related Performance Issues and Effective Analytical Models for System Design Guide.

Li, K., Chan, T. H. T., Yau, M. H., Thambiratnam, D. P., & Tam, H. Y. [2014]. Experimental verification of the modified spring-mass theory of fiber Bragg grating accelerometers using transverse forces. Applied Optics, 53(6), 1200.

Li, T., Guo, J., Tan, Y., & Zhou, Z. [2020]. Recent Advances and Tendency in Fiber Bragg Grating-Based Vibration Sensor: A Review. IEEE Sensors Journal, 20(20), 12074–12087.

Li, T., Tan, Y., Han, X., Zheng, K., & Zhou, Z. [2017]. Diaphragm Based Fiber Bragg Grating Acceleration Sensor with Temperature Compensation. Sensors, 17(12), 218.

Lim, T. C., & Singh, R. [1990]. Vibration transmission through rolling element bearings, part I: Bearing stiffness formulation. Journal of Sound and Vibration, 139(2), 179–199.

Lim, T. C., & Singh, R. [1991]. Vibration transmission through rolling element bearings. Part III: Geared rotor system studies. Journal of Sound and Vibration, 151(1), 31–54.

Lim, T. C., & Singh, R. [1992]. Vibration transmission through rolling element bearings, part IV: statistical energy analysis. Journal of Sound and Vibration, 153(1), 37–50.

Matsushita, O., Tanaka, M., Kanki, H., Kobayashi, M., & Keogh, P. [2017]. Vibrations of Rotating Machinery (Vol. 16). Springer Japan. https://doi.org/10.1007/978-4-431-55456-1

Preizler, R. R., Davidi, R., Motil, A., Botsev, Y., Hahami, M., & Tur, M. [2017]. On the actual bandwidth of some dynamic fiber optic strain/temperature interrogators. 25th International Conference on Optical Fiber Sensors, 10323, 103235C.

Randall, R. B. [2011]. Vibration-based Condition Monitoring. Wiley.

Szeidl, G., & Kiss, L. P. [2020]. Mechanical Vibrations. Springer International Publishing.

Tozzetti, L., Barsanti, T., Gambini, F., Manzo, G., Filippi, S., Matteucci, L., Izzo, I., Di Pasquale, F., & Faralli, S. [2021]. Fiber Bragg Grating Sensors for Dynamic Strain Measurements in Gasoline Direct Injectors. IEEE Transactions on Vehicular Technology, 70(6), 5658–5668.

Vance, J., Zeidan, F., & Murphy, B. [2010]. Machinery Vibration and Rotordynamics. Wiley.

Xiong, L., Guo, Y., Zhou, W., Chen, M., & Zhou, X. [2021]. Fiber Bragg Grating-Based Three-Axis Vibration Sensor. IEEE Sensors Journal, 21(22), 25749–25757.

Xu, H., Li, F., Gao, Y., & Wang, W. [2020]. Simultaneous Measurement of Tilt and Acceleration Based on FBG Sensor. IEEE Sensors Journal, 20(24), 14857–14864.

Yang, J., Liu, Y., Wang, X., & Wu, H. [2017]. An improved steady inverse method for turbomachinery aerodynamic design. Inverse Problems in Science and Engineering, 25(5), 633–651.

Zingoni, A. [2014]. Group-theoretic insights on the vibration of symmetric structures in engineering. Philosophical Transactions of the Royal Society A: Mathematical, Physical and Engineering Sciences, 372(2008), 20120037.

ISSN: 2524-2121
RENIECYT-SECIHTI: 1702902

Hernández-González, Josué Iván, Torres-Cedillo, Sergio Guillermo, Hernández-Moreno, Hilario and Cortés-Pérez, Jacinto. [2025]. Optical Sensing Technology for Capturing Vibrations in the Automotive Industry. ECORFAN-Journal Taiwan. 9 [16]1-11: e4916111.
https://doi.org/10.35429/EJT.2025.9.16.4.1.11

ECORFAN-Journal Taiwan 9[16]1-8: e5916108
Article

Effect of frying on pork rinds quality

Efecto del freído en la calidad del chicharrón de cerdo

Reynoso-Ocampo, Carlos Abraham*[a], Arroyo-Cruz, Celerino[b], Trejo-Trejo, Elia[c] and Cervantes-Miranda, Jesús[d]

[a] Universidad Tecnológica del Valle del Mezquital • 0000-0002-1620-584X
[b] Universidad Tecnológica del Valle del Mezquital • T-2543-2018 • 0000-0002-7027-101
[c] Universidad Tecnológica del Valle del Mezquital • ISB-6748-2023 • 0000-0003-0184-1795
[d] Universidad Tecnológica del Valle del Mezquital • KHC-4616-2024 • 0009-0003-8349-2409

SECIHTI classification:

Area: Biotechnology and Agricultural Sciences
Field: Biotechnology
Discipline: Food Technology
Subdiscipline: Nutrition and food

https://doi.org/10.35429/EJT.2025.9.16.5.1.8
History of the article:
Received: June 11, 2025
Accepted: December 10, 2025

* ✉ [carroyo@utvm.edu.mx]

Abstract

Saturated fatty acids (SFA) are endogenously synthesized and necessary for some physiological and structural functions, while trans fatty acids (TFA) are almost always derived from the ingestion of hydrogenated foods and have no health benefits. The alteration of the lipid profile is a risk factor for cardiocerebrovascular diseases. Reducing their consumption may present a protective effect for cardiovascular events (Cabezas et al., 2015). The concern in Mexico is alarming because more than 50% of the population does not consume vegetables daily, while 20% reported not consuming plain water every day; 80% of the population reported consuming sweetened beverages and about 60% of the population under 20 years of age reported consuming snacks among which corn chips (58%), potato chips (29%), wheat flour snacks and cracklings (4%) highly rich in fat and sodium. With these figures, we can be classified as a country of snackers, since the population consumes at least 90 grams of fried foods per week (Gaona, 2022). Therefore, it was proposed to evaluate the effect of different thermal treatments for frying pork crackling for low-fat snacks. Three formulations were developed to evaluate the heat treatment, dehydration method, penetrability, composition and sensory tests. The results showed that there were no significant differences between the parameters evaluated, showing a preference for the microwave oven chicharrón with a significant decrease in fat according to the analyses performed.

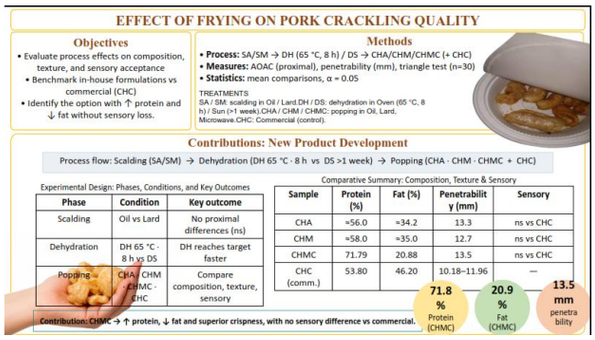

Pork Rinds, low fat, fried

Resumen

Los ácidos grasos saturados (AGS) son de síntesis endógena, necesarios para algunas funciones fisiológicas y estructurales, mientras que los ácidos grasos trans (AGT) provienen casi siempre de la ingesta de alimentos hidrogenados y no tienen beneficios en la salud. La alteración del perfil lipídico es un factor de riesgo para sufrir enfermedades cardiocerebrovasculares. La reducción del consumo de los mismos puede presentar un efecto protector para eventos cardiovasculares (Cabezas et al., 2015). La preocupación en México es alarmante debido a que más del 50% de la población no consume verduras diariamente, mientras que el 20% reportó no consumir agua sola todos los días; el 80% de la población reportó el consumo de bebidas endulzadas y cerca del 60% de la población menor de 20 años reportó consumir botanas entre las que destacan frituras de maíz (58%), papas fritas (29%), botanas de harina de trigo y chicharrón (4%) altamente ricas en grasas y sodio. Con estas cifras bien podemos clasificarnos como un país botanero, ya que la población consume por lo menos 90 gramos de frituras por semana (Gaona, 2022). Por lo anterior, se planteó evaluar el efecto de diferentes tratamientos térmicos de freído del chicharrón de cerdo para snack bajo en grasa. Se desarrollaron 3 formulaciones para evaluar el tratamiento térmico, método de deshidratado, penetrabilidad, composición y pruebas sensoriales. Los resultados mostraron que no presentan diferencias significativas entre los parámetros evaluados, mostrando una preferencia por el chicharrón para horno de microondas con una disminución significativa de grasa de acuerdo a los análisis realizados.

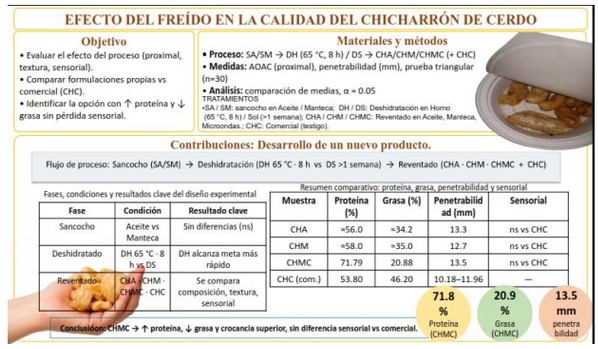

Chicharrón de cerdo, bajo en grasa, freído

Area: Promotion of frontier research and basic science in all fields of knowledge

Citation: Reynoso-Ocampo, Carlos Abraham, Arroyo-Cruz, Celerino, Trejo-Trejo, Elia and Cervantes-Miranda, Jesús. [2025]. Effect of frying on pork rinds quality. ECORFAN-Journal Taiwan. 9 [16]1-8: e5916108.

Introduction

The popularity of snacks is due to various advantages such as easy access (they are sold everywhere), relatively low cost, and attractive presentation and packaging. Hence, we find a wide variety of salty products, mainly made from cereal flours (corn and wheat) or tubers (potatoes and taro) obtained by extrusion; sweet snacks made from fried plantains; flour and pork cracklings; popcorn; natural or dehydrated nuts with salt or sugar (blueberries, raisins, figs, walnuts), among the best known.

With regard to consumption statistics, it is difficult to estimate figures, as there are few measurements for each type of snack and, above all, because a large part of sales are made by street vendors. However, in 2020, per capita consumption of fried snacks was 4.7 kilograms, equivalent to $31.4 per capita. The most commonly consumed salty snacks in Mexico are fried corn (58%), potato chips (29%), and wheat flour and pork rind snacks (4%). With these figures, we can certainly classify ourselves as a snacking country, as the population consumes at least 90 grams of fried snacks per week (Estrada et al., 2022).

About pork rinds

Snacks in Mexico are an industry that spans various markets and continues to grow rapidly. Pork rinds, made from pork skin that has been cleaned and fried in animal fat, are foods that provide a large amount of calories (699 kcal per 30 g serving), which come mainly from lipids, due to the lack of control in the frying of the skin. In some countries, chicharron is made by melting pork fat, while in others, the fat is used to fry the skin, with or without meat.

The Pork Rinds can also be made from other animals such as cows, chickens, fish, or lambs, although they are generally considered to be of lower sensory quality. In Mexico, “chicharron” refers to clean pork skin, which is fried almost whole in animal fat (lard) until it becomes fluffy and crispy. The main objective of frying pork rinds is to achieve a specific texture and color on their surface, as well as a characteristic aroma. The crispy texture is associated with changes that occur in proteins, fats, and carbohydrates (Pérez et al., 2016).

Crispiness in fried foods

Frying food is one of the oldest culinary processes on record, probably dating back to the 6th century BC, and was likely one of the first technical culinary processes that allowed food to be preserved for longer.

Technically, frying refers to methods of cooking food by immersing it in edible oil (mainly vegetable oil) or hot fat (mostly vegetable or animal fat) above the boiling point of water (160-180°C) (3,4). The oil acts as a heat transfer medium, producing rapid and uniform heating of the product.

The high temperatures during the frying process cause the water to evaporate, transferring it from the food to the surrounding oil. The oil absorbed by the food partially replaces the water released, constituting up to 40% of the final product and thus influencing all its organoleptic properties, especially flavor, color, crispness, and aroma (Montes *et al*., 2016).

Effect of moisture on pork rinds

The moisture content of the product definitely influences the number of pellets that pop and also their expansion rate. The pellet pops when heated to around 200°C, as the water inside it is superheated and turns into steam. The steam pressure breaks in an explosion, resulting in expansion and a product with a moisture content of less than 4%. Although popping is usually achieved using lard or oil, the use of radiant heat may be more feasible for a quick snack.

That is why during the dehydration process, the aim is to have a moisture content in the product below 4%, as this way it is quicker for the small amount of water to turn into steam when subjected to high temperatures, which generates a quick and uniform bursting of the pellets.

In addition to the above, as it is a product with relatively low moisture content, it has a long shelf life of up to 60 days. Furthermore, as it does not contain a significant amount of water, it is almost certain to be free of microorganisms that accelerate its deterioration, as they cannot find a medium in which to live (Espinel, 2010).

ISSN: 2524-2121
RENIECYT-SECIHTI: 1702902

Reynoso-Ocampo, Carlos Abraham, Arroyo-Cruz, Celerino, Trejo-Trejo, Elia and Cervantes-Miranda, Jesús. [2025]. Effect of frying on pork rinds quality. ECORFAN-Journal Taiwan. 9 [16]1-8: e5916108.
https://doi.org/10.35429/EJT.2025.9.16.5.1.8

Dehydration

This is one of the most widely used techniques for food preservation throughout history. Mesh trays are used for dehydration to allow heat to circulate, facilitating the process. The pieces of skin, cut and cooked in butter or oil and seasoned, are spread evenly on the tray and placed in a hot air oven at 50°C for 8 hours or three days in the sun so that they lose as much water as possible (Espinel, 2010).

Materials and methods

Through experimental research, a new product was developed (low-fat pork rind snack) whose main ingredient was pork skin fried using different heat treatments to evaluate the impact of fat reduction. The project was therefore developed in the following stages.

Process for making pork rinds

To begin processing instant pork rinds, the most suitable skin for this type of product was selected, which in this case was American pork skin due to its lower fat content and colour, in order to facilitate the process. After that, all excess fat was removed from the pork rinds to facilitate the next step. Once the skin was clean, it was cut into 5x5 cm pieces, adding 2% iodized salt per kilogram of skin.

Two methods were selected for heat treatment of the skin (frying in oil and lard) in order to evaluate which, heat treatment is most viable for the process. The skin is subjected to a temperature of 200°C for 50 seconds. Once the pork rind has been boiled, it is dehydrated using two methods: drying in an oven for 8 hours at a temperature of 65°C, and drying in the sun for an indefinite period of time until it reaches a moisture content of less than 4%, in order to prevent the development of pathogenic microorganisms.

Three heat treatments were used to pop the dehydrated pork pellets (frying in lard, frying in oil, and popping in a microwave oven) to verify whether there were significant differences between treatments.

Physicochemical analyses

Physicochemical analyses were performed on the final product. These included determining the carbohydrate, fat, protein, moisture, and mineral content in accordance with the methods recommended by the AOAC (Association of Official Analytical Chemists). These analyses were performed at each critical point in the process (boiling, dehydration, and cracking). The results obtained were expressed as averages. The results obtained were compared with those of a commercial Pork Rind (CPR). The aim was to develop a snack with the typical characteristics of commercial pork rinds with a low level of saturated fat and to determine whether there is a difference between the boiling and dehydration heat treatments.

To determine the differences between pork rinds popped in the microwave, oil, and lard (MPR, OPR, LPR) and CPR, the results were analyzed using a randomized block design with a significance level of $\alpha=0.5$, with three replicates; CPR was considered the control, so a Dunnet's test with $\alpha=0.5$ was performed. Minitab version 19 was used for statistical analysis.

Determination of drying curve

For this process, two formulations of instant pork rinds, fried in oil and fried in lard, were analysed. For the dehydrated method of instant pork rinds, two methods were used: oven drying and sun drying. For the oven drying method, a temperature of 65°C was maintained for 8 hours, obtaining a product with a moisture content of 4%. On the other hand, using the sun drying method, the product took a week and a half to reach the desired moisture content of 4%, due to the fact that changes in atmospheric temperature can delay the dehydration process.

Determination of penetrability

A penetrometer was used to determine the penetrability of pork rinds.

A completely randomized design was used for this, with five replicates, in order to verify whether there was a significant difference in the hardness of instant pork rinds and commercial brands.

ISSN: 2524-2121
RENIECYT-SECIHTI: 1702902

Reynoso-Ocampo, Carlos Abraham, Arroyo-Cruz, Celerino, Trejo-Trejo, Elia and Cervantes-Miranda, Jesús. [2025]. Effect of frying on pork rinds quality. ECORFAN-Journal Taiwan. 9 [16]1-8: e5916108.
https://doi.org/10.35429/EJT.2025.9.16.5.1.8

Results and discussion

To obtain the final formulation for instant microwave pork rinds, it was necessary to conduct various tests to ensure that the product matched the sensory characteristics of commercial pork rinds. Table 1 shows the formulation, which features a lower sodium content.

Box 1

Table 1

Formulation for pork pellets

Ingredient	Amount (%)
Pork rind	97
Salt	2
Lard	1

Source: own elaboration, 2025

Once the product formulation was obtained, standardization was carried out considering the different formulations of interest to observe possible changes, as described in Figure 1. It is important to mention that during the manufacturing process, it was observed that the main control point that affects product quality is dehydration, which allows the protein to burst in the microwave.

Drying curves

According to Heldman and Lund (2007), drying is defined as the removal of moisture due to the simultaneous transfer of heat and mass. Sharma *et al*. (2003) point out that food drying kinetics is a complex phenomenon and requires reliable models to predict this process. These models are useful tools for estimating the time needed to reduce the water content of the product under different conditions and the ideal temperature, thus improving the efficiency of the process (Iglesias et al., 2018).

Box 2

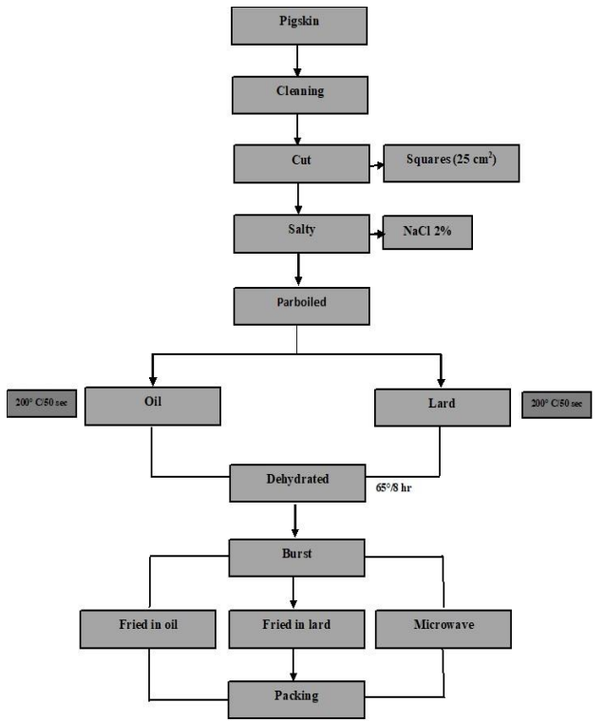

Figure 1

Standardization of the pork rind production process

Source: own elaboration (2025)

Once the product was obtained, the dehydration process was evaluated in order to observe whether there was a difference between the blanching time when dehydrating the pellets in the sun or in an oven (DS and DO). The results are shown in Figures 2 and 3.

Box 3

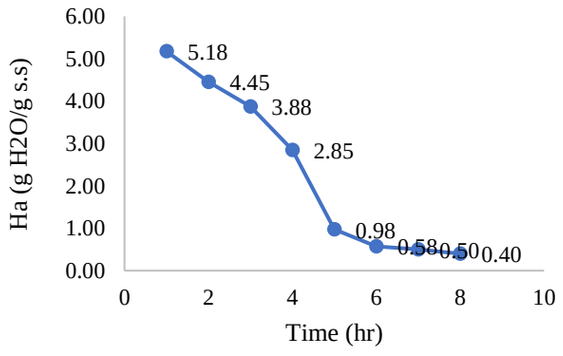

Figure 1

Drying curve in an oven at 65°C

Source: own elaboration, 2025

Looking at both graphs, it was found that temperature control (65°C) reduces drying time to 8 hours by obtaining the required moisture content for cooking the pork pellets, compared to sun drying, which does not achieve the required water content after 13 hours.

ISSN: 2524-2121
RENIECYT-SECIHTI: 1702902

Reynoso-Ocampo, Carlos Abraham, Arroyo-Cruz, Celerino, Trejo-Trejo, Elia and Cervantes-Miranda, Jesús. [2025]. Effect of frying on pork rinds quality. ECORFAN-Journal Taiwan. 9 [16]1-8: e5916108.
https://doi.org/10.35429/EJT.2025.9.16.5.1.8

Box 4

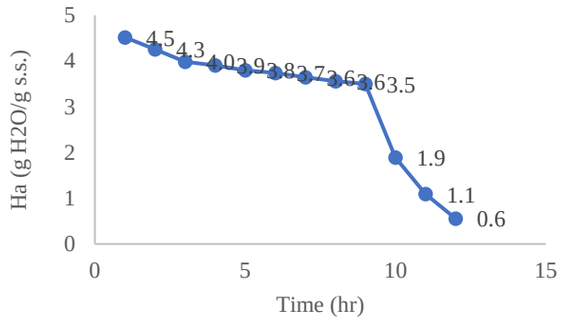

Figure 2
Sun drying curve

Source: Own Elaboration, 2025

Drying is one of the oldest techniques used for food preservation since the dawn of humanity, as it provides the possibility of subsistence in times of scarcity. Although natural drying is the most economical, it has some limitations. Under normal conditions, it takes two to three days; however, in times of low solar radiation and rainfall, the drying time is extended to five days or more, and the product can be negatively affected by biological agents. Due mainly to these disadvantages, it is advisable to consider the use of solar dryers and not just expose the product to the sun (Iglesias *et al*., 2018).

Bromatological tests

Once the product was standardized, its moisture, ash, protein, fat, and carbohydrate content were evaluated in the boiled in oil and lard (BO, BL) process, finding no significant difference between the parameters evaluated, as shown in Table 2.

Box 5

Table 2
Bromatological evaluation of boiled in oil (BO) and boiled in lard (SM)

Parameter	BO	BL
Moisture	30.49 ^{A}	29.40 ^{A}
Minerals	1.42 ^{A}	1.79 ^{A}
Fats	8.84 ^{A}	6.28 ^{A}
Protein	58.68 ^{A}	61.63 ^{A}
Carbohydrates	0.8 ^{A}	0.9 ^{A}

Source: Own Elaboration, 2025

Note: Different letters for each parameter evaluated indicate a significant difference ($p<0.05$).

Bromatological analyses were performed on oven-dried (OD) and sun-dried (SD) sancochos in order to evaluate whether there is a difference between the two methods (Table 3).

Box 6

Table 3
Bromatological evaluation between oven-dried and sun-dried products

Parameter	BO	BL
Moisture	4.57^{A}	5.54 ^{A}
Minerals	2.66 ^{A}	3.29 ^{A}
Fats	26.69 ^{A}	23.44 ^{A}
Protein	62.29 ^{A}	61.72 ^{A}
Carbohydrates	3.78 ^{A}	5.50 ^{A}

Source: Own Elaboration (2025)

Note: Different letters for each parameter evaluated indicate a significant difference ($p<0.05$).

Finally, it was decided to conduct a bromatological evaluation of the different pork rinds: pork rinds fried in oil (PRFO), pork rinds fried in lard (PRFL), and pork rinds fried in a microwave oven (PRFM), comparing them with a commercial brand.

According to the results of the proximate chemical analysis presented in Table 4, it can be observed that microwave pork rinds have a higher protein content and lower fat content, with percentages of 71.79% and 20.88%, respectively. These differences are statistically significant ($\alpha=0.5$) compared to the control (CPR). This is explained by the fact that microwave pork rinds have a 133.43% increase in protein content and a 43.31% decrease in fat content compared to the control sample.

Box 7

Table 4
Bromatological evaluation of different types of popcorn vs. commercial brand

Parameter	PRFO	PRFL	PRFM	CPR
Moisture	4.10^{A}	4.07 ^{A}	4.19^{A}	3.63^{A}
Minerals	2.81^{A}	3.80 ^{A}	2.16 ^{A}	1.86^{A}
Fats	35.35^{A}	34.1 ^{A}	20.88^{B}	46.20^{A}
Protein	56.71^{A}	57.80^{A}	71.79^{B}	53.8 ^{A}
Carbohydrates	1^{C}	0.2^{B}	0.9^{C}	0^{A}

Source: Own Elaboration (2025)

ISSN: 2524-2121
RENIECYT-SECIHTI: 1702902

Reynoso-Ocampo, Carlos Abraham, Arroyo-Cruz, Celerino, Trejo-Trejo, Elia and Cervantes-Miranda, Jesús. [2025]. Effect of frying on pork rinds quality. ECORFAN-Journal Taiwan. 9 [16]1-8: e5916108.
https://doi.org/10.35429/EJT.2025.9.16.5.1.8

Note: Different letters for each parameter evaluated indicate a significant difference ($p<0.05$).

Once the standardization process was complete, a completely randomized design was developed, as shown in Table 5, to observe whether there was a significant difference between the penetrability of the formulations developed compared to two commercial brands.

Box 8

Table 5

Evaluation of the penetrability of different formulations compared to commercial brands

Product	Penetrability (mm)
PRFO	13.32^{A}
PRFL	12.72^{AB}
PRFM	13.46^{A}
CPR1	11.96^{B}
CPR2	10.18^{B}

Source: Own Elaboration (2023)

Note: Different letters for each parameter evaluated indicate a significant difference ($p<0.05$).

The results shown in the table above demonstrate that the formulations developed have greater penetrability; this suggests that they are firmer and therefore do not crumble easily, which may be related to the fact that they are crunchier than commercially available brands.

Sensory tests

The study was conducted using a discriminatory (triangular) test in which, once the instant pork rind process had been standardized, a sensory evaluation was carried out. This consisted of forming a group of 30 consumer panelists who were selected through an exam or test in which they demonstrated their ability to detect basic flavors (sweet, salty, sour, and bitter) in order to evaluate and compare whether there were significant differences between the formulations developed and a commercial brand. sour, and bitter) in order to evaluate and compare whether there were significant differences between the formulations developed and a commercial brand. The results obtained from the sensory analysis can be interpreted using Table 3 from Pedrero and Pangborn, 1989.

Depending on the number of judges and the level of significance chosen, the (minimum) thresholds necessary to determine whether there are significant differences are obtained. This analytical differentiation test was performed to determine the participants' ability to discriminate between similar samples. For this test, three samples were used for evaluation by trained panelists. The test consists of a triad, where two samples are the same and one is different.

Based on the problem posed to determine the discriminating ability of the judges, whose test questions have dichotomous YES or NO answers, they distinguish the different sample. It was determined that the most suitable statistical hypothesis test was to use the binomial test resulting from several Bernoulli-type trials according to Infante and Zárate (2000). In the Binomial probability model, the sample space consists of the sequences of successes and failures resulting from *n* independent repetitions of an experiment whose probability model is Bernoulli with a constant probability p of success.

Therefore, the following set of hypotheses was established: H0: $p > 1/3$ vs. Ha: $p \leq 1/3$ Where: Ho: The judge does not distinguish the sample as different from the instant pork rind test triad. Vs. Ha: The judge does distinguish the different sample from the instant pork rind test triad. $p= 1/3$ is the constant probability of success that the judge will distinguish the different sample from the triad. The decision rule is to reject H0 if: $X \leq c$", where c is such that $P(X \leq c \mid p = 1/3) \leq \alpha$ Where X represents the minimum number of judges required to discriminate between samples and c is the number of judges who discriminated between samples in the test with a significance level of $\alpha=0.05$ error.

Based on the above, when conducting the analysis with 30 panelists, only 17 detected the different sample of instant pork rinds in oil and 15 in lard, so it is concluded that there is no significant difference between the instant pork rinds formulation and the commercial brand because a minimum of 20 of them must detect the different sample to say that there is a significant difference, as shown in the following tables of results.

ISSN: 2524-2121
RENIECYT-SECIHTI: 1702902

Reynoso-Ocampo, Carlos Abraham, Arroyo-Cruz, Celerino, Trejo-Trejo, Elia and Cervantes-Miranda, Jesús. [2025]. Effect of frying on pork rinds quality. ECORFAN-Journal Taiwan. 9 [16]1-8: e5916108.
https://doi.org/10.35429/EJT.2025.9.16.5.1.8

Box 9

Table 7
Results of the triangular test of the sensory evaluation

Sample	Panelists	
	Noticed a difference	**Did not notice any differences**
In oil	17	13
In Lard	15	15

Source: Own Elaboration, 2023

Box 10

Figure 2
Final product (microwave pork rinds)
Source: Own Elaboration, 2025

Conclusions

In conclusion, the evaluation of heat treatments and parameters for instant pork rinds demonstrates that it is feasible to develop instant pork rinds for microwave ovens. A key advantage of the developed product is its high protein content and low-fat content, which gives it a competitive edge over other commercial brands.

Another advantage of this product is that it is considered safe in terms of microorganism development, since it uses a heat treatment of boiling at a temperature of 200°C and then dehydrates to 4% moisture to prevent the development of microorganisms. Similarly, the product is crunchier than commercial brands, which is an advantage as this is the main appeal of this type of snack on the market.

Declarations

Conflict of interest

The authors declare no interest conflict. They have no known competing financial interests or personal relationships that could have appeared to influence the article reported in this article.

Author contribution

Carlos Abraham Reynoso Ocampo: Conceived and supervised the overall research project, directed the intellectual framework, and led the process development and product standardisation.

Celerino Arroyo Cruz: Provided specialised technical review and critical validation of the analytical methodologies.

Elia Trejo Trejo: Designed the experimental methodology and performed the statistical analysis and interpretation.

Jesús Cervantes Miranda: Conducted the editorial review and manuscript style correction.

Availability of data and materials

The datasets used and/or analyzed during the current study are available from the corresponding author on reasonable request.

Funding

This research did not receive any specific grant from funding agencies in the public, commercial, or not-for-profit sectors. The work was supported entirely by the institutional resources of the Universidad Tecnológica del Valle del Mezquital.

Availability of data and materials

Indicate the availability of the data obtained in this research.

Acknowledgements

This study was not funded by any government institution or scientific association.

ISSN: 2524-2121
RENIECYT-SECIHTI: 1702902

Reynoso-Ocampo, Carlos Abraham, Arroyo-Cruz, Celerino, Trejo-Trejo, Elia and Cervantes-Miranda, Jesús. [2025]. Effect of frying on pork rinds quality. ECORFAN-Journal Taiwan. 9 [16]1-8: e5916108.
https://doi.org/10.35429/EJT.2025.9.16.5.1.8

Abbreviations

AOAC: Association of Official Analytical Chemists.
CPR**:** Commercial Pork Rind
BL: Boiled in Lard
BO: Boiled in Oil
LPR: Lard Pork Rinds
MPR: Microwave Pork Rinds
OD: Oven Dried
OPR: Oil Pork Rinds
PRFL: Pork Rinds Fried in Lard
PRFM: Pork Rinds Fried in Microwave
PRFO: Pork Rinds Fried in Oil
SFA: Satured Fatty Acids
SD: Sun dried
TFA: Trans Fatty Acids

References

Association of Official and Analytucal Chemists (1984). Official Methods of Analysis. 14 th. Editorial Arlington.

Cabezas *et al.,* (2016). Aceites y grasas: efectos en la salud y regulación mundial. Rev. Fac. Med. 2016 vol. 64 No. 4: 761-8.

Espinel, O. N. C. (2010). Establecimiento de las condiciones de elaboración de Pellet de piel de cerdo destinado para snack. Escuela Politécnica Nacional.

Estrada *et al*., (2022). Tendencias en el consumo de botanas en México.

Gaona *et al*., (2023). Consumidores de grupos de alimentos en población mexicana. Salud Pública de México/vol. 65.

Heldman y Lund. (2006). Handbook of Food Engineering. Second Edition. CRC Press. Taylos & Francis Group. Boca Raton, Florida: 756 -810 pp.

Iglesias *et al*. (2018). Cinética de secado de Moringa oleífera. Revista Mexicana de Ciencias Agrícolas volumen 9 número 5.

Infante y Zarate. (2012). Métodos estadísticos: un enfoque disciplinario. La Gaya Ceincia. Tercera Edición.

Montes *et al*., (2016). Absorción de aceite en alimentos fritos. Rev. Chil. Nutr. vol.43 no.1.

Pedrero, D. L. y Pangborn, R. M. (1989). Evaluación sensorial de los alimentos. Métodos analíticos. Editorial Alhambra mexicana. D. F. México.

Sharma et al. (2003). Drying kinetics of garlic cloves under convective drying conditions. J. Food Sci. Technol. 40(1):45-51.

ISSN: 2524-2121
RENIECYT-SECIHTI: 1702902

Reynoso-Ocampo, Carlos Abraham, Arroyo-Cruz, Celerino, Trejo-Trejo, Elia and Cervantes-Miranda, Jesús. [2025]. Effect of frying on pork rinds quality. ECORFAN-Journal Taiwan. 9 [16]1-8: e5916108.
https://doi.org/10.35429/EJT.2025.9.16.5.1.8

ECORFAN-Journal Taiwan 9[16]1-15: e6916115
Article

PID control for tracking A 5 DOF robotic manipulator subjected to exogenous forces

Control PID para el seguimiento de un manipulador robótico de 5 GDL bajo fuerzas exógenas

Pacheco, Jorge[a], Cortés-Vega, David[b], Sanchez-Lara, Rafael[c], Alazki, Hussain[d]

[a] Universidad Autónoma del Carmen • 0009-0000-7434-0663 • 246083
[b] Universidad Autónoma del Carmen • 0000-0002-6209-2081 • 593408
[c] Universidad Autónoma del Carmen • 0000-0001-6587-1972 • 88144
[d] Universidad Autónoma del Carmen • 0000-0002-1960-3624 • 274587

SECIHTI classification:

Area: Engineering
Field: Engineering
Discipline: Electronic Engineering
Subdiscipline: Control

https://doi.org/10.35429/EJT.2025.9.16.6.1.15
History of the article:
Received: September 11, 2025
Accepted: December 10, 2025

Abstract

In this work, a differentiator-based PID control scheme was developed and applied to a robot manipulator. It was considered that the system contains uncertainties in the payload; also, exogenous forces, such as bounded disturbances in the force torques acting on the robot joints and affecting the action of the actuators; and noise in the measurements. The control scheme was tested at the simulation level, to verify its versatility in following different three-dimensional trajectories, two curves were used in 3D space, the first a cardioid and the second a lemniscate. The differentiator used, which works in conjunction with the PID, aims to obtain a good position estimate, despite the presence of noise in the measurements. The convergence of the differentiator used is guaranteed and is referenced in this work.

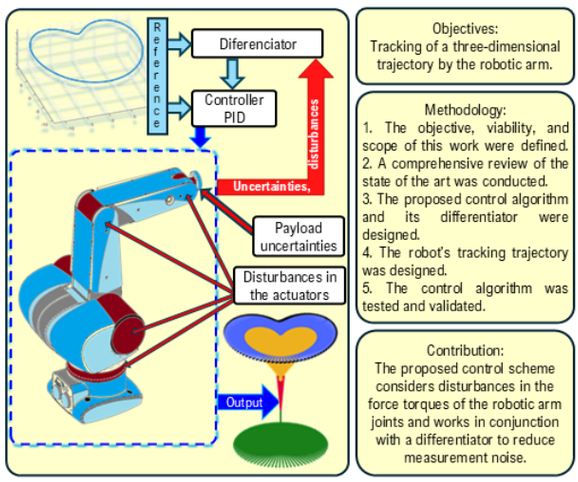

Motion control; sensorless; noises and disturbances

Resumen

En este trabajo se desarrolló un esquema de control PID basado en un diferenciador y aplicado a un Robot Manipulador. Se consideró que en el sistema existe la presencia de incertidumbres en la carga útil; asimismo la presencia de fuerzas exógenas, tales como, perturbaciones acotadas en los torques que actúan en las articulaciones del robot y afectan la acción de los actuadores; y también ruido en las mediciones. El esquema de control se probó a nivel de simulación; para verificar su versatilidad de seguimiento de trayectorias tridimensionales distintas, se utilizaron 2 curvas en el espacio 3D, la primera un cardioide y la segunda una lemniscata. El diferenciador utilizado y que trabaja en conjunto con el PID tiene como objetivo realizar una buena estimación de la posición, a pesar de la presencia de ruido en las mediciones. La convergencia del diferenciador empleado está garantizada y es referenciada en el presente trabajo.

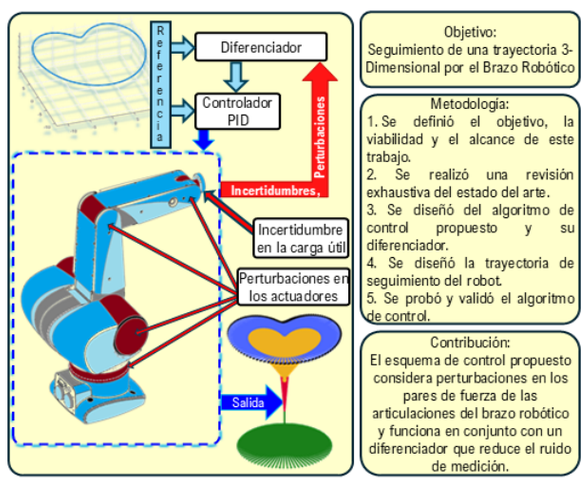

Control de movimiento; medición sin sensores; ruidos y perturbaciones

Area: Development of strategic leading-edge technologies and open innovation for social transformation

Citation: Pacheco, Jorge, Cortés-Vega, David, Sanchez-Lara, Rafael, Alazki, Hussain. [2025]. PID control for tracking A 5 DOF robotic manipulator subjected to exogenous forces. ECORFAN-Journal Taiwan. 9 [16]1-15: e6916115.

Introduction

The great importance that robotic manipulators have had in industries and in various application areas is based mainly on the core points mentioned below: efficient increase in productivity; improvement in the quality of products and processes, since precision and repeatability are a characteristic of robotic manipulators; reduction in production costs; versatility, since their programming algorithm can be changed and they can be adapted to this change to perform other tasks; safety, since they can perform highly dangerous tasks, such as transporting heavy loads or handling hazardous or contaminated materials, thus reducing the risk of occupational accidents (Álvarez et. al, 2024; Pérez, Castro, Alonso, Castillo, & Salichs, 2017).

To realize these advantages and avoid poor system performance and instability, the control algorithms designed and applied to manipulator robots must command the robotic arm to follow pre-established trajectories with a high degree of precision and speed. These characteristics must be preserved even when there are uncertainties in the mathematical model and/or perturbations in the robot's environment, such as those typically encountered in the links, the payload (Reboucas, Da Silva, Praxedes, Hemanth, & De Albuquerque, 2019) or the force torques acting on the actuator joints. It is worth mentioning that no work has been reported so far in the state-of-the-art review that considers perturbations in the force torques mentioned above.

Trajectory tracking work has been carried out with various control techniques, for example, in the area of intelligent control, work has been presented using fuzzy logic (Yilmaz, Tatlicioglu, Savran, & Alci, 2021; Urrea, & Alvarado, 2020; Bae et. al, 2017), which is useful when there is no adequate mathematical model of the system, however, some knowledge of the system dynamics is required to generate the fuzzy rules, and it is also necessary to have a large capacity of computational resources to train fuzzy or neuro-fuzzy networks (NFN), another drawback of fuzzy systems is low efficiency when the systems present uncertainties and are exposed to external disturbances; a similar thing happens in the field of neural networks (NN),

Although they have proven to be very good when there is no mathematical model of the system (Huang, Cheng, & Huang, 2023; Zhang, Zheng, Yu, Li, & Yu, 2017), they have the drawback that they require a large number of input-output data from the system to train this type of networks, which produces two other disadvantages, which are, having a large computing equipment and time to train said network; another type of intelligent control are those that use genetic algorithms (Lin, Sie, Chu, Yau, & Ding, 2021), but likewise, these require a powerful computing system, which entails an increase in the cost of the system and is sometimes not profitable; further intelligent control technique that has been used in manipulator robots is predictive control, which is based on the system model, however (Klančar, & Škrjanc 2007), this technique requires an accurate model of the system because it is sensitive to the uncertainty that arises when changes occur in the model parameters, an additional drawback is that it requires a computer to carry out the algorithm optimization process, which increases the cost of the control system.

For linear systems, or systems that are nonlinear but can be linearized around the operating point, PID controllers can be used (Božek, & Nikitin, 2021). It should be noted that its control action is only efficient in a region close to the operating point, and its efficiency decreases as it moves away from this region. PID controllers lack robustness to external disturbances that directly affect the system, and due to the uncertainties, that arise when the mathematical model does not faithfully represent the system to be controlled.

Having an exact mathematical model of the system improves the performance of most control systems. Normally, mathematical models do not fully represent the dynamics of systems and uncertainties are generated, and they may not be reliable in the presence of disturbances. A good option to overcome this problem would be to measure the variables required by the control algorithm; thus, ensuring that the control does not require a very exact model of the system.

ISSN: 2524-2121
RENIECYT-SECIHTI: 1702902

Pacheco, Jorge, Cortés-Vega, David, Sanchez-Lara, Rafael, Alazki, Hussain. [2025]. PID control for tracking A 5 DOF robotic manipulator subjected to exogenous forces. ECORFAN-Journal Taiwan. 9 [16]1-15: e6916115.
https://doi.org/10.35429/EJT.2025.9.16.6.1.15

In order not to increase the cost of the control system, instead of using sensors to measure the variables, observers (Sariyildiz & Ohnishi, 2014; Li, Yang, Chen, & Chen, 2016; Liu, Chen, Mei, & Wu, 2022; Dao, Nguyen, & Ahn, 2023) or differentiators can be used. For example, numerical differentiation (Loria, 2015; Brunot, 2019; Cao, Gan & Dai, 2019; Vo, Truong & Kang, 2021) could be useful in certain situations where the variables do not change very quickly and a high sampling rate is not required; high gain observers are another option as long as there is no high frequency noise present, since the overshoots grow greatly during transients (Stotsky, & Kolmanovsky, 2001).

There is also a type of observers that require a good mathematical model, however, precisely what is intended is not to depend too much on the model, furthermore they do not guarantee convergence in finite time (Levant, 1998); on the other hand, with the Levante differentiator the convergence in finite time can be guaranteed (Levant, 2003), when overshoots occur, they can be attenuated by means of a convenient tuning of the gains defined in its structure, furthermore they show satisfactory conditions in the case of the presence of measurement noise, and/or disturbances, and do not require large computing resources (Shtessel, Edwards, Fridman, & Levant, 2014; Na, 2019).

The Thermo CRS CataLyst 5-DOF robotic arm will track a 3-dimensional reference trajectory using a PID control scheme based on a Sliding Mode differentiator (SMD), which will allow the robot state variables required by the control algorithm to be estimated and will help eliminate the need for a highly accurate model of the system. The advantages of this differentiator structure will be leveraged to minimize undesirable effects caused by model uncertainties, as well as by the bounded perturbations that can occur at the robot manipulator joints and directly affect the torques applied to the actuators. In this way, the PID controller, working in conjunction with the aforementioned differentiator, will meet the established requirements.

The mathematical model used in this article is based on the Euler-Lagrange equations of motion.

The following sections of this work are organized as follows:

Section II mentions the methodology applied in this article; Section III describes the mathematical model used in this paper; Section IV presents the problem statement, describing SMD-based PID control algorithm, as well as mentioning the stability of the SMD; Section V presents the results obtained in this work as a result of using the aforementioned control scheme in the tracking of the 2 three-dimensional trajectories, the cardioid and the lemniscate.; Section VI describes the conclusions of this work.

Methodology

The methodology applied in this article was the following:

1. The objective, viability and scope of the research of this work were defined.
2. A exhaustive review of the state of the art was carried out.
3. The proposed control algorithm scheme was designed, as well as its differentiator.
4. The robot's tracking trajectories were proposed and designed.
5. Testing and validation of the control algorithm were carried out.

Model of the manipulator robot

A schematic drawing of the 5-DOF Thermo CRS CataLyst Robot Manipulator is presented in Figure 1, where the angles of action of each of its joints can be seen (*CRS Catalyst-5Articulated Robot*, n.d.), this robot has the following mathematical model (Okubanjo, Oyetola, Osifeko, Olaluwoye, & Alo, 2017; Lavín, Solís, Gómez, & Escobar, 2020):

$$M_i\ddot{\alpha} + M_c\dot{\alpha} + v_g = \tau(t) \quad [1]$$

In this mathematical expression:

$$\alpha \in \mathbb{R}^{5x1}, \qquad \dot{\alpha} \in \mathbb{R}^{5x1}, \qquad \ddot{\alpha} \in \mathbb{R}^{5x1}$$

are vectors representing respectively the position state, the velocity state and the acceleration of the joint angles; $\tau(t) \in \mathbb{R}^{5x1}$ is the vector of torques applied at the input of the system $M_i \in \mathbb{R}^{5x5}$; is the inertia matrix, which is symmetrical and positive definite, and depends on the manufacturer parameters *"*m, I, l, lc*"* and α, which can be expressed as follows:

$$M_i = F_{M_i}([m, I, l, lc], \alpha)$$

ISSN: 2524-2121
RENIECYT-SECIHTI: 1702902

Pacheco, Jorge, Cortés-Vega, David, Sanchez-Lara, Rafael, Alazki, Hussain. [2025]. PID control for tracking A 5 DOF robotic manipulator subjected to exogenous forces. ECORFAN-Journal Taiwan. 9 [16]1-15: e6916115.
https://doi.org/10.35429/EJT.2025.9.16.6.1.15

$M_c \in \mathbb{R}^{5x5}$ is the centripetal and Coriolis force matrix, which depends on the manufacturer parameters "m, l, lc" as well as on α and $\dot{\alpha}$, which can be written as follows:

$$M_c = F_{M_c}([m, l, lc], \alpha, \dot{\alpha})$$

$v_g \in \mathbb{R}^{5x1}$ is the vector of gravitational torques, which depends on the manufacturer parameters "g, m, l, lc" and α, which can be written as follows:

$$v_g = F_{v_g}([g, m, l, lc], \alpha)$$

g is the gravitational constant; the values of the manufacturer's parameters just mentioned are given in Table 1 and represent, "I" the inertia of the links, l" the length of the links, lc the length from the axis to the center of mass and m" the mass of the links.

It is considered that there is the presence of bounded uncertainty in the mass of the end-effector link, then the matrices M_i, M_c and the vector v_g of Eq. 1, will be affected, since they depend on the mass of the links. If it is considered that:

$$\Delta^u_{M_i}, \quad \Delta^u_{M_c}, \quad \Delta v^u_{v_g}$$

represent the increases in:

$$M_i, \quad M_c, \quad v_g$$

due to the uncertainties in the masses of the links, it can be written:

$$M^u_i = M_i + \Delta^u_{M_i},$$

$$M^u_c = M_c + \Delta^u_{M_c},$$

$$v^u_g = v_g + \Delta v^u_{v_g},$$

representing in this same order, the inertia matrix, the Coriolis matrix and centripetal forces and the gravitational force vector but already modified by the effects of the uncertainties in the masses of the links. The presence of bounded perturbations in the force torques applied to the joints of the manipulator robot will also be considered. If τ_d is considered to represent the presence of bounded disturbances in the force pairs applied to the joints, the mathematical model expressed in Eq. 1 is modified by the following expression:

$$M^u_i \ddot{\alpha} + M^u_c \dot{\alpha} + v^u_g + \tau_d = \tau(t) \qquad [2]$$

The parameters and working angles of the joints provided by the manufacturer of the Thermo CRS CataLyst 5 DOF robotic manipulator are presented in Table 1 and Table 2 respectively.

Box 1

Table 1

Parameters provided by the manufacturer of the Robot Manipulator

Link Mass (kg)	Link Length (m)	Link Inertia (kg-m^2)	Axis length to center of mass (m)
m1=5.47	l1=0.254	I1=88.22$x10^{-3}$	lc1=0.127
m2=2.09	l2=0.254	I2=33.70$x10^{-3}$	lc2=0.127
m3=1.36	l3=0.254	I3=21.93$x10^{-3}$	lc3=0.127
m4=0.006	l4=0.0508	I4=21.93$x10^{-3}$	lc4=0.0254
m5=0.6	l5=0.01	I5=39$x10^{-8}$	lc5=0.005

Source: CRS Catalyst-5Articulated Robot, n.d. https://www.equipx.net

Box 2

Table 2

Working angles of the joints provided by the manufacturer of the Robot Manipulator

values associated with the joint:				
J1	**J2**	**J3**	**J4**	**J5**
+180°/-180°	+110°/0°	+90°/-35°	+110°/-110°	+180°/-180°

Source: CRS Catalyst-5Articulated Robot, n.d. https://www.equipx.net

Box 3

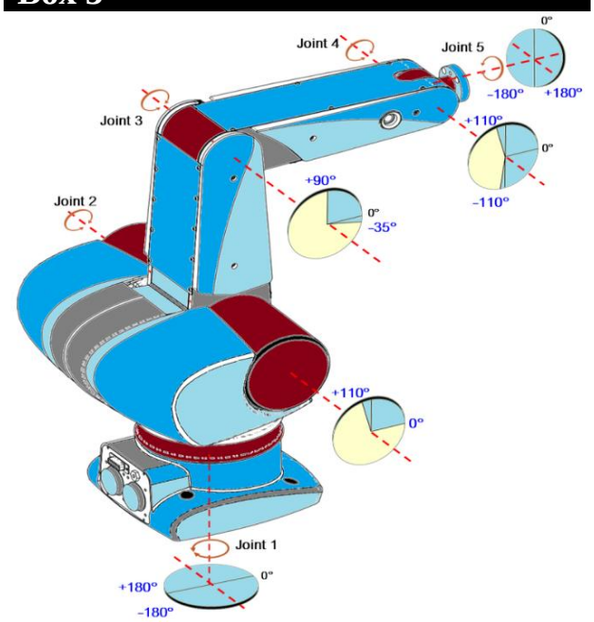

Figure 1

Manipulator Robot: Thermo CRS CataLyst 5 DOF

Source: CRS Catalyst-5Articulated Robot, n.d. https://www.equipx.net

ISSN: 2524-2121
RENIECYT-SECIHTI: 1702902

Pacheco, Jorge, Cortés-Vega, David, Sanchez-Lara, Rafael, Alazki, Hussain. [2025]. PID control for tracking A 5 DOF robotic manipulator subjected to exogenous forces. ECORFAN-Journal Taiwan. 9 [16]1-15: e6916115.
https://doi.org/10.35429/EJT.2025.9.16.6.1.15

4. Problem statement

To achieve satisfactory results with a robotic manipulator designed to perform trajectory tracking tasks in 3D space, the control algorithm used in the robot must be able to command the robotic arm's actuators to execute rapid and precise movements, even in the face of possible uncertainties in the mathematical model, such as unexpected variations in the payload of the end effector, which would directly affect the mass of the last link; as well as the presence of exogenous forces, i.e. bounded disturbances that affect the action of the actuators; noise in the force torques acting on the joints; and noise in the measurements of each of the joint angles. It is worth mentioning that the works presented with manipulator robots consider certain perturbations, but not those occurring to the force torques acting on the joints.

To address this problem, a PID control scheme will be designed in the Manipulator Robot: Thermo CRS CataLyst 5 DOF, acting in collaboration with a SMD, which will allow the system states to be estimated and at the same time its good qualities will be taken advantage of, that is, the values of the state variables will be obtained from the SMD and a high-precision mathematical model will not be necessary, its effective characteristics will also be taken advantage of when noise is present in the measurements. Figure 2 illustrates a block diagram of the proposed control scheme, and the considerations made.

Box 4

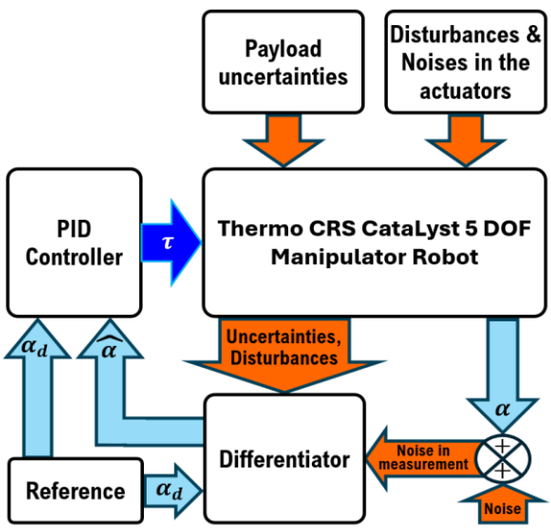

Figure 2
Block diagram of SMD-based PID control scheme.
Source: Own design and elaboration

From the following mathematical structures of the SMD Eq. 3 and Eq. 4, the position and velocity of the joint angles will be estimated:

$$\dot{\widehat{\alpha_0}} = -\lambda_1\sqrt{L}\sqrt{|\widehat{\alpha_0} - \alpha|}sign(\widehat{\alpha_0} - \alpha) + \widehat{\alpha_1} \quad [3]$$

$$\dot{\widehat{\alpha_1}} = -\lambda_0\, L\, sign\left(\widehat{\alpha_1} - \dot{\widehat{\alpha_0}}\right) \quad [4]$$

In these expressions, $\widehat{\alpha_0}$ and $\widehat{\alpha_1} \in \mathbb{R}^{5x1}$ represent the estimates of the velocity and acceleration, respectively, of the joint angles. Therefore, by integrating these equations, the position and velocity of the joint angles are obtained; $\lambda_1 > 0$ and $\lambda_0 > 0$ are parameters used to adjust the estimation of the variables; and $L > 0$ is a Lipschitz constant.

The position errors of the joint angles are obtained from Eq. 5.

$$e = \alpha_d - \widehat{\alpha_0} = x_1^d - \hat{x}_1^0 \quad [5]$$

In this expression, α_d and x_1^d represent the desired position, of the joint angles; $\widehat{\alpha_0}$ and $\hat{x}_1^0$ represent the position estimation. The position estimation errors derived from the SMD are obtained from Eq. 6.

$$e_{x_1} = x_1 - \hat{x}_1^0 \quad [6]$$

The convergence of this differentiator is demonstrated in (Levant, 1998). It can be observed how the phase trajectories of the differentiator converge. Likewise, in (Levant, 2003; Levant, 2005), the convergence of the differentiator structure is demonstrated through homogeneity properties.

The control law used, that is, the proposed PID scheme that works in conjunction with the SMD, is described below in Eq. 7:

$$\tau(t) = K_p e(t) + K_i \int e(t)dt + K_d \frac{de(t)}{dt} \quad [7]$$

In this expression K_p , K_i, & K_d, $\in \mathbb{R}^{5x1}$ represent the proportional, integral and derivative gains of the PID controller respectively, and $e \in \mathbb{R}^{5x1}$, is the tracking error, which is calculated from the estimated output position provided by the SMD, as indicated in Eq. 5.

ISSN: 2524-2121
RENIECYT-SECIHTI: 1702902

Pacheco, Jorge, Cortés-Vega, David, Sanchez-Lara, Rafael, Alazki, Hussain. [2025]. PID control for tracking A 5 DOF robotic manipulator subjected to exogenous forces. ECORFAN-Journal Taiwan. 9 [16]1-15: e6916115.
https://doi.org/10.35429/EJT.2025.9.16.6.1.15

5. Results

In this section, the results obtained from the use of a PID control scheme based on a SMD in the robotic manipulator are presented. The results shown correspond to simulations performed with MATLAB software and its Simulink Toolbox. To verify its versatility in following different three-dimensional trajectories, two curves were used in 3D space, the first a cardioid and the second a lemniscate. The tracking of the proposed trajectories will be performed with the first 4 joints of the robot, the fifth joint or end effector is used for the working angle with the payload, therefore, it is not part of the trajectory and will be proposed arbitrarily within its operating range.

The tuned gains for the PID that are expressed in Eq. 7, as well as the parameters expressed in Eq. 3, and Eq. 4 that correspond to the SMD, which were obtained to track the trajectories are shown in Table 3 and Table 4 respectively.

Box 5

Table 3
Tuned PID gains

	values associated with the joint:				
	1	**2**	**3**	**4**	**5**
K_p	675	600	600	600	$8x10^{-4}$
K_i	7.5	7.5	7.5	7.5	$5x10^{-6}$
K_d	57.75	66	40	20	$4x10^{-5}$

Source: Own design and elaboration

The graphs obtained from the simulation results of testing the SMD-based PID control algorithm on the 5-DOF Thermo CRS CataLyst robot manipulator model while tracking the 3D reference trajectories are presented below.

In the test performed with the aforementioned control scheme, the following conditions are considered:

a) Unknown, sudden, and bounded variations in the end-effector load.

b) The presence of noise in the measurements of the five joints.

c) Presence of external and bounded disturbances in the actuators that act on the first four joints of the robot.

d) Presence of noise in the force torques acting on the joints.

Box 6

Table 4
Tuned parameters corresponding to the SMD.

	values associated with the joint:				
	1	**2**	**3**	**4**	**5**
λ_1	3.06	1.836	1.836	1.224	1.652
λ_0	0.94	1.81	1.81	18.1	0.073
L	1250	1500	1375	1000	1000

Source: Own design and elaboration

Figure 3 shows the bounded uncertainty applied to the mass of the end-effector, or payload. The uncertainty was limited to 1 kg, as this is the maximum working load indicated in the manufacturer's specifications.

Box 7

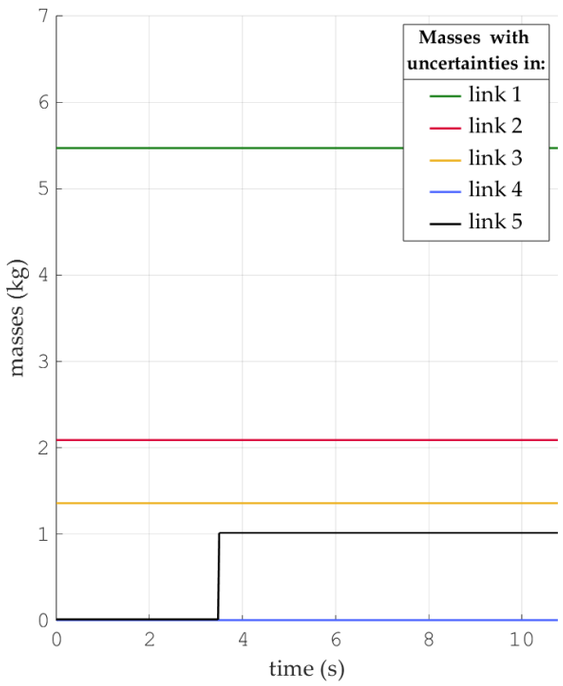

Figure 3
Graph of the bounded uncertainty applied to the mass of the 5th link or end effector
Source: Own design and elaboration.

Figure 4 shows the noises that were present in the angle measurements of the five joints.

Figure 5 shows the disturbances present in the actuators that operate on the joints of the robotic manipulator. These perturbations, as mentioned above, are external and bounded.

ISSN: 2524-2121
RENIECYT-SECIHTI: 1702902

Pacheco, Jorge, Cortés-Vega, David, Sanchez-Lara, Rafael, Alazki, Hussain. [2025]. PID control for tracking A 5 DOF robotic manipulator subjected to exogenous forces. ECORFAN-Journal Taiwan. 9 [16]1-15: e6916115.
https://doi.org/10.35429/EJT.2025.9.16.6.1.15

Box 8

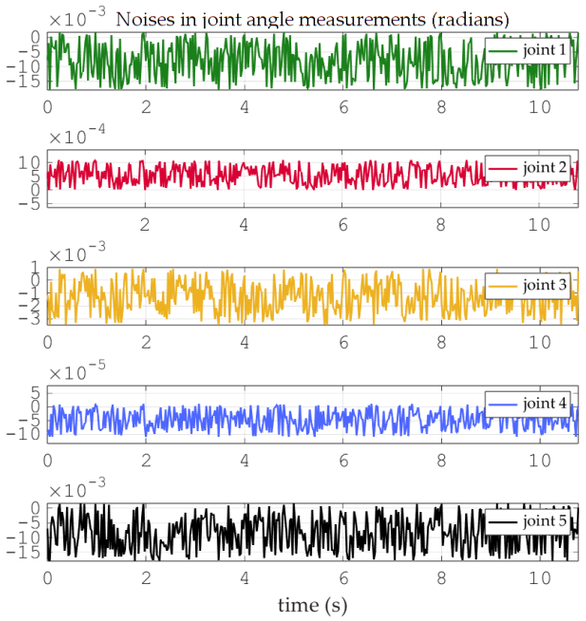

Figure 4

Graphs of the noises present at the time of joint angle measurements.

Source: Own design and elaboration.

Box 9

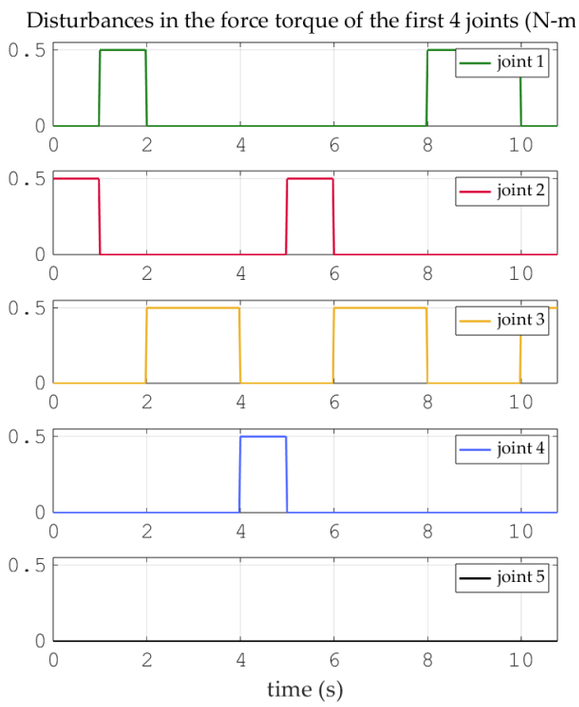

Figure 5

Graphs of the external and bounded disturbances affecting the torques of the first 4 joints of the manipulator robot

Source: Own design and elaboration

Figure 6 shows the graphs of the presence of noise in the five joints of the manipulator robot.

Box 10

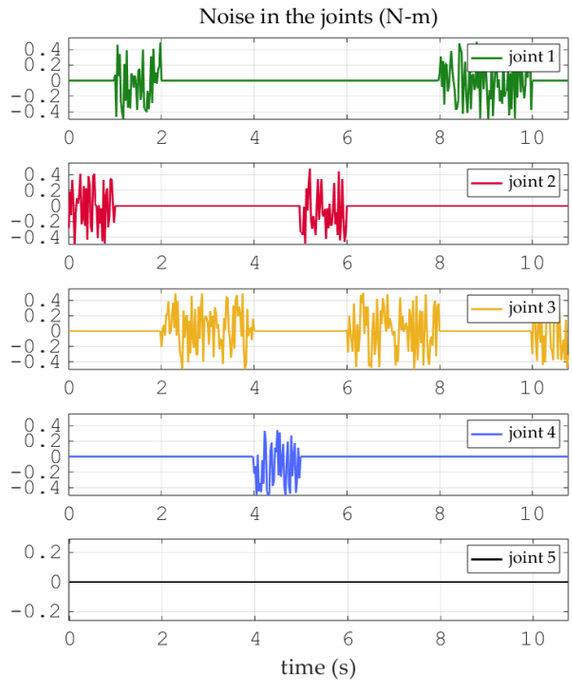

Figure 6

Graph of the presence of noise in the five joints of the manipulator robot

Source: Own design and elaboration

A) Simulations with the 3D cardioid

Figures 7 show an ideal reference trajectory for the cardioid, but they do not consider the intrinsic limitations of the manipulator robot, so it should not be used as shown. Therefore, an adjustment was made so that the manipulator robot can track said trajectory optimally without having to suffer mechanical overstress and at the same time excessive overshoots do not occur (Feng, Dai, Zhou, Xu & Wang, 2024; Haselirad & Neubert, 2014). Figure 8 shows the reference trajectory to be used, and Figure 9 shows the reference angles for each joint that form the 3D reference trajectory in Figure 8.

Figure 10 shows the graph describing the robotic manipulator as it tracks the trajectory presented in Figure 8.

Figure 11 shows the tracking of the 5 joint angles that describe the trajectory of the 3D cardioid represented in Figure 8. The angles of the desired trajectory are shown as dashed segments, and the corresponding tracking with solid segments. This graph shows that, after approximately 0.6s, accurate tracking of the reference angles for all 5 joints is achieved. A slight overshoot in the angle of the fifth joint is also observed when there is a sudden change in the reference angle of the first.

ISSN: 2524-2121
RENIECYT-SECIHTI: 1702902

Pacheco, Jorge, Cortés-Vega, David, Sanchez-Lara, Rafael, Alazki, Hussain. [2025]. PID control for tracking A 5 DOF robotic manipulator subjected to exogenous forces. ECORFAN-Journal Taiwan. 9 [16]1-15: e6916115.
https://doi.org/10.35429/EJT.2025.9.16.6.1.15

Box 11

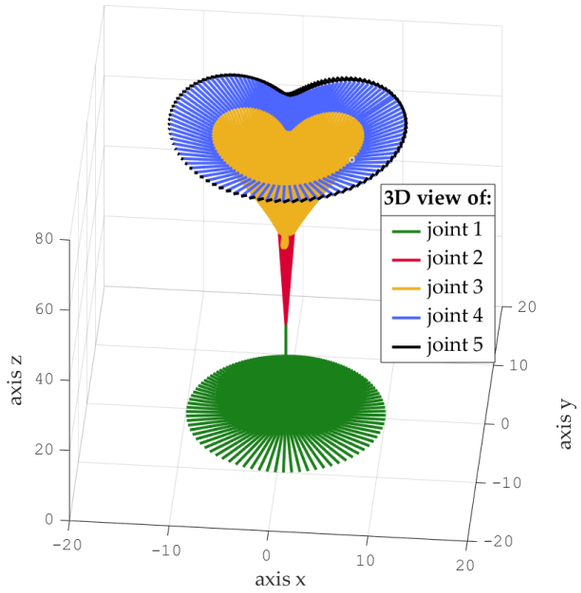

Figure 7

Ideal 3D reference trajectory of the cardioid.

Source: Own design and elaboration.

Box 12

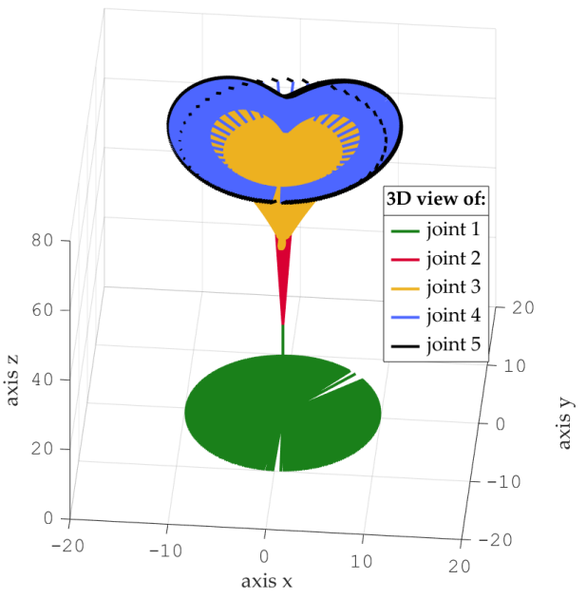

Figure 8

3D reference trajectory used for the cardioid.

Source: Own design and elaboration

Figure 12 shows the tracking error graphs for each of the angles corresponding to the 5 joints of the robotic manipulator. The errors are expressed in radians. In these graphs, it is observed that the tracking errors for each of the 5 angles always converge to zero, even though the system is permanently subject to noise in the force torques, as well as to noise in the measurements and the presence of disturbances in said torques.

It is also observed that the convergence remains towards zero when a sudden change in the trajectory of the first joint occurs, this arises in at 7.5 and 8.5 seconds. The percentage tracking error at steady state for each angle of the five joints is shown in Table 5.

Box 13

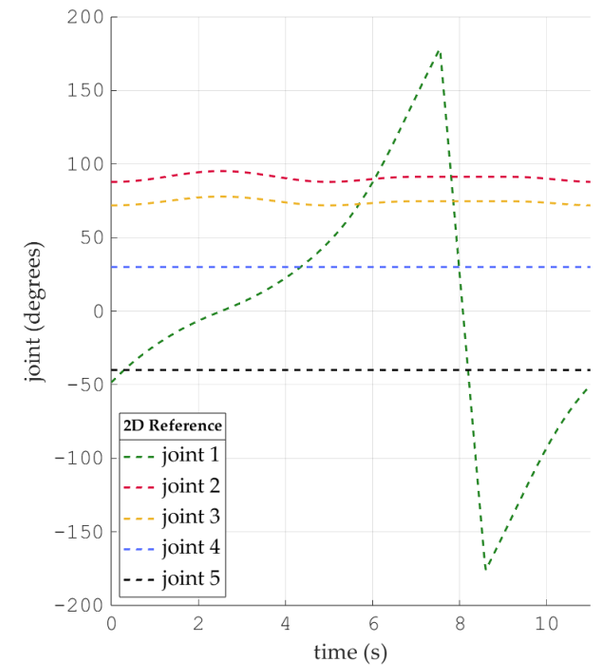

Figure 9

Graphs of the reference angles of each joint for the cardioid.

Source: Own design and elaboration

Box 14

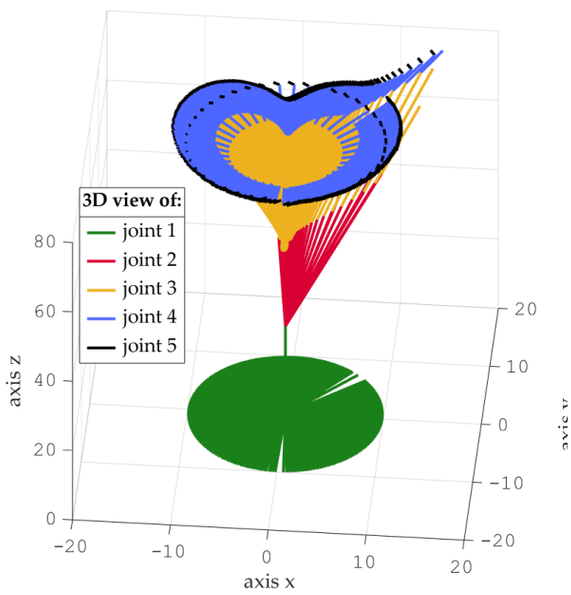

Figure 10

3D cardioid reference trajectory tracking.

Source: Own design and elaboration

ISSN: 2524-2121
RENIECYT-SECIHTI: 1702902

Pacheco, Jorge, Cortés-Vega, David, Sanchez-Lara, Rafael, Alazki, Hussain. [2025]. PID control for tracking A 5 DOF robotic manipulator subjected to exogenous forces. ECORFAN-Journal Taiwan. 9 [16]1-15: e6916115.
https://doi.org/10.35429/EJT.2025.9.16.6.1.15

Box 15

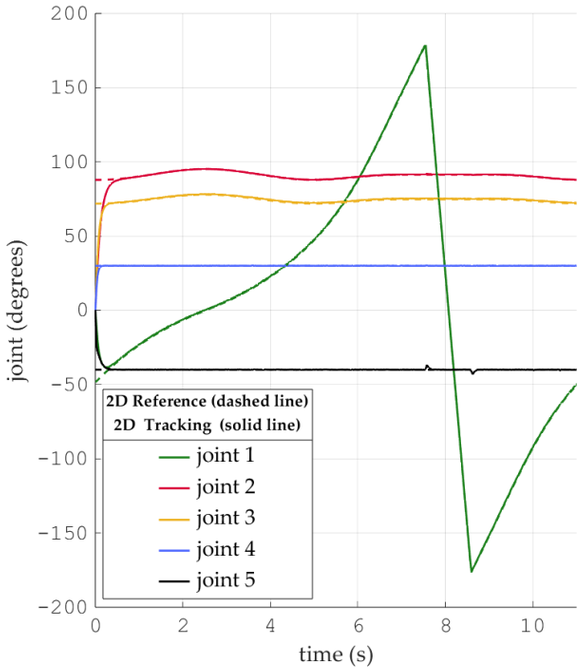

Figure 11

Graphs of the angles of the desired trajectory of the cardioid and its tracking for each joint.

Source: Own design and elaboration

Box 16

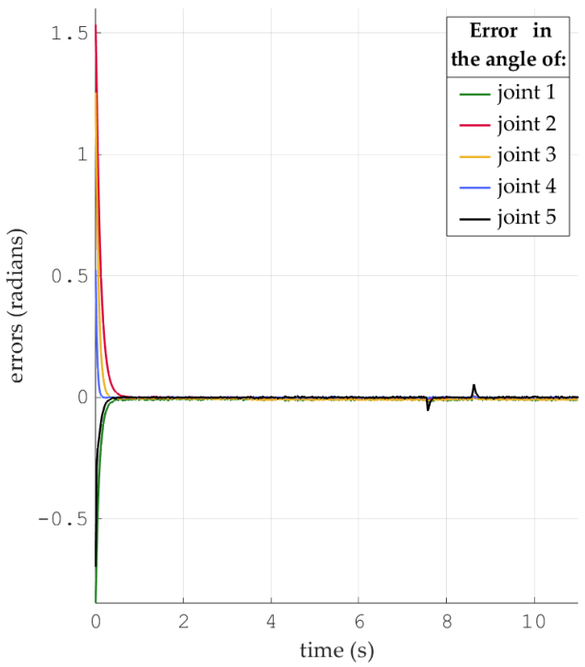

Figure 12

Graphs of the cardioid tracking errors for each of the 5 joint angles.

Source: Own design and elaboration

The percentage of steady-state tracking error for each angle of the five joints is shown in Table 5. Figure 13 shows the graphs of the estimated errors in the angles of the 5 joints using the SMD.

Box 17

Table 5

Percentage of tracking error in steady state for each angle of the 5 joints that make up the cardioid

values associated with the joint (%):				
J1	**J2**	**J3**	**J4**	**J5**
0.6614	0.1435	0.621	0.1974	0.3245

Source: Own design and elaboration.

Box 18

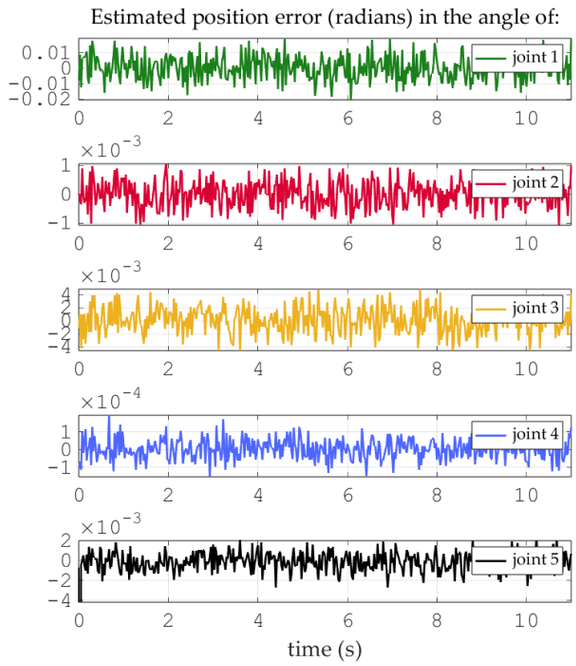

Figure 13

Graphs of the position measurement errors resulting from the estimate made by the SMD when tracking the cardioid.

Source: Own design and elaboration

The percentage error in the estimation of each of the 5 angles is shown in Table 6.

Box 19

Table 6

Percentage error of position measurement made by the estimator.

values associated with the joint (%):				
J1	**J2**	**J3**	**J4**	**J5**
305.5×10^{-3}	4.986×10^{-3}	63.96×10^{-3}	6.04×10^{-3}	97.41×10^{-3}

Source: Own design and elaboration.

Figure 14 shows the control signal, that is, the force torques applied in tracking the trajectory of the robotic manipulator.

ISSN: 2524-2121
RENIECYT-SECIHTI: 1702902

Pacheco, Jorge, Cortés-Vega, David, Sanchez-Lara, Rafael, Alazki, Hussain. [2025]. PID control for tracking A 5 DOF robotic manipulator subjected to exogenous forces. ECORFAN-Journal Taiwan. 9 [16]1-15: e6916115.
https://doi.org/10.35429/EJT.2025.9.16.6.1.15

Box 20

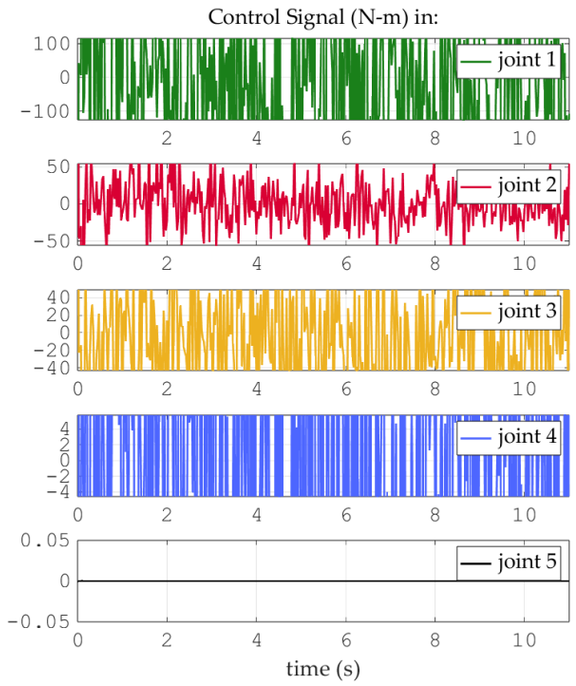

Figure 14

Graphs of the control signal applied to each joint in cardioid tracking.

Source: Own design and elaboration.

B) Simulations with the 3D lemniscate.

Figure 15 shows an ideal reference trajectory for the lemniscate, but it does not consider the intrinsic limitations of the manipulator robot. Therefore, an adjustment was made so that the manipulator robot could optimally follow this trajectory without suffering mechanical overexertion and, at the same time, avoid excessive overshoots.

Figure 16 shows the reference trajectory to be used, and Figure 17 shows the reference angles for each joint that form the 3D reference trajectory in Figure 16.

Figure 18 shows the graph describing the robotic manipulator as it tracks the trajectory presented in Figure 16.

Figure 19 shows the tracking of the five joint angles that describe the 3D lemniscate trajectory represented in Figure 16. The desired trajectory angles are shown as dashed segments, and the corresponding tracking angles are shown as solid segments. This graph shows that, after approximately 0.65s, accurate tracking of the reference angles for all five joints is achieved. A slight overshoot in the angle of the fifth joint is also observed when there is a sudden change in the reference angle of the first.

Box 21

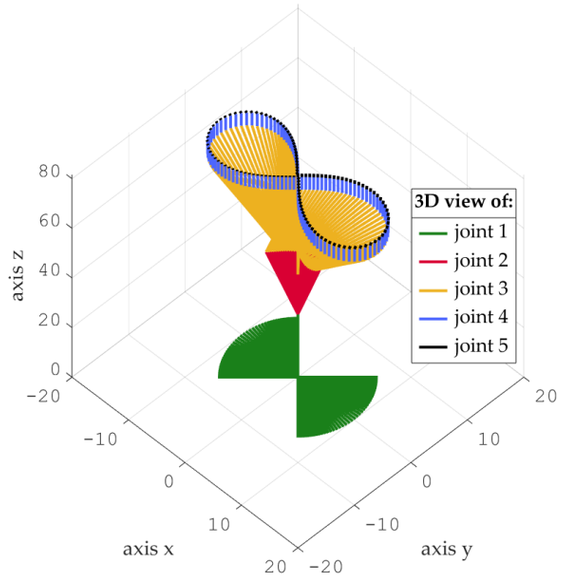

Figure 15

Ideal 3D reference trajectory of the lemniscate.

Source: Own design and elaboration

Box 22

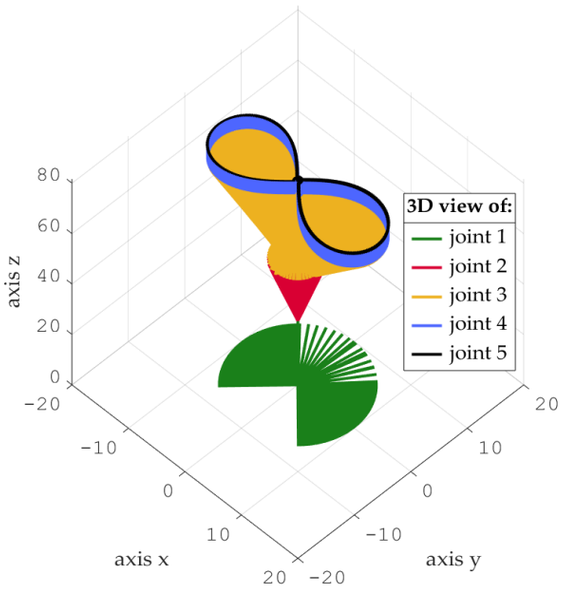

Figure 16

3D reference trajectory used for the lemniscate.

Source: Own design and elaboration.

Figure 20 shows the tracking error graphs for each of the angles corresponding to the 5 joints of the robotic manipulator. In these graphs, it is observed that the tracking errors for each of the 5 angles always converge to zero, even though the system is permanently subject to noise in the force torques, as well as to noise in the measurements and the presence of disturbances in said torques. It is also observed that convergence remains towards zero when a sudden change occurs in the trajectory of the first joint, this arises at 5 seconds and 6 seconds.

ISSN: 2524-2121
RENIECYT-SECIHTI: 1702902

Pacheco, Jorge, Cortés-Vega, David, Sanchez-Lara, Rafael, Alazki, Hussain. [2025]. PID control for tracking A 5 DOF robotic manipulator subjected to exogenous forces. ECORFAN-Journal Taiwan. 9 [16]1-15: e6916115.
https://doi.org/10.35429/EJT.2025.9.16.6.1.15

Box 23

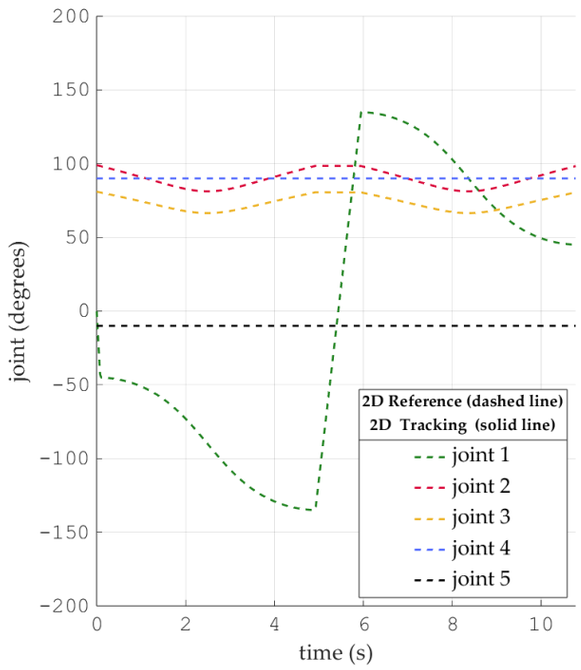

Figure 17

Graphs of the reference angles of each joint for the lemniscate.

Source: Own design and elaboration

Box 24

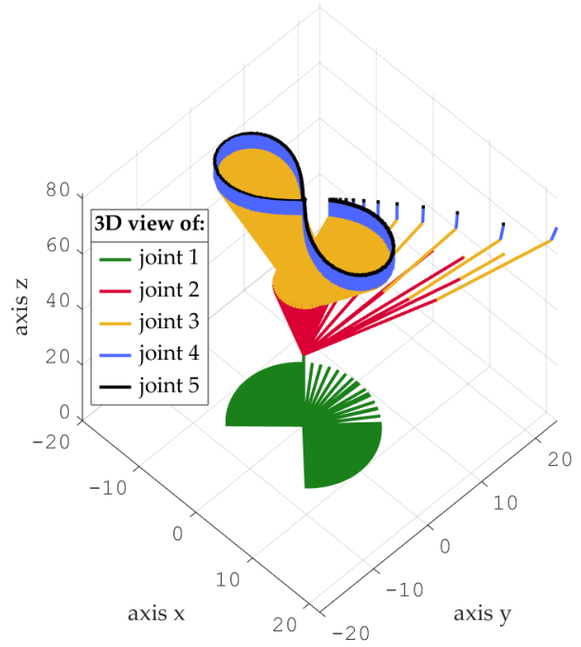

Figure 18

Tracking the reference trajectory of the 3D lemniscate.

Source: Own design and elaboration

Box 25

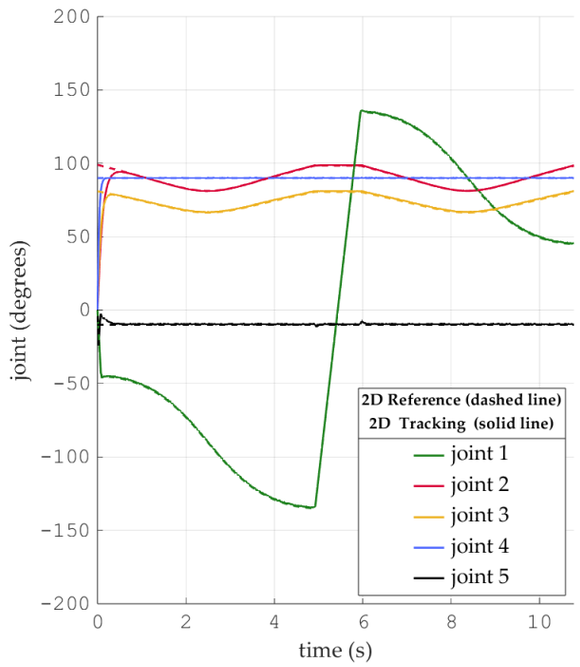

Figure 19

Graphs of the angles of the desired trajectory of the lemniscate and its tracking for each joint

Source: Own design and elaboration

Box 26

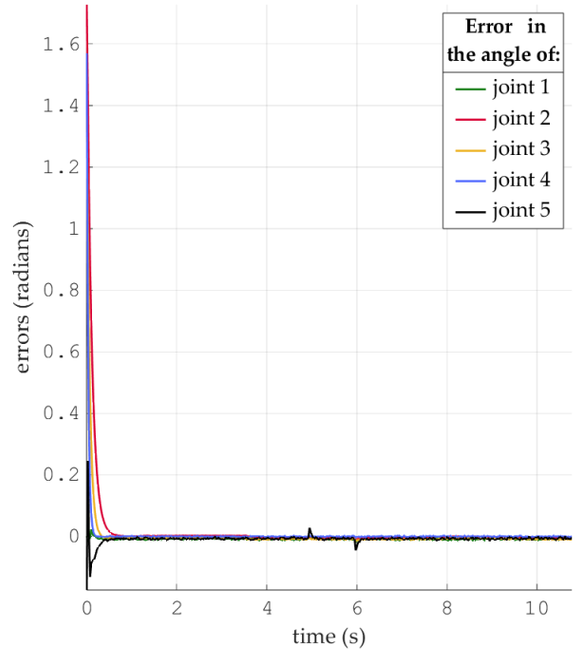

Figure 20

Graphs of the lemniscate tracking errors for each of the 5 joint angles.

Source: Own design and elaboration

The percentage of steady-state tracking error for each angle of the five joints is shown in Table 7.

ISSN: 2524-2121
RENIECYT-SECIHTI: 1702902

Pacheco, Jorge, Cortés-Vega, David, Sanchez-Lara, Rafael, Alazki, Hussain. [2025]. PID control for tracking A 5 DOF robotic manipulator subjected to exogenous forces. ECORFAN-Journal Taiwan. 9 [16]1-15: e6916115.
https://doi.org/10.35429/EJT.2025.9.16.6.1.15

Box 27

Table 7

Percentage of tracking error in steady state for each angle of the 5 joints that form the lemniscate.

values associated with the joint (%):				
J1	**J2**	**J3**	**J4**	**J5**
0.5379	0.1693	0.6350	0.0742	1.1310

Source: Own design and elaboration

Figure 21 shows the graphs of the estimated errors in the angles of the 5 joints using the SMD. The percentage error in the estimation of each of the 5 angles is shown in Table 8.

Box 28

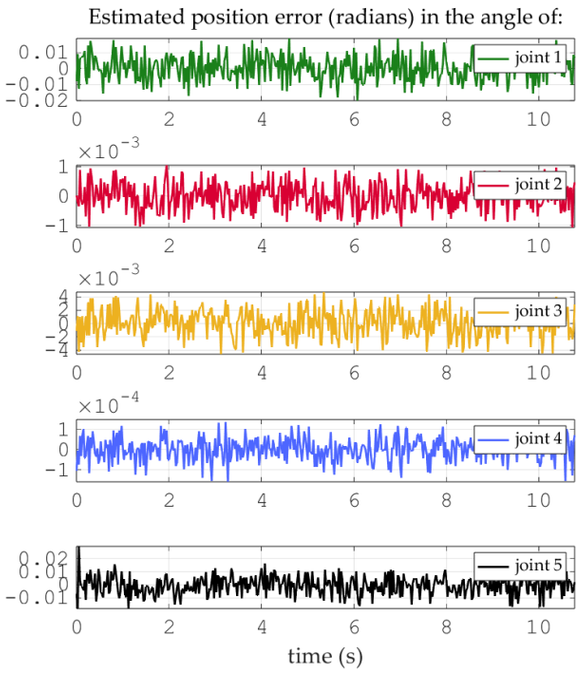

Figure 21

Graphs of the position measurement errors resulting from the estimation made by the SMD when tracking the lemniscate.

Source: Own design and elaboration

Box 29

Table 8

Percentage error of position measurement made by the SMD

values associated with the joint (%):				
J1	**J2**	**J3**	**J4**	**J5**
228×10^{-3}	5.076×10^{-3}	64.36×10^{-3}	2.173×10^{-3}	393.5×10^{-3}

Source: Own design and elaboration

Figure 22 shows the control signal, that is, the force torques applied in tracking the trajectory of the robotic manipulator.

Box 30

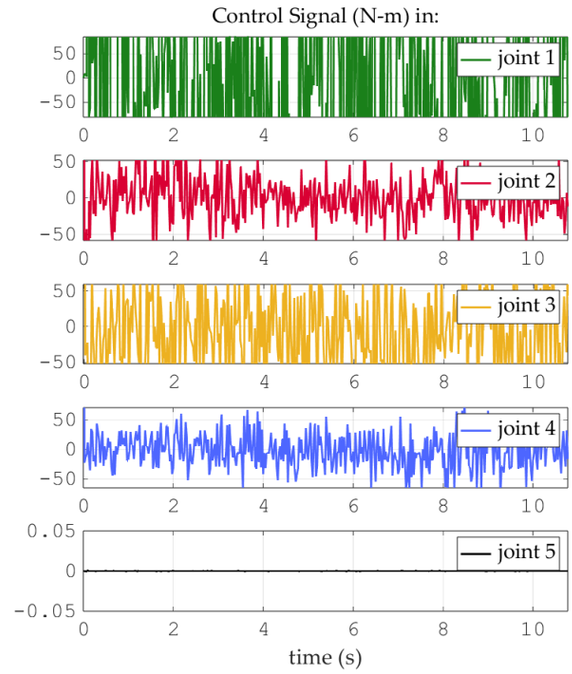

Figure 22

Graphs of the control signal applied to each joint in the tracking of the lemniscate.

Source: Own design and elaboration

6. Conclusions

A SMD-based PID control scheme was applied at the simulation level to the Thermo CRS CataLyst 5-degree-of-freedom robotic manipulator. To verify the tracking versatility of the control scheme, two three-dimensional trajectories were employed: the first a cardioid and the second a lemniscate.

Simulation tests were performed considering the following: Uncertainties in end-effector payload; the presence of noise in the measurements of the five joints; presence of exogenous forces, i.e. bounded disturbances in the actuators acting on the first 4 joints of the robot and noise in the torques acting on the joints.

It was verified that the SMD performed an excellent estimation of the states while the system tracked the proposed trajectories. The stability of SMD is guaranteed and was mentioned in this work.

ISSN: 2524-2121
RENIECYT-SECIHTI: 1702902

Pacheco, Jorge, Cortés-Vega, David, Sanchez-Lara, Rafael, Alazki, Hussain. [2025]. PID control for tracking A 5 DOF robotic manipulator subjected to exogenous forces. ECORFAN-Journal Taiwan. 9 [16]1-15: e6916115.
https://doi.org/10.35429/EJT.2025.9.16.6.1.15

Furthermore, the percentage tracking errors were found to be very small. It was also observed that the control signals obtained for tracking did not exhibit excessive overshoots. After testing and validating the control scheme, it can be determined that the development proposed in this work offers a solution to the needs previously expressed in the problem statement.

Annexes

Declarations

Conflict of interest

As authors of this research article, we declare no conflicts of interest. We have no known financial conflicts of interest or personal relationships that could have influenced the article submitted to this journal.

Author contribution

Pacheco, Jorge: He developed the proposed research; conducted an exhaustive search of the state of the art; designed the tracking trajectories, cardioid and lemniscate; tested and validated the complete control algorithm; and wrote the article.

Alazki, Hussein: He contributed the main research proposal, the method and the control technique applied in the robotic manipulator and also participated in reviewing the article's writing.

Cortés Vega, David: He tested and fine-tuned the complete control algorithm; tested and validated the structures of various differentiators for application in the control scheme; and participated in reviewing the article's editorial work.

Availability of data and materials

The control algorithm, data and graphs presented in this work were obtained from MATLAB® R2024a/Simulink version 24.1, (Natick, MA, USA) Software, are available for sharing upon request.

Funding

This research did not receive funding from any institution.

Abbreviations

3D	Three dimensions.
DOF	Degrees Of Freedom.
GDL	Degrees Of Freedom, in Spanish.
PID	Proportional Integral Derivative.
SMD	Sliding Mode Differentiator.

References

Basics

Alvarez-Sánchez, E. J., Aldana-Franco, F., Leyva-Retureta, J. G., Aldana-Franco, R., Villafuerte-Segura, R., & Domínguez-Ramírez, O. A. (2024). Tendencias Actuales en el Desarrollo de la Robótica en México. Pädi Boletín Científico de Ciencias Básicas e Ingenierías del ICBI, 12(Especial2), I-IV. DOI: 10.29057/icbi.v12iEspecial2.12560.

Bae, H. J., Jin, M., Suh, J., Lee, J. Y., Chang, P. H., & Ahn, D. S. (2017). Control of robot manipulators using time-delay estimation and fuzzy logic systems. Journal of Electrical Engineering and Technology, 12(3), 1271-1279. DOI: 10.5370/jeet.2017.12.3.1271.

Božek, P., & Nikitin, Y. The Development of an Optimally-Tuned PID Control for the Actuator of a Transport Robot. Actuators 2021, 10, 195. DOI: 10.3390/act10080195.

Brunot, M. (2019). Comparison of Numerical Differentiation Techniques for Aircraft Identification. Journal of Aerospace Engineering, 32(5), 06019002. DOI: 10.1061/(ASCE)AS.1943-5525.0001003

Cao, P., Gan, Y., & Dai, X. (2019). Finite-time disturbance observer for robotic manipulators. Sensors, 19(8), 1943. DOI: 10.3390/s19081943

CRS Catalyst-5Articulated Robot, n.d. https://acortar.link/Gx5RWx

Dao, H. V., Nguyen, M. H., & Ahn, K. K. (2023). Nonlinear functional observer design for robot manipulators. Mathematics, 11(19), 4033. DOI: 10.3390/math11194033

Feng, M., Dai, J., Zhou, W., Xu, H., & Wang, Z. (2024). Kinematics analysis and trajectory planning of 6-DOF hydraulic robotic arm in driving side pile. Machines, 12(3), 191. DOI: 10.3390/machines12030191.

ISSN: 2524-2121
RENIECYT-SECIHTI: 1702902

Pacheco, Jorge, Cortés-Vega, David, Sanchez-Lara, Rafael, Alazki, Hussain. [2025]. PID control for tracking A 5 DOF robotic manipulator subjected to exogenous forces. ECORFAN-Journal Taiwan. 9 [16]1-15: e6916115.
https://doi.org/10.35429/EJT.2025.9.16.6.1.15

Haselirad, A., & Neubert, J. (2014). A comparison of three trajectory planning methods for smooth motion in 5-DOF manipulators. *tC*, *60*(24), 6.

Huang, H. L., Cheng, M. Y., & Huang, T. Y. (2023). A rapid base parameter physical feasibility test algorithm for industrial robot manipulator identification using a recurrent neural network. IEEE Access, 11, 145692-145705. DOI: 10.1109/ACCESS.2023.3344490.

Klančar, G., & Škrjanc, I. (2007). Tracking-error model-based predictive control for mobile robots in real time. Robotics and autonomous systems, 55(6), 460-469. DOI: 10.1016/j.robot.2007.01.002.

Lavín-Delgado, J. E., Solís-Pérez, J. E., Gómez-Aguilar, J. F., & Escobar-Jiménez, R. F. (2020). Trajectory tracking control based on non-singular fractional derivatives for the PUMA 560 robot arm. Multibody System Dynamics, 50(3), 259-303. DOI: 10.1007/s11044-020-09752-y.

Levant, A. (2005). Homogeneity approach to high-order sliding mode design. Automatica, 41(5), 823-830. DOI: 10.1016/j.automatica.2004.11.029.

Levant, A. (2003). Higher-order sliding modes, differentiation and output-feedback control. International journal of Control, 76(9-10), 924-941. DOI: 10.1080/0020717031000099029.

Levant, A. (1998). Robust exact differentiation via sliding mode technique. automatica, 34(3), 379-384. DOI:10.1016/s0005-1098(97)002094.

Li, S., Yang, J., Chen, W. H., & Chen, X. (2016). *Disturbance observer-based control: methods and applications*. CRC press.

Lin, C. J., Sie, T. Y., Chu, W. L., Yau, H. T., & Ding, C. H. (2021, March). Tracking control of pneumatic artificial muscle-activated robot arm based on sliding-mode control. In Actuators (Vol. 10, No. 3, p. 66). MDPI. DOI: 10.3390/act10030066.

Liu, Y., Chen, X., Mei, Y., & Wu, Y. (2022). Observer-based boundary control for an asymmetric output-constrained flexible robotic manipulator. *Science China. Information Sciences*, *65*(3), 139203. DOI: 10.1007/s11432-019-2893-y

Loria, A. (2015). Observers are unnecessary for output-feedback control of Lagrangian systems. IEEE Transactions on Automatic Control, 61(4), 905-920. DOI: 10.1109/TAC.2015.2446831.

Na, G., Jo, N. H., & Eun, Y. (2019). Performance degradation due to measurement noise in control systems with disturbance observers and saturating actuators. Journal of the Franklin Institute, 356(7), 3922-3947. DOI: 10.1016/j.jfranklin.2019.03.001

Okubanjo, A. A., Oyetola, O. K., Osifeko, M. O., Olaluwoye, O. O., & Alao, P. O. (2017). Modeling of 2-DOF robot arm and control. Futo J Series (FUTOJNLS), 3(2), 80-92.

Pérez Vidal, A. J., Castro-González, Á., Alonso Martín, F., Castillo, J. C., & Salichs, M. Á. (2017). Evolución de la robótica social y nuevas tendencias. Actas de las XXXVIII Jornadas de Automática. http://hdl.handle.net/10651/46926.

Rebouças Filho, P. P., da Silva, S. P. P., Praxedes, V. N., Hemanth, J., & de Albuquerque, V. H. C. (2019). Control of singularity trajectory tracking for robotic manipulator by genetic algorithms. Journal of computational science, 30, 55-64. DOI: 10.1016/j.jocs.2018.11.006.

Sariyildiz, E., & Ohnishi, K. (2014). Stability and robustness of disturbance-observer-based motion control systems. IEEE Transactions on Industrial Electronics, 62(1), 414-422. DOI: 10.1109/TIE.2014.2327009

Shtessel, Y., Edwards, C., Fridman, L., & Levant, A. (2014). Sliding mode control and observation (Vol. 10). New York: Springer New York. DOI: 10.1007/978-0-8176-4893-0.

Stotsky, A., & Kolmanovsky, I. (2001, June). Simple unknown input estimation techniques for automotive applications. In Proceedings of the 2001 American Control Conference. (Cat. No. 01CH37148) (Vol. 5, pp. 3312-3317). IEEE. DOI: 10.1109/ACC.2001.946139.

Urrea, C., Kern, J., & Alvarado, J. (2020). Design and evaluation of a new fuzzy control algorithm applied to a manipulator robot. Applied sciences, 10(21), 7482. DOI: 10.3390/app10217482.

ISSN: 2524-2121
RENIECYT-SECIHTI: 1702902

Pacheco, Jorge, Cortés-Vega, David, Sanchez-Lara, Rafael, Alazki, Hussain. [2025]. PID control for tracking A 5 DOF robotic manipulator subjected to exogenous forces. ECORFAN-Journal Taiwan. 9 [16]1-15: e6916115.
https://doi.org/10.35429/EJT.2025.9.16.6.1.15

Vo, A. T., Truong, T. N., & Kang, H. J. (2021). A novel tracking control algorithm with finite-time disturbance observer for a class of second-order nonlinear systems and its applications. *IEEE Access*, *9*, 31373-31389. DOI: 10.1109/ACCESS.2021.3060381

Yilmaz, B. M., Tatlicioglu, E., Savran, A., & Alci, M. (2021). Self-adjusting fuzzy logic based control of robot manipulators in task space. IEEE Transactions on Industrial Electronics, 69(2), 1620-1629. DOI: 10.1109/TIE.2021.3063970.

Zhang, Z., Zheng, L., Yu, J., Li, Y., & Yu, Z. (2017). Three recurrent neural networks and three numerical methods for solving a repetitive motion planning scheme of redundant robot manipulators. IEEE/ASME Transactions on Mechatronics, 22(3), 1423-1434. DOI: 10.1109/TMECH.2017.2683561.

ISSN: 2524-2121
RENIECYT-SECIHTI: 1702902

Pacheco, Jorge, Cortés-Vega, David, Sanchez-Lara, Rafael, Alazki, Hussain. [2025]. PID control for tracking A 5 DOF robotic manipulator subjected to exogenous forces. ECORFAN-Journal Taiwan. 9 [16]1-15: e6916115.
https://doi.org/10.35429/EJT.2025.9.16.6.1.15

ECORFAN-Journal Taiwan 9[16]1-7: e7916107
Article

Current sensorless robust voltage regulation discontinuous control for DC-DC buck converter

Control discontinuo robusto sin sensor de corriente para regulación de voltaje en un convertidor reductor

Hernandez-Salazar, Jesus Emmanuel[a], Cortes-Vega, David[b], Alazki, Hussain[c] and Vázquez-Ávila, José Luis[d]

[a] Universidad Autónoma del Carmen • 0009-0000-2306-2923 • 1322453
[b] Universidad Autónoma del Carmen • 0000-0002-6209-2081 • 593408
[c] Universidad Autónoma del Carmen • 0000-0002-1960-3624 • 274587
[d] Universidad Autónoma del Carmen • 0000-0002-9654-2431 • 92331

SECIHTI classification:

Area: Engineering
Field: Engineering
Discipline: Electronic engineering
Subdiscipline: Control

https://doi.org/10.35429/EJT.2025.9.16.7.1.7
History of the article:
Received: June 11, 2025
Accepted: December 10, 2025

* ✉ []

Abstract

This paper presents the development of a robust discontinuous controller based on the super twisting algorithm and a simultaneous state and disturbance estimation scheme to regulate efficiently output voltage of a DC-DC converter in buck topology under load and input voltage variations. Such changes are handled by an appropriate rearranging of the system and the use of an Extended State Observer scheme to estimate the disturbance of the new model. This observer scheme also allows the estimation of the system states which permits the elimination of the current sensor reducing the overall system cost. The stability of the proposed robust discontinuous controller based on disturbance and state estimations is ensured using Lyapunov stability concepts. Simulation tests of the proposal in contrast to classic control techniques are presented to verify its adequate performance

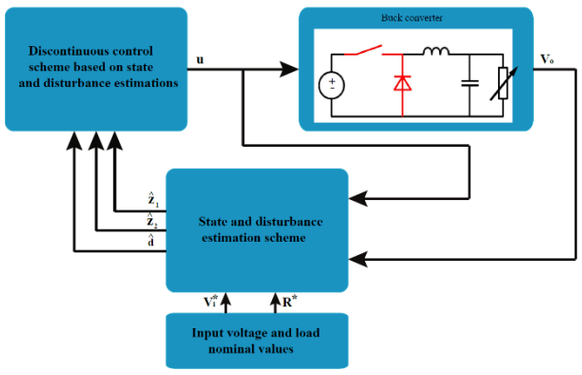

Robust control, Power electronics, Disturbance estimation

Resumen

En este artículo se presenta el desarrollo de un controlador discontinuo robusto basado en el algoritmo Super Twisting y en un esquema de estimación simultanea de estados y perturbaciones para regular de forma eficiente el voltaje de salida de un convertidor CD-CD en topología reductora bajo cargas y voltajes de entrada variantes. Tales cambios son incluidos en el modelo mediante una reestructuración del sistema y el uso posterior de un Observador de Estados Extendido que permita estimar la perturbación acoplada del nuevo modelo. Este esquema de estimación tambien permite la estimación de estados lo cual permite la eliminación de un sensor de corriente reduciendo con esto el costo total del sistema. La estabilidad del controlador robusto discontinuo basado en estimaciones de estado es asegurada mediante conceptos de estabilidad de Lyapunov. Se presentan pruebas de simulación del control propuesto en comparación con técnicas de control clásicas para verificar su efectividad.

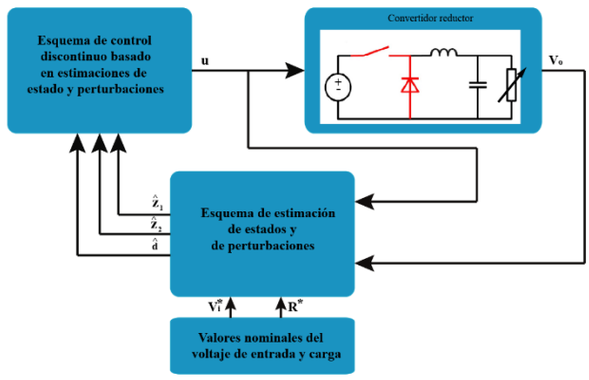

Control robusto, Electrónica de potencia, Estimación de perturbación

Area: Development of strategic leading-edge technologies and open innovation for social transformation

Citation: Hernandez-Salazar, Jesus Emmanuel, Cortes-Vega, David, Alazki, Hussain and Vázquez-Ávila, José Luis. [2025]. Current sensorless robust voltage regulation discontinuous control for DC-DC buck converter. ECORFAN-Journal Taiwan. 9 [16]1-7: e7916107.

1. Introduction

Nowadays, with the great advance and development that has been carried out globally in the field of renewable energies, the use of DC-DC converters in their different topologies has become an essential part of the processes of generation and conversion of energy based in renewable sources. A known example of this can be found in photovoltaic systems, which require of these types of converters to guarantee operation in optimal conditions that ensure maximum extraction of the available energy at every moment, through the use of maximum power point tracking algorithms as shown in [13].

Therefore, it is a necessity to have control schemes that allow operating DC-DC converters in an efficient way under various situations specific of each particular application. A typical operation scenario of a system fed by DC-DC converters is the load change, which may affect the voltage regulation of the converter output deteriorating the overall system performance. For such scenario, various proposals can be found in the literature. In [18] a scheme model-based predictive control (MPC) is proposed for systems subject to disturbances, where a disturbance observer (DO) is developed for estimating disturbances value and using it in the output prediction to correct errors caused by disturbances and uncertainties. A fuzzy sliding control scheme is presented in [3], obtaining a better performance in comparison to conventional schemes based on Proportional Integral (PI) controllers.

A passivity-based controller with PI complementary control was developed in [19], guaranteeing a proper output voltage regulation, stability and fast response against load changes. Some other control schemes for output voltage regulation under load changes can be found in [15], [14], [4], [8]. Nevertheless, the previous control strategies show an efficient operation, most of them are complex techniques that entail a high computational burden which can limit its application, especially in low cost applications. In order to cope with this limitation a common robust control approach used for power converters control is sliding modes control theory [16].

Several proposals based on sliding modes can be found in the literature as the ones shown in [12], [17], [10], [9] achieving an efficient output power regulation even under disturbances along with easy implementation. Although sliding modes controllers have proved to be an excellent alternative to DC-DC converters, its major drawback is the high frequency commutation generated in the control signal, known as chattering, which can deteriorate severely the actuators. The Super Twisting control is a sliding modes technique that reduces chattering while keeping the robustness against disturbances [7]. To reduce the overall cost of the system it is a common practice the use of observation schemes that allow us to dispense of physical sensors to make measurements of the variables of interest, particularly for the buck converter the desired variables to estimate are the inductor current and the disturbances.

To estimate inductor current, several methods have been developed, in [1] and [11] such estimation is performed by means of observer schemes but this approach require additional measurements of load current, inductor voltage and output voltage. In [2] a method based on estimation of inductor's resistance and inductance parameters is proposed. Disturbance observers (DO) based methods only performs the estimation of disturbance without considering system states [6], [5] so it is required to carry out a scheme which estimates simultaneously both parts.

This work proposes the design of a simultaneous estimation scheme for states and disturbances that allows the elimination of sensors and at the same time operates efficiently under disturbance scenarios related to load and input voltage changes. To this end, the load and input voltage changes are modeled into a coupled term which can be estimated by an ESO, and use such estimation to attenuate disturbance effects. State and disturbance estimations are used to design a ST controller that ensures output voltage regulation in desired values. To guarantee system stability a Lyapunov analysis is performed. The remainder of the paper is organized as follows: Section II presents the mathematical model of the buck converter, Section III analyzes the design conditions for the ESO estimation scheme, Section IV describes the ESO based ST controller, Section V shows the results of simulation tests and finally Section VI states the main conclusions of the work

ISSN: 2524-2121
RENIECYT-SECIHTI: 1702902

Hernandez-Salazar, Jesus Emmanuel, Cortes-Vega, David, Alazki, Hussain and Vázquez-Ávila, José Luis. [2025]. Current sensorless robust voltage regulation discontinuous control for DC-DC buck converter. ECORFAN-Journal Taiwan. 9 [16]1-7: e7916107
https://doi.org/10.35429/EJT.2025.9.16.7.1.7

2. Mathematical model of the buck converter

A step-down converter, also called buck converter, is a DC-DC converter topology that, as its name indicates, allows you to reduce the input voltage. A typical buck converter configuration is shown in Figure 1, where v_i, i_L, v_o are input voltage, inductor current and output voltage respectively. The converter components are denoted by R, L, C. This basic structure is affected mainly by two uncertainty sources, namely, input voltage variations and load changes.

Box 1

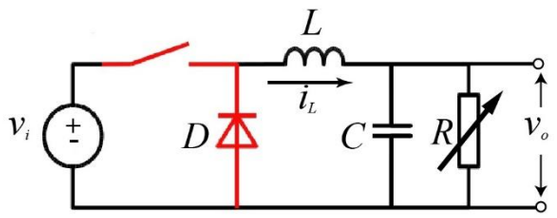

Figure 1
Buck converter topology

Depending on the Switch state the converter can be analyzed as two different circuits.

When S=ON (switch is closed), the current will increase, the inductor generates an opposing voltage in response to the change of current. This reduces the voltage across the load. The equations describing this scenario are:

$$\frac{di_L}{dt} = \frac{(v_i - v_o)}{L} \quad [1]$$

$$\frac{dv_o}{dt} = \frac{i_L}{C} - \frac{v_o}{RC} \quad [2]$$

When S=OFF (switch is open), the voltage source will be removed from the circuit, and the current will decrease. The equations for this case are:

$$\frac{di_L}{dt} = \frac{-v_o}{L}$$

$$\frac{dv_o}{dt} = \frac{i_L}{C} - \frac{v_o}{RC}$$

Using the state–space averaging method [20], [21], the dynamic model of the buck converter can be written as:

$$\frac{di_L}{dt} = \frac{-v_o}{L} + \frac{v_i}{L}u \quad [3]$$

$$\frac{dv_o}{dt} = \frac{i_L}{C} - \frac{v_o}{RC} \quad [4]$$

where u is the duty ratio of the converter.

3. ESO estimation scheme

The model described by (3-4) can be transformed to include the load and input voltage changes as

$$\dot{z}_1 = z_2 \quad [5]$$

$$\dot{z}_2 = -n_{11}n_{21}z_1 - n_{23}z_2 + n_{11}n_{21}v_i(u + w) \quad [6]$$

with

$$n_{11} = {}^1\!/_L \,, n_{21} = {}^1\!/_C$$
$$n_{22} = {}^1\!/_{RC} - {}^1\!/_{R^*C} \,, n_{23} = {}^1\!/_{R^*C}$$
$$w = \frac{1}{n_{11}n_{21}v_i}\left[-n_{11}n_{21}v_{ref} + n_{11}n_{21}(v_i - v^*)u - n_{23}\dot{v}_{ref} - n_{22}\left(z_2 + \dot{v}_{ref}\right) - \ddot{v}_{ref}\right]$$

where $z_1 = v_o - v_{ref}$ and R^*, v^* describe the load nominal value and input voltage nominal value respectively. System (5-6) can be rewritten in matrix form as

$$\dot{z} = Az + Bu + B_w w \quad [7]$$

with

$$\dot{z} = [z_1\ z_2]^T \,, A = \begin{bmatrix} 0 & 1 \\ -n_{11}n_{21} & -n_{23} \end{bmatrix}$$

$$B = \begin{bmatrix} 0 \\ n_{11}n_{21}v_i \end{bmatrix} \,, B_w = B$$

An extended variable $z_{n+1} = w$ is added to linearize system (7), so the extended system is described as [22]

$$\begin{cases} \dot{\bar{z}} = A_e\bar{z} + B_e u + Dh \\ y = C\bar{z} \end{cases}$$

where

$$\bar{z} = \begin{bmatrix} z \\ z_{n+1} \end{bmatrix} \,, h = \dot{w}$$

$$A_e = \begin{bmatrix} 0 & 1 & 0 \\ -n_{11}n_{21} & -n_{23} & n_{11}n_{21}v_i \\ 0 & 0 & 0 \end{bmatrix}$$

ISSN: 2524-2121
RENIECYT-SECIHTI: 1702902

Hernandez-Salazar, Jesus Emmanuel, Cortes-Vega, David, Alazki, Hussain and Vázquez-Ávila, José Luis. [2025]. Current sensorless robust voltage regulation discontinuous control for DC-DC buck converter. ECORFAN-Journal Taiwan. 9 [16]1-7: e7916107
https://doi.org/10.35429/EJT.2025.9.16.7.1.7

$$B_e = \begin{bmatrix} 0 \\ n_{11}n_{22}v_i \\ 0 \end{bmatrix}, D = \begin{bmatrix} 0 \\ 0 \\ 1 \end{bmatrix}, C_e = \begin{bmatrix} 1 \\ 0 \\ 0 \end{bmatrix}^T$$

An ESO scheme for system (8) can be designed as

$$\begin{cases} \dot{\hat{\bar{z}}} = A_e\hat{\bar{z}} + B_e u + L(y - \hat{y}) \\ \hat{y} = C_e\hat{\bar{z}} \end{cases} \quad [9]$$

where $\hat{\bar{z}}$ is the vector of estimations of $\bar{z}$ and $L = [L_1\ L_2\ L_3]^T$ is the observer gain matrix.

4. Controller design

For the discontinuous control scheme design, the ST algorithm is selected considering the following surface

$$s = c_1\hat{\bar{z}}_1 + c_2\hat{\bar{z}}_2 \quad [10]$$

where $c_1, c_2 > 0$. The surface dynamics is described as

$$\dot{s} = c_1\dot{\hat{\bar{z}}}_1 + c_2\dot{\hat{\bar{z}}}_2$$

$$\dot{s} = c_1\hat{\bar{z}}_2 + L_1(\bar{z}_1 - \hat{\bar{z}}_1)c_1 + c_2[-n_{11}n_{21}\hat{\bar{z}}_1 - n_{23}\hat{\bar{z}}_2 + n_{11}n_{21}v_i(u + \hat{w}) + L_2(\bar{z}_1 - \hat{\bar{z}}_1)] \quad [11]$$

Considering a quadratic Lyapunov function

$$V(s) = \frac{1}{2}s^2$$

the condition $\dot{V} = s\dot{s} \leq 0$ must be fulfilled to guarantee system stability. Therefore, the proposed discontinuous control has the form

$$u = \frac{1}{n_{11}n_{21}v_i}\left(-\frac{c_1}{c_2}\hat{\bar{z}}_2 - L_1c_1(\bar{z}_1 - \hat{\bar{z}}_1) + n_{11}n_{21}\hat{\bar{z}}_1 + n_{22}\hat{\bar{z}}_2 - L_2(\bar{z}_1 - \hat{\bar{z}}_1) - n_{11}n_{21}v_i\hat{w} + v\right) \quad [12]$$

where v is the ST algorithm defined as

$$v = -\alpha\|s\|^{1/2}sign(s) - \beta\int sign(s)\,dt \quad [13]$$

Finally, by using (12) in (11), the surface dynamics results in

$$\dot{s} = v$$

then

$$\dot{V} = s\left[-\alpha\|s\|^{1/2}sign(s) - \beta\int sign(s)\,dt\right] \quad [14]$$

and by using the relation $\|s\| = sign(s)s$, the last equation can be transformed as

$$\dot{V} \leq -\alpha\|s\|^{1/2}\|s\| - \beta\int\|s\|\,dt \quad [15]$$

which ensures that $\dot{V} < 0$ if $\alpha + \beta > 0$.

5. Results

To verify the performance of the proposed control scheme, simulation tests have been developed using Simulink and the Simscape/Power Systems libraries. The selected parameters of the buck converter are shown in Table 1. The proposed controller parameters are presented in Table 2 which were selected empirically based on the condition (15). The proposed controller performance is compared with a PI control scheme and a first order sliding mode controller. The simulated scenario consists of an input voltage signal that changes from 20V-24V at $t = 6s$ and has small sinusoidal variation as shown in Figure 2. The desired output voltage is selected as 10V and a load change is presented at $t = 1s$ from 25Ω to 9.75Ω.

Box 2

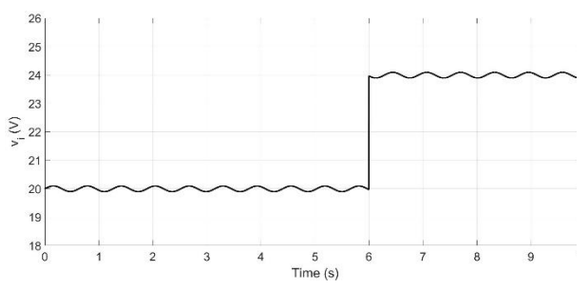

Figure 2
Input voltage signal

The output voltage regulation is illustrated in Figure 3. It can be seen that the 3 schemes perform an adequate regulation around the 10V reference but the proposed scheme shows an oscillation of lower magnitude. The load change at $1s$ generates a greater oscillation from the current increment, which is better handled by the proposed controller. The other disturbance effects produced by the input voltage change is also attenuated in a more accurate way by the proposed controller than the other schemes.

ISSN: 2524-2121
RENIECYT-SECIHTI: 1702902

Hernandez-Salazar, Jesus Emmanuel, Cortes-Vega, David, Alazki, Hussain and Vázquez-Ávila, José Luis. [2025]. Current sensorless robust voltage regulation discontinuous control for DC-DC buck converter. ECORFAN-Journal Taiwan. 9 [16]1-7: e7916107
https://doi.org/10.35429/EJT.2025.9.16.7.1.7

Box 3

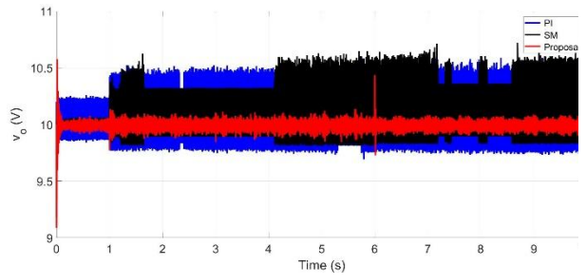

Figure 3
Output voltage

Figure 4 depicts the inductor current behaviour, which shows similar characteristics to the one seen for the output voltage case with a more accurate response for the proposed controller.

Box 4

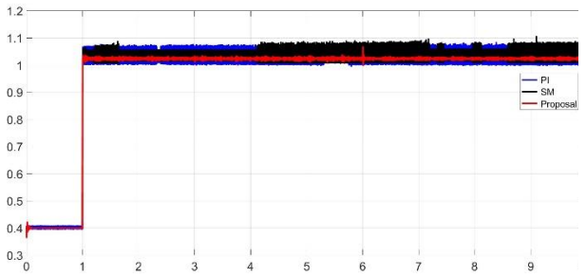

Figure 4
Inductor current

The control signal is shown in Figure 5. The three control signals keep his values in the desired range from 0 to 1.

Box 5

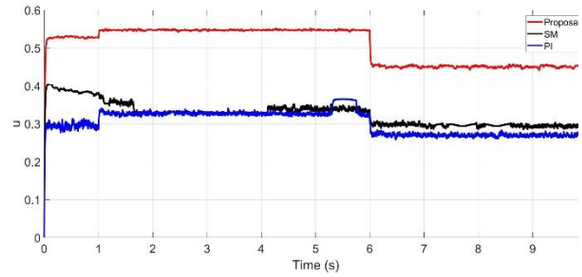

Figure 5
Control signal

The estimation error of the first state corresponding to the output voltage error $(v_o - v_{ref})$ is presented in Figure 6, a very low error is generated which contributes to the proper performance of the proposed controller.

Box 6

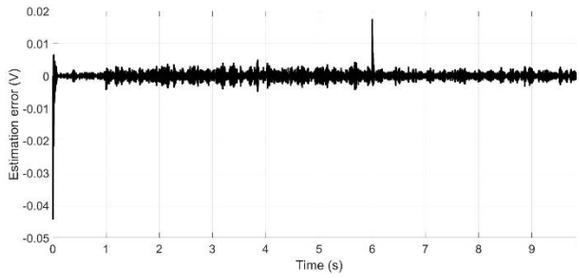

Figure 6
Estimation error of state $\hat{z}_1$

6. Conclusions

The proposed robust discontinuous control scheme using a ST controller based on ESO is able to effectively regulate the output voltage of the selected DC-DC buck converter under load changes and input voltage variations. The ESO scheme for simultaneous estimation of states and disturbances operates with low estimation errors contributing to an adequate voltage regulation. It was demonstrated system stability of the proposed controller by means of Lyapunov analysis. Simulation tests shown that the proposed controller has a better performance that conventional PID based schemes and is capable of handle disturbances generated from load changes and input voltage variations. It is possible to enhance the controller response in a future work by implementing an appropriate gain selection method which allows a more precise control of the desired variables.

Annexes

Box 7

Table 1
Buck converter parameters

Parameter	Value
Nominal load (R*)	11 Ω
Inductance (L)	200 µH
Capacitance (C)	220 µF
Input voltage (V_i)	20V

Box 8

Table 2
Proposed controller parameters

Parameter	Value
α	21
β	15
L_1	5000
L_2	1000
L_3	1000

ISSN: 2524-2121
RENIECYT-SECIHTI: 1702902

Hernandez-Salazar, Jesus Emmanuel, Cortes-Vega, David, Alazki, Hussain and Vázquez-Ávila, José Luis. [2025]. Current sensorless robust voltage regulation discontinuous control for DC-DC buck converter. ECORFAN-Journal Taiwan. 9 [16]1-7: e7916107
https://doi.org/10.35429/EJT.2025.9.16.7.1.7

Declarations

Conflict of interest

The authors declare no interest conflict. They have no known competing financial interests or personal relationships that could have appeared to influence the article reported in this article.

Funding

This research received no external funding.

Availability of data and materials

Data sharing is not applicable to this article as no new data were created or analyzed in this study.

Abbreviations

DC	Direct Current
DO	Disturbance Observer
ESO	Extended State Observer
MPC	Model Predictive Control
PID	Proportional Integral Derivative
ST	Super Twisting

References

Antecedents

[7] Kamal, S., Chalanga, A., Moreno, J. A., Fridman, L., & Bandyopadhyay, B. "Higher order super-twisting algorithm". 13th International Workshop on Variable Structure Systems (VSS) IEEE, 2014. DOI: 10.1109/VSS.2014.6881129

[9] Lopez-Santos, O., Martinez-Salamero, L., Garcia, G., Valderrama-Blavi, H., & Sierra-Polanco, T. "Robust sliding-mode control design for a voltage regulated quadratic boost converter." *IEEE transactions on power electronics*, Vol. 30, No. 4, 2014. DOI: 10.1109/TPEL.2014.2325066

[10] Midya, P., Greuel, M., & Krein, P. T. "Sensorless current mode control-an observer-based technique for DC-DC converters." PESC97. Record 28th Annual IEEE Power Electronics Specialists Conference. Formerly Power Conditioning Specialists Conference 1970-71. Power Processing and Electronic Specialists Conference 1972, IEEE, 1997. DOI: 10.1109/63.931070

[12] Pandey, S. K., Patil, S. L., Chaskar, U. M., & Phadke, S. B. "State and disturbance observer-based integral sliding mode-controlled boost DC–DC converters". *IEEE Transactions on Circuits and Systems II: Express Briefs*, Vol. 66, No. 9, 2018. DOI: 10.1109/TCSII.2018.2888570

[13] Podder, Amit Kumer; Roy, Naruttam Kumar; Pota, Hemanshu Roy. "MPPT methods for solar PV systems: a critical review based on tracking nature". *IET Renewable Power Generation*, Vol. 13, No. 10, 2019. DOI: https://doi.org/10.1049/iet-rpg.2018.5946

[16] Utkin, Vadim. "Variable structure systems with sliding modes". IEEE Transactions on Automatic Control Vol.22, No. 2, 1977. DOI: 10.1109/TAC.1977.1101446

[17] Wang, Zuo; Li, Shihua; Li, Qi. "Continuous nonsingular terminal sliding mode control of DC–DC boost converters subject to time-varying disturbances". *IEEE Transactions on Circuits and Systems II: Express Briefs*, Vol. 67, No 11, 2019. DOI: 10.1109/TCSII.2019.2955711

Basics

[20] R. D. Middlebrook and S. Cuk, "A general unified approach to modeling switching converter power stages", in Proc. IEEE Power Electron. Spec. Conf., Jun. 8–10, 1976, pp. 18–34. DOI: 10.1109/PESC.1976.7072895

[21] P. T. Krein, J. Bentsman, R. M. Bass, and B. C. Lesieutre, "On the use of averaging for the analysis of power electronic systems", in Proc. 20th Annu. IEEE Power Electron. Spec. Conf., Jun. 26–29, 1989, pp. 463–467. DOI: 10.1109/63.53155

[22] Li, S., Yang, J., Chen, W. H., & Chen, X. (2011). Generalized extended state observer based control for systems with mismatched uncertainties. IEEE Transactions on Industrial Electronics, 59(12), 4792-4802. DOI: 10.1109/TIE.2011.2182011

ISSN: 2524-2121
RENIECYT-SECIHTI: 1702902

Hernandez-Salazar, Jesus Emmanuel, Cortes-Vega, David, Alazki, Hussain and Vázquez-Ávila, José Luis. [2025]. Current sensorless robust voltage regulation discontinuous control for DC-DC buck converter. ECORFAN-Journal Taiwan. 9 [16]1-7: e7916107
https://doi.org/10.35429/EJT.2025.9.16.7.1.7

Supports

[1] Bhartiya, P.; Rathore, N.; Fulwani, D. "A tutorial on implementation of Sliding mode observer for DC/DC power converters using FPGA". IECON 2014-40th Annual Conference of the IEEE Industrial Electronics Society. IEEE, 2014. DOI: 10.1109/IECON.2014.7049126

[2] Chen, C., Li, L., Zhang, Q., Tong, Q., Liu, K., Lyu, D., & Min, R. "Online inductor parameters identification by small-signal injection for sensorless predictive current controlled boost converter". *IEEE Transactions on Industrial Informatics*, Vol. 13, No. 4, 2016. DOI: 10.1109/TII.2016.2647079

[5] Han, J. "From PID to active disturbance rejection control". *IEEE transactions on Industrial Electronics*, Vol. 56, No. 3, 2009. DOI: 10.1109/TIE.2008.2011621

[6] Jiang, L.; Wu, Q. H. "Nonlinear adaptive control via sliding-mode state and perturbation observer". *IEE Proceedings-Control Theory and Applications*, Vol. 149, No. 4, 2002. DOI: 10.1049/ip-cta:20020470

[11] Naik, B. B.; Mehta, A. J. "Sliding mode controller with modified sliding function for DC-DC Buck Converter". *ISA transactions*, Vol. 70, 2017. DOI: https://doi.org/10.1016/j.isatra.2017.05.009

Differences

[3] Guo, Liping; Hung, John Y.; Nelms, R. M. "Comparative evaluation of sliding mode fuzzy controller and PID controller for a boost converter". *Electric Power Systems Research*, Vol. 81, No 1, 2011. DOI: https://doi.org/10.1016/j.epsr.2010.07.018

[4] Hajihosseini, M., Andalibi, M., Gheisarnejad, M., Farsizadeh, H., & Khooban, M. H. "DC/DC power converter control-based deep machine learning techniques: Real-time implementation". *IEEE Transactions on Power Electronics*, Vol. 35, No. 10, 2020. DOI: 10.1109/TPEL.2020.2977765

[8] Jiazhou, L., Guosheng, Z., Liaoxuan, D., Huifang, M., & Shang, S. (2024). "Volterra operator-based fixed-time adaptive parameter estimation for DC-DC buck converters without current sensors". *Transactions of the Institute of Measurement and Control*. DOI: https://doi.org/10.1177/01423312241262540

[14] Riffo, S., Gil-González, W., Montoya, O. D., Restrepo, C., & Muñoz, J. "Adaptive Sensorless PI+ Passivity-Based Control of a Boost Converter Supplying an Unknown CPL". *Mathematics*, Vol. 10, No. 22, 2022. DOI: https://doi.org/10.3390/math10224321

[15] Soriano-Rangel, C. A., He, W., Mancilla-David, F., & Ortega, R. "Voltage regulation in buck–boost converters feeding an unknown constant power load: An adaptive passivity-based control". *IEEE Transactions on Control Systems Technology*, Vol. 29, No.1, 2020. DOI: 10.1109/TCST.2019.2959535

[18] Yang, J., Zheng, W. X., Li, S., Wu, B., & Cheng, M. "Design of a prediction-accuracy-enhanced continuous-time MPC for disturbed systems via a disturbance observer". *IEEE Transactions on Industrial Electronics*, Vol. 62, No.9,2015. DOI: 10.1109/TIE.2015.2450736

[19] Zeng, Jianwu; Zhang, Zhe; Qiao, Wei. "An interconnection and damping assignment passivity-based controller for a DC–DC boost converter with a constant power load". *IEEE Transactions on Industry Applications*, Vol. 50, No 4, 2013. DOI: 10.1109/IAS.2012.6374043

ISSN: 2524-2121
RENIECYT-SECIHTI: 1702902

Hernandez-Salazar, Jesus Emmanuel, Cortes-Vega, David, Alazki, Hussain and Vázquez-Ávila, José Luis. [2025]. Current sensorless robust voltage regulation discontinuous control for DC-DC buck converter. ECORFAN-Journal Taiwan. 9 [16]1-7: e7916107
https://doi.org/10.35429/EJT.2025.9.16.7.1.7

[[Title in TNRoman and Bold No. 14 in English and Spanish]

Surname, Name 1st Author*[a], Surname, Name 1st Co-author[b], Surname, Name 2nd Co-author[c] and Surname, Name 3rd Co-author[d] [No.12 TNRoman]

[a] Affiliation institution, Researcher ID, ORC ID, SNI-SECIHTI ID or CVU PNPC [No.10 TNRoman]
[b] Affiliation institution, Researcher ID, ORC ID, SNI-SECIHTI ID or CVU PNPC [No.10 TNRoman]
[c] Affiliation institution, Researcher ID, ORC ID, SNI-SECIHTI ID or CVU PNPC [No.10 TNRoman]
[d] Affiliation institution, Researcher ID, ORC ID, SNI-SECIHTI ID or CVU PNPC [No.10 TNRoman]

All ROR-Clarivate-ORCID and SECIHTI profiles must be hyperlinked to your website.
Prot- University of South Australia • 7038-2013• 0000-0001-6442-4409 • 416112

SECIHTI classification:
https://marvid.org/research_areas.php [No.10 TNRoman]
Area:
Field:
Discipline:
Subdiscipline:

DOI: https://doi.org/
Article History:
Received: [Use Only ECORFAN]
Accepted: [Use Only ECORFAN]
Contact e-mail address:
* ✉ [example@example.org]

Abstract [In English]
Must contain up to 150 words
Graphical abstract [In English]

Authors must provide an original image that clearly represents the article described in the article. Graphical abstracts should be submitted as a separate file. Please note that, as well as each article must be unique. File type: the file types are MS Office files.No additional text, outline or synopsis should be included. Any text or captions must be part of the image file. Do not use unnecessary white space or a "graphic abstract" header within the image file.

Keywords [In English]
Indicate 3 keywords in TNRoman and Bold No. 10

Abstract [In Spanish]
Must contain up to 150 words
Graphical abstract [In Spanish]

Authors must provide an original image that clearly represents the article described in the article. Graphical abstracts should be submitted as a separate file. Please note that, as well as each article must be unique. File type: the file types are MS Office files.No additional text, outline or synopsis should be included. Any text or captions must be part of the image file. Do not use unnecessary white space or a "graphic abstract" header within the image file.

Keywords [In Spanish]
Indicate 3 keywords in TNRoman and Bold No. 10

Citation: Surname, Name 1st Author, Surname, Name 1st Co-author, Surname, Name 2nd Co-author and Surname, Name 3rd Co-author. Article Title. ECORFAN Journal- Taiwan. Year. V-N: Pages [TN Roman No.10].

Introduction

Text in TNRoman No.12, single space.

General explanation of the subject and explain why it is important.

What is your added value with respect to other techniques?

Clearly focus each of its features.

Clearly explain the problem to be solved and the central hypothesis.

Explanation of sections Article.

Development of headings and subheadings of the article with subsequent numbers

[Title No.12 in TNRoman, single spaced and bold]

Products in development No.12 TNRoman, single spaced.

Including figures and tables-Editable

In the article content any table and figure should be editable formats that can change size, type and number of letter, for the purposes of edition, these must be high quality, not pixelated and should be noticeable even reducing image scale.

[Indicating the title at the bottom with No.10 and Times New Roman Bold]

Box

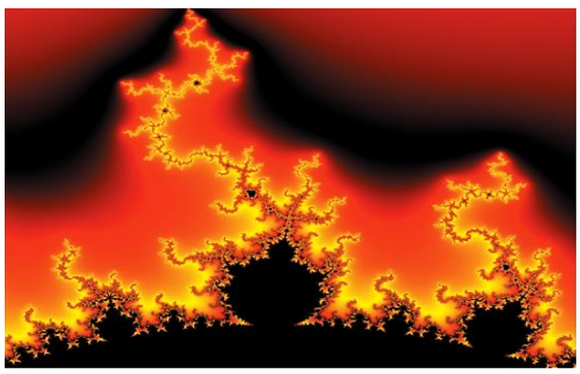

Figure 1

Title [Should not be images-everything must be editable]

Source [in italic]

Box

Table 1

Title [Should not be images-everything must be editable]

Source [in italic]

The maximum number of Boxes is 10 items

For the use of equations, noted as follows:

$$Y_{ij} = \alpha + \sum_{h=1}^{r} \beta_h X_{hij} + u_j + e_{ij} \quad [1]$$

Must be editable and number aligned on the right side.

Methodology

Develop give the meaning of the variables in linear writing and important is the comparison of the used criteria.

Results

The results shall be by section of the article.

Conclusions

Clearly explain the results and possibilities of improvement.

Annexes

Tables and adequate sources.

The international standard is 7 pages minimum and 14 pages maximum.

Declarations

Conflict of interest

The authors declare no interest conflict. They have no known competing financial interests or personal relationships that could have appeared to influence the article reported in this article.

ISSN: 2524-2121.
RENIECYT-SECIHTI: 1702902

Surname, Name 1st Author, Surname, Name 1st Co-author, Surname, Name 2nd Co-author and Surname, Name 3rd Co-author. Article Title. ECORFAN Journal Taiwan. Year. V-N: Pages [Times New Roman No. 8].
https://doi.org/10.35429/

Author contribution

Specify the contribution of each researcher in each of the points developed in this research.

Prot-
Benoit-Pauleter, Gerard: Contributed to the project idea, research method and technique.

Availability of data and materials

Indicate the availability of the data obtained in this research.

Funding

Indicate if the research received some financing.

Acknowledgements

Indicate if they were financed by any institution, University or company.

Abbreviations

List abbreviations in alphabetical order.

Prot-

ANN	Artificial Neural Network

References

Use APA system. Should not be numbered, nor with bullets, however if necessary numbering will be because reference or mention is made somewhere in the Article.

Use the Roman alphabet, all references you have used should be in Roman alphabet, even if you have cited an article, book in any of the official languages of the United Nations [English, French, German, Chinese, Russian, Portuguese, Italian, Spanish, Arabic], you should write the reference in Roman alphabet and not in any of the official languages.

Citations are classified the following categories:

Antecedents. The citation is due to previously published research and orients the citing document within a particular scholarly area.

Basics. The citation is intended to report data sets, methods, concepts and ideas on which the authors of the citing document base their work.

Supports. The citing article reports similar results. It may also refer to similarities in methodology or, in some cases, to the reproduction of results.

Differences. The citing document reports by means of a citation that it has obtained different results to those obtained in the cited document. This may also refer to differences in methodology or differences in sample sizes that affect the results.

Discussions. The citing article cites another study because it is providing a more detailed discussion of the subject matter.

The URL of the resource is activated in the DOI or in the title of the resource.

Prot-
Mandelbrot, B. B. [2020]. Negative dimensions and Hölders, multifractals and their Hölder spectra, and the role of lateral preasymptotics in science. Journal of Fourier Analysis and Applications Special. 409-432.

Intellectual Property Requirements for editing:

- Authentic Signature in Color of Originality Format Author and Coauthors.
- Authentic Signature in Color of the Acceptance Format of Author and Coauthors.
- Authentic Signature in blue color of the Conflict of Interest Format of Author and Co-authors.

ISSN: 2524-2121.
RENIECYT-SECIHTI: 1702902

Surname, Name 1st Author, Surname, Name 1st Co-author, Surname, Name 2nd Co-author and Surname, Name 3rd Co-author. Article Title. ECORFAN Journal Taiwan. Year. V-N: Pages [Times New Roman No. 8].
https://doi.org/10.35429/

Reservation to Editorial Policy

ECORFAN Journal-Taiwan reserves the right to make editorial changes required to adapt the Articles to the Editorial Policy of the Journal. Once the Article is accepted in its final version, the Journal will send the author the proofs for review. ECORFAN® will only accept the correction of errata and errors or omissions arising from the editing process of the Journal, reserving in full the copyrights and content dissemination. No deletions, substitutions or additions that alter the formation of the Article will be accepted.

Code of Ethics - Good Practices and Declaration of Solution to Editorial Conflicts

Declaration of Originality and unpublished character of the Article, of Authors, on the obtaining of data and interpretation of results, Acknowledgments, Conflict of interests, Assignment of rights and Distribution.

The ECORFAN-Mexico, S.C Management claims to Authors of Articles that its content must be original, unpublished and of Scientific, Technological and Innovation content to be submitted for evaluation.

The Authors signing the Article must be the same that have contributed to its conception, realization and development, as well as obtaining the data, interpreting the results, drafting and reviewing it. The Corresponding Author of the proposed Article will request the form that follows.

Article title:

– The sending of an Article to ECORFAN Journal- Taiwan emanates the commitment of the author not to submit it simultaneously to the consideration of other series publications for it must complement the Format of Originality for its Article, unless it is rejected by the Arbitration Committee, it may be withdrawn.

– None of the data presented in this article has been plagiarized or invented. The original data are clearly distinguished from those already published. And it is known of the test in PLAGSCAN if a level of plagiarism is detected Positive will not proceed to arbitrate.

– References are cited on which the information contained in the Article is based, as well as theories and data from other previously published Articles.

– The authors sign the Format of Authorization for their Article to be disseminated by means that ECORFAN-Mexico, S.C. In its Holding Taiwan considers pertinent for disclosure and diffusion of its Article its Rights of Work.

– Consent has been obtained from those who have contributed unpublished data obtained through verbal or written communication, and such communication and Authorship are adequately identified.

– The Author and Co-Authors who sign this work have participated in its planning, design and execution, as well as in the interpretation of the results. They also critically reviewed the paper, approved its final version and agreed with its publication.

– No signature responsible for the work has been omitted and the criteria of Scientific Authorization are satisfied.

– The results of this Article have been interpreted objectively. Any results contrary to the point of view of those who sign are exposed and discussed in the Article.

Copyright and Access

The publication of this Article supposes the transfer of the copyright to ECORFAN-Mexico, SC in its Holding Taiwan for its ECORFAN Journal- Taiwan, which reserves the right to distribute on the Web the published version of the Article and the making available of the Article in This format supposes for its Authors the fulfilment of what is established in the Law of Science and Technology of the United Mexican States, regarding the obligation to allow access to the results of Scientific Research.

Article Title:

Name and Surnames of the Contact Author and the Co-authors	Signature
1.	
2.	
3.	
4.	

Principles of Ethics and Declaration of Solution to Editorial Conflicts

Editor Responsibilities

The Publisher undertakes to guarantee the confidentiality of the evaluation process, it may not disclose to the Arbitrators the identity of the Authors, nor may it reveal the identity of the Arbitrators at any time.

The Editor assumes the responsibility to properly inform the Author of the stage of the editorial process in which the text is sent, as well as the resolutions of Double-Blind Review. The Editor should evaluate manuscripts and their intellectual content without distinction of race, gender, sexual orientation, religious beliefs, ethnicity, nationality, or the political philosophy of the Authors.

The Editor and his editing team of ECORFAN® Holdings will not disclose any information about Articles submitted to anyone other than the corresponding Author.

The Editor should make fair and impartial decisions and ensure a fair Double-Blind Review.

Responsibilities of the Editorial Board

The description of the peer review processes is made known by the Editorial Board in order that the Authors know what the evaluation criteria are and will always be willing to justify any controversy in the evaluation process. In case of Plagiarism Detection to the Article the Committee notifies the Authors for Violation to the Right of Scientific, Technological and Innovation Authorization.

Responsibilities of the Arbitration Committee

The Arbitrators undertake to notify about any unethical conduct by the Authors and to indicate all the information that may be reason to reject the publication of the Articles. In addition, they must undertake to keep confidential information related to the Articles they evaluate.

Any manuscript received for your arbitration must be treated as confidential, should not be displayed or discussed with other experts, except with the permission of the Editor.

The Arbitrators must be conducted objectively, any personal criticism of the Author is inappropriate.

The Arbitrators must express their points of view with clarity and with valid arguments that contribute to the Scientific, Technological and Innovation of the Author.

The Arbitrators should not evaluate manuscripts in which they have conflicts of interest and have been notified to the Editor before submitting the Article for Double-Blind Review.

Responsibilities of the Authors

Authors must guarantee that their articles are the product of their original work and that the data has been obtained ethically.

Authors must ensure that they have not been previously published or that they are not considered in another serial publication.

Authors must strictly follow the rules for the publication of Defined Articles by the Editorial Board.

The authors have requested that the text in all its forms be an unethical editorial behavior and is unacceptable, consequently, any manuscript that incurs in plagiarism is eliminated and not considered for publication.

Authors should cite publications that have been influential in the nature of the Article submitted to arbitration.

Information services

Indexation - Bases and Repositories

RESEARCH GATE (Germany)
GOOGLE SCHOLAR (Citation indices-Google)
MENDELEY (Bibliographic References Manager)
HISPANA (Information and Bibliographic Orientation-Spain)

Publishing Services

Citation and Index Identification H
Management of Originality Format and Authorization
Testing Article with PLAGSCAN
Article Evaluation
Certificate of Double-Blind Review
Article Edition
Web layout
Indexing and Repository
ArticleTranslation
Article Publication
Certificate of Article
Service Billing

Editorial Policy and Management

69 Street. YongHe district, ZhongXin. Taipei-Taiwan. Phones: +52 1 55 6159 2296, +52 1 55 1260 0355, +52 1 55 6034 9181; Email: contact@ecorfan.org www.ecorfan.org

ECORFAN Journal-Taiwan

2524-2121
ISSN 2524-2121

www.ecorfan.org